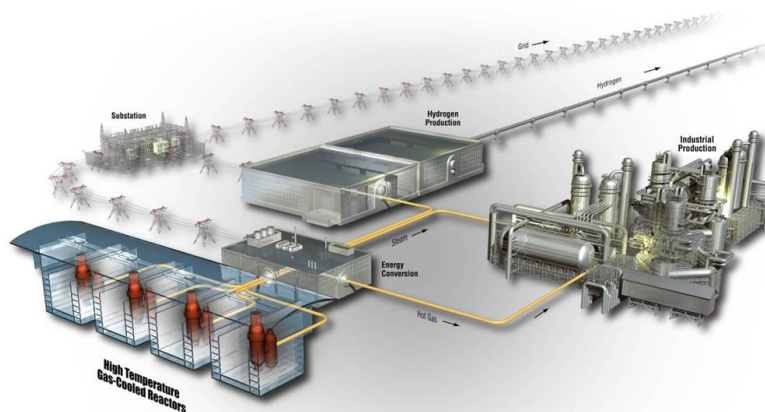# AGR-5/6/7 Experiment Monitoring and Simulation Progress

June 2021

Changing the World's Energy Future

Binh T. Pham
James W. Sterbentz
Grant L. Hawkes
Dawn M. Scates
Joe J. Palmer

Idaho National Laboratory

INL is a U.S. Department of Energy National Laboratory operated by Battelle Energy Alliance, LLC

AGR-5/6/7 Experiment Monitoring and Simulation Progress

Binh T. Pham
James W. Sterbentz
Grant L. Hawkes
Dawn M. Scates
Joe J. Palmer

June 2021

Idaho National Laboratory
Advanced Reactor Technologies
Idaho Falls, Idaho 83415

http://www.ART.INL.gov

Page intentionally left blank

INL ART Program

AGR-5/6/7 Experiment Monitoring and Simulation Progress

INL/EXT-19-55429
Revision 2

July 2021

Author:

CBsignature   7/15/2021
_____   _____
Binh T. Pham   Date

Technical Reviewer: (Confirmation of mathematical accuracy, and correctness of data, and appropriateness of assumptions.)
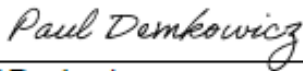
Mitchell Plummer   7/15/2021
_____   _____
Mitchell A. Plummer   Date
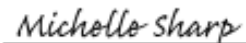
Approved by:

Paul Demkowicz   7/15/2021
_____   _____
Paul Demkowicz   Date
TRISO Fuel Director

Michelle Sharp   7/15/21
_____   _____
Michelle T. Sharp   Date
INL ART Quality Assurance

REVISION LOG

Rev.	Date	Affected Pages	Revision Description
0	09/2019	All	New issue that covered data from the first four cycles, 162B-164B.
1	09/2020	all	Add data from the last five cycles, 165A-168A.
2	07/2021	1, 26	To address an error, in Section 5.1.4, that incorrectly referred to a radionuclide dose rate of 0.1 mrem/yr as a public exposure limit rather than a criterion requiring a change in emission monitoring frequency, according to 40 CFR 61.93(4)(i).

SUMMARY

Advanced Gas Reactor (AGR)-5/6/7 is the last of a series of experiments conducted in the Advanced Test Reactor (ATR) at Idaho National Laboratory (INL) in support of development and qualification of tri-structural isotropic (TRISO) low-enriched fuel for use in high-temperature gas-cooled reactors. The test train contains five separate capsules that are independently controlled and monitored. Each capsule contains multiple 12.51-mm-long compacts filled with low-enriched uranium carbide/oxide (UCO) TRISO fuel particles. The objectives of the AGR-5/6/7 experiment are to:

1. Irradiate reference-design fuel particles to support fuel qualification.

2. Establish operating margins for the fuel beyond normal operating conditions.

3. Provide irradiated-fuel performance data and irradiated-fuel samples for post-irradiation examination (PIE) and safety testing.

The primary objective of the AGR-5/6 test (Capsules 1, 2, 4, and 5) is to verify successful performance of the reference-design fuel under normal-operating conditions. The AGR-7 test (Capsule 3) was designed to explore fuel performance at higher temperatures. Its primary objective is to demonstrate the capability of the fuel to withstand conditions beyond normal operating conditions in support of plant design and licensing. AGR 5/6/7 will also provide irradiated-fuel performance data on fission-gas release from failed particles during irradiation.

To achieve the test objectives, the AGR-5/6/7 experiment is being irradiated in the northeast flux trap of the ATR with a planned duration of 500 effective full-power days (EFPDs). The northeast flux trap was selected because its larger diameter provided greater flexibility for test-train design compared to the Large B positions used for the AGR-1 and AGR-2 irradiations, significantly enhancing test capabilities for the combined irradiation campaigns. Due to delays in the ATR schedule, the AGR-5/6/7 irradiation was significantly shorter than the originally planned 13-cycle schedule. Irradiation began on February 16, 2018 and ended on July 22, 2020, spanning nine ATR cycles over two and a half years. Thus, the AGR-5/6/7 fuel compacts were irradiated for a total of approximately 360.9 EFPDs.

This document presents a summary of the irradiation-monitoring and simulation data for the AGR 5/6/7 experiment. The report covers measured data for Cycles 162B–168A but calculated data only for Cycles 162B–167A because Cycle 168A simulation data were not completed in time to include in this progress report. At the end of 167A, burnup values on a per-compact basis range from 4.65 to 13.23% fissions per initial heavy metal atom, while fast fluence values range from 1.32 to 4.47×10^{25} n/m^2 (E >0.18 MeV). Time-averaged volume-averaged fuel temperatures on a capsule basis ranged from 705°C in Capsule 5 to 1381°C in Capsule 3.

During the first five cycles (162B – 165A), fission-gas isotope release-rate-to-birthrate (R/B) ratios were stable in the 10^{-8}–10^{-6} range, and no in-pile particle failures were observed based on the gross gamma counts. During this time the high exposed kernel fraction and high fuel particle temperatures in Capsule 1 led

to the maximum R/B value of around 2×10^{-6} for Kr-85m. Gas line issues in Capsule 1 occurred from the fourth cycle (164B), and were rigorously mitigated to minimize fission product crosstalk between capsules. This gas line problem prevented fission product release measurement for Capsule 1 during the last three cycles and caused various fission gas leakage events into the other four capsules.

By the end of the sixth cycle, 166A, a significant number of in-pile particle failures occurred in Capsule 1, causing a substantial increase in R/B values. In addition, numerous particle failures were observed in Capsule 3 and perhaps a small number of failures might have occurred in Capsule 2 during the last cycle, 168A. In contrast, no in-pile failures are likely in the top two capsules (4 and 5) based on absence of the typical spike in gross gamma counts and low failure estimates by the end of Cycle 168A using the AGR-3/4 R/B per exposed kernel model. Increased and unstable R/Bs in Capsules 4 and 5 can be contributed to fission gas leakage from Capsule 1.

Page intentionally left blank

ACKNOWLEDGEMENTS

CONTENTS

FIGURES

TABLES

Page intentionally left blank

ACRONYMS

AGR	Advanced Gas Reactor
ART	Advanced Reactor Technologies
ATR	Advanced Test Reactor
DU	dispersed uranium
ECAR	engineering calculation and analysis report
EFPD	effective full-power day
EK	exposed kernel
FG	fission gas
FPMS	Fission Product Monitoring System
GG	gross gamma
HTGR	high-temperature gas-cooled reactor
INL	Idaho National Laboratory
MCNP	Monte Carlo n-Particle (code)
NDMAS	Nuclear Data Management and Analysis System
NEFT	northeast flux trap
PALM	powered axial locator mechanism
PIE	post-irradiation examination
R/B	release-to-birth ratio
TC	thermocouple
TRISO	tri-structural isotropic
UCO	uranium carbide/oxide

AGR-5/6/7 Experiment Monitoring and Simulation Progress

1. INTRODUCTION

AGR-5/6/7 is the last of a series of Advanced Gas Reactor (AGR) experiments sponsored by Advanced Reactor Technologies (ART) and conducted in the Advanced Test Reactor (ATR) at Idaho National Laboratory (INL) in support of development and qualification of tri-structural isotropic (TRISO) low-enriched fuel for use in a high-temperature gas-cooled reactor (HTGR). The configuration and irradiation conditions of the AGR experiments are based on prismatic HTGR technology, a technology involving the use of helium coolant, a low-power-density ceramic core capable of withstanding very high temperatures, and coated-particle fuel (PLN-3636 2020). The objectives of the AGR-5/6/7 experiment (PNL-5245 2018) are to:

1. Irradiate reference-design fuel containing low-enriched uranium carbide/oxide (UCO) TRISO fuel particles to support fuel qualification.

2. Establish operating margins for the fuel beyond normal operating conditions.

3. Provide irradiated fuel performance data and irradiated fuel samples for post-irradiation examination (PIE) and safety testing.

The primary objective of the AGR-5/6 test is to verify successful performance of the reference-design fuel by demonstrating compliance with statistical performance requirements under normal-operating conditions. The AGR-7 test was designed to explore fuel performance at higher fuel temperatures. Its primary objective is to demonstrate the capability of the fuel to withstand conditions beyond normal operating conditions in support of plant design and licensing.

AGR-5/6/7 will also provide irradiated-fuel performance data on the release of fission-gas from failed particles during irradiation. The in-pile gas release, PIE, and safety-testing data on fission-gas and metal release from kernels will be used in the development of improved fuel performance and fission-product transport models.

This document presents irradiation-monitoring and simulation progress of the AGR-5/6/7 experiment. The AGR-5/6/7 fuel test has been irradiated for nine completed cycles, resulting in approximately 360.9 effective full-power days (EFPDs). Due to delays in the ATR schedule, the irradiation campaign did not complete the full 13-cycle schedule or the planned 500 EFPDs. Monitoring data include sweep-gas flow rates, thermocouple (TC)-measured temperatures, and fission-gas release rates. Simulation data include burnup, fast neutron fluence, fission heat rates, fission-gas birthrates (results from neutronics analysis), and temperatures (results from thermal analysis) for fuel compacts and components. Fission-gas release-rate-to-birth-rate (R/B) ratios, calculated from the measured release rates and calculated birthrates for twelve isotopes (Kr-85m, Kr-87, Kr-88, Kr-89, Kr-90, Xe-131m, Xe-133, Xe-135, Xe-135m, Xe-137, Xe-138, and Xe-139) are also included. Performance of the 54 installed TCs and issues with the sweep-gas system are also discussed.

The second revision is to address an error in the description of the federally mandated limits on dose to the public (i.e., the dose limit at Frenchman's Cabin) in Section 5.1.4.

2. ADVANCED GAS REACTOR-5/6/7 IRRADIATION EXPERIMENT DESIGN

To achieve the test objectives outlined above, AGR-5/6/7 was irradiated in the northeast flux trap (NEFT) position of the ATR at INL. A core cross-section indicating this location is displayed in Figure 1. The NEFT provides greater flexibility for test train design compared to the Large B positions used for the AGR-1 and AGR-2 irradiations, significantly enhancing the test capabilities for the combined irradiation campaigns [PLN-5245 (Collin 2018), "AGR-5-6-7 Irradiation Experiment Test Plan"]. Advantages of the NEFT position include that it:

- Efficiently utilizes the ample space afforded by the NEFT to accommodate enough fuel for the needs of qualification and margin tests

- Reduces irradiation time required by taking advantage of the higher flux levels relative to other ATR irradiation locations

- Allows the use of neutron filters to maintain more consistent compact power as the fuel burns out

- Allows power-level control (corner lobes are controlled independently).
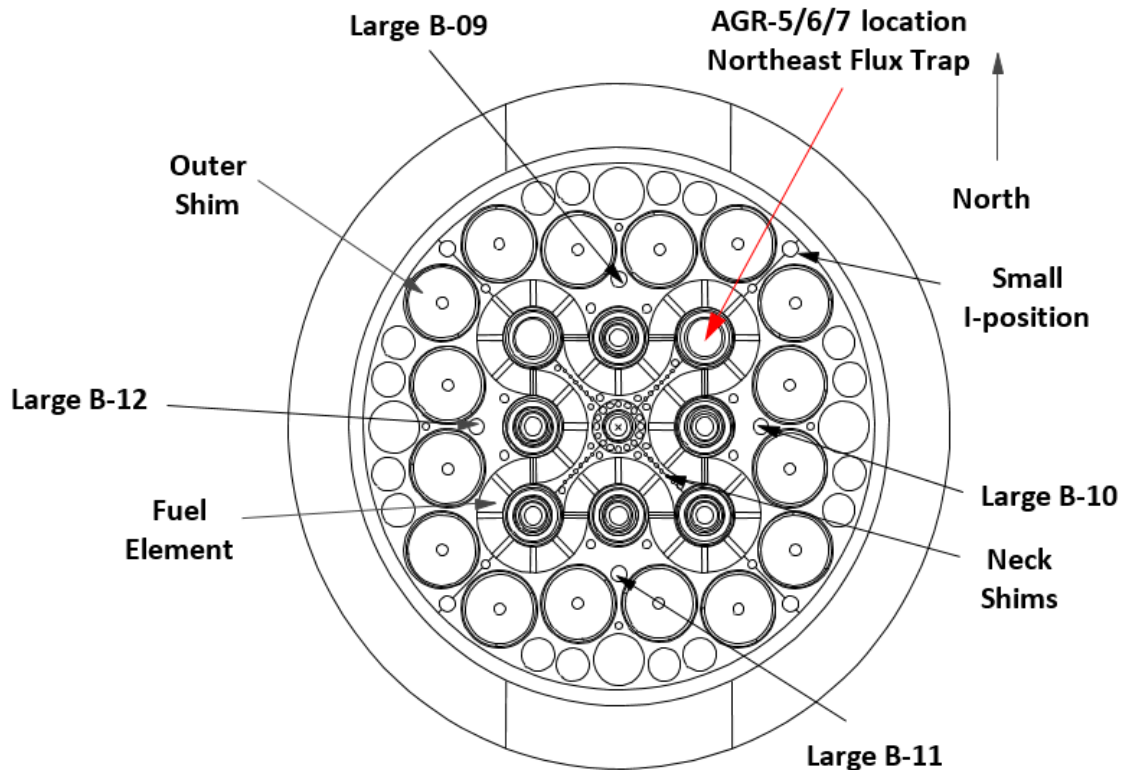
Figure 1. ATR core cross-section displaying the NEFT position.

2.1 Test Train Description

The experimental test train consists of five independently controlled and monitored capsules stacked on top of each other, as shown in Figure 2, which was rotated for ease of display. Capsules 1, 2, 4, and 5 comprise the AGR-5/6 experiment while Capsule 3 is the AGR-7 experiment.
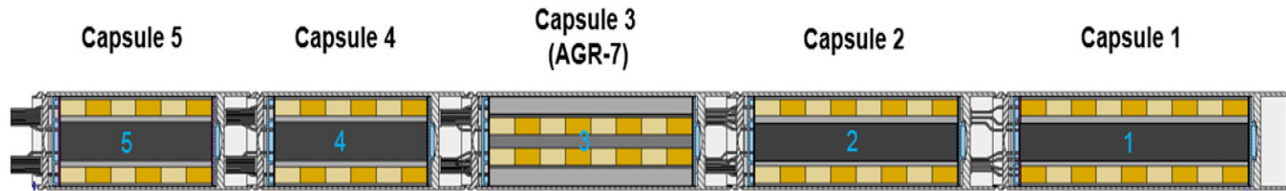
Figure 2. Schematic view of the AGR-5/6/7 test train (Note: Capsule 5 is at the top of the test train).

The five separate capsules use the full 1.2-m active core height in ATR to maximize the amount of irradiated fuel (~515,000 particles in AGR-5/6 and ~55,000 particles in AGR-7) and span the broad range of fuel-burnup and temperature combinations expected in a modular HTGR. To achieve test goals and still be able to control the capsule temperatures, compacts with two different packing fractions of particles were included in the test train. Packing fraction is defined as the total volume of particles divided by the total volume of the compact; Capsules 1 and 5 contain compacts with a 40% nominal packing fraction, and Capsules 2, 3, and 4 contain compacts with a 25% nominal packing fraction. Capsule 1 contains the greatest number of compacts (90). Capsules 3, 4, and 5 each contain 24 compacts; and Capsule 2 contains 32 compacts (Table 1).

Table 1. AGR-5/6/7 capsules (PNL-5245).

Capsule	Numbers of			Average Packing Fraction (%) [a]	Approximate Number of Particles [b]
	Levels	Stacks	Compacts		
5	6	4	24	38.4	3393 [c]
4	6	4	24	24.9	2197 [c]
3	8	3	24	25.5	2265 [c]
2	8	4	32	25.5	2264 [c]
1	9	10	90	38.4	3434 [c]
AGR-5/6			170		515,668
AGR-7	—	—	24	—	54,360
Total			194		570,028

(a) Average packing fraction for each compact lot.
(b) Number of particles obtained by dividing uranium mass content of a compact by uranium mass content of a particle.
(c) Number of particles per compact.

In each AGR-5/6 capsule, the fuel stacks are contained in a graphite holder, separated from the capsule shell by a gas gap (top capsules in Figure 3). AGR-7 Capsule 3 has two gas gaps because fuel stacks are contained in the inner graphite holder, which is separated from the outer graphite holder by an inner gas gap (bottom capsule in Figure 3). These temperature-control gas gaps have axially varying width to compensate for the axial variation in heating. The temperature of the graphite holder is monitored by TCs to ensure the fuel is operating at the target irradiation temperatures. Each capsule contains an individual gas line to provide the helium-neon gas mixture used in the control gas gap to adjust the temperature in the capsule based on TC readings. The capsules are welded together to form the core section of the test train. The plenum regions between capsules have been extended over previous AGR designs to accommodate the bending of larger and stiffer TCs. The core section is welded to a lead-out tube that houses and protects the gas lines and TC leads. The lead-out is routed from the NEFT position straight up from the ATR core to the experiment penetration in the reactor vessel top head. Above the vessel top head, the gas lines and TC leads are connected to their facility counterparts in the temperature-monitoring, control, and data-collection systems.

3

To shape the temporal and spatial fuel power distribution, two techniques are used to adjust the neutron flux incident on the test train: placing a neutron filter around the capsules and raising the northeast lobe power throughout irradiation as the test fuel is depleted. Two different filters (shrouds) were used during irradiation (Figure 4): a standard filter (partial tube of hafnium foil sandwiched between stainless-steel tubes on the left) and a light filter (stainless-steel tube on the right). The hafnium foil is centered axially about the ATR core mid-plane and extends 50.8 cm above and below the core mid-plane for a total axial length of 101.6 cm. The axial extent of the hafnium does not fully cover the top of Capsule 5 or the bottom of Capsule 1 to increase the compact power densities and burnup in these regions. As a result, the compact power densities can remain relatively constant and uniform despite the northeast-lobe power variations incurred during irradiation.
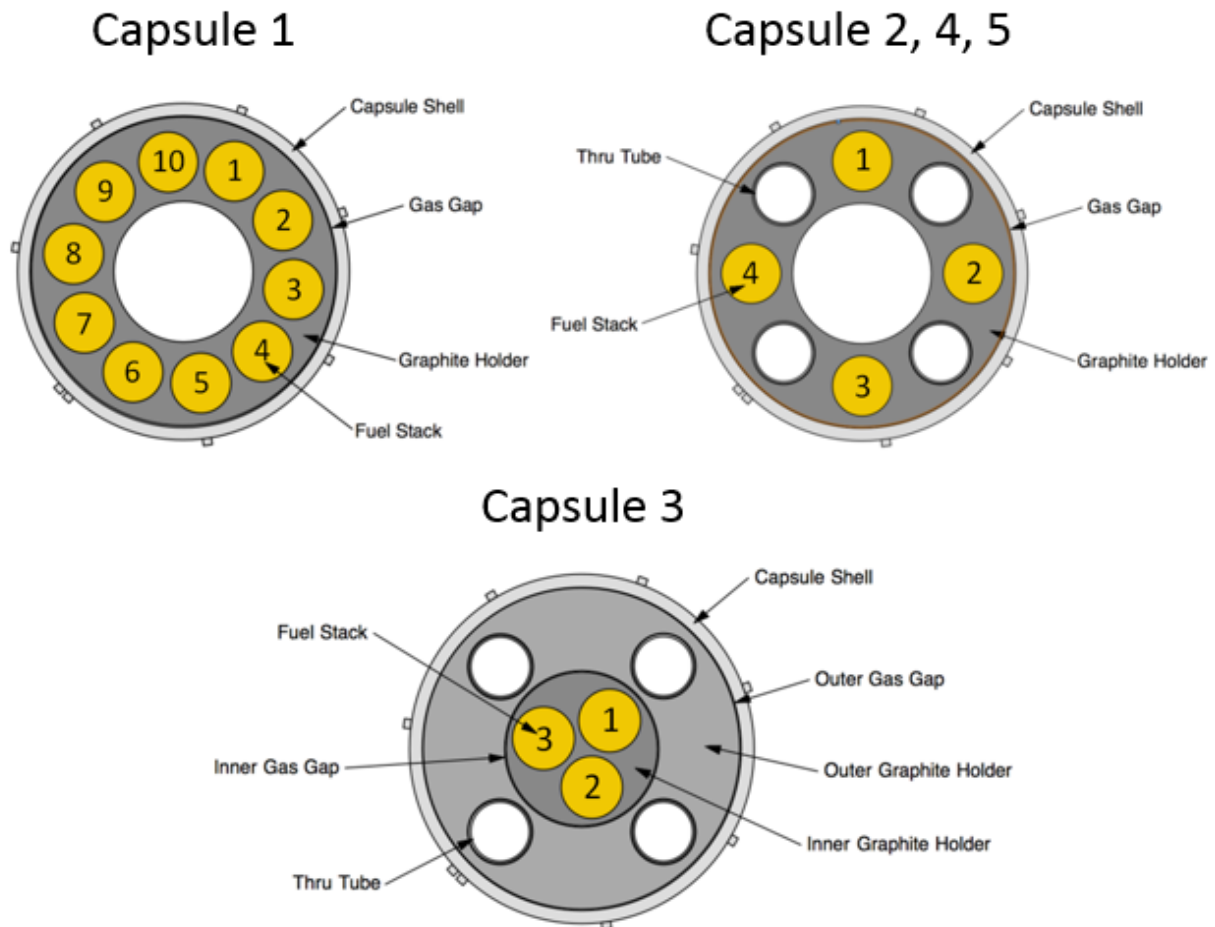
Figure 3. Cross-sections of the AGR 5/6/7 capsules showing the compact stacks (Top: Capsule 1 [left] and Capsules 2, 4, and 5 [right]; Bottom: Capsule 3).
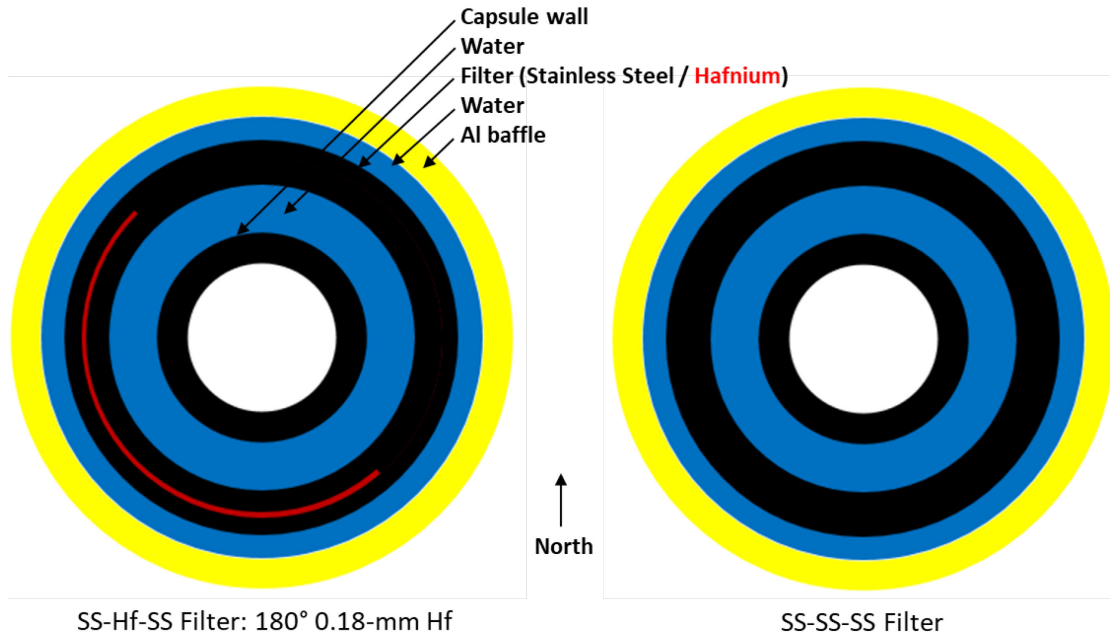
Figure 4. The AGR-5/6/7 neutron filters.

2.2 Instrumentation

2.2.1 Thermocouples

The number of TCs installed in the AGR-5/6/7 capsules was substantially increased, relative to previous experiments, based on the high failure rate among TCs previously experienced. Seventeen TCs were installed in the highest-temperature capsules (i.e., 1 and 3) to maximize the likelihood that at least one TC would survive the entire irradiation campaign. TCs are essential for independent temperature control in the capsules. The four types of TCs used in the capsules are

- Type N (Ni/Cr/Si/Mg wire), with Inconel 600 (Ni/Cr/Fe/Mn alloy) sheath, MgO insulation, and sleeved with Nb (standard baseline).

- Type N, with Cambridge low-drift pure Ni sheath, MgO insulation, and sleeved with Nb in the AGR-5/6 capsules and with ZrO_2 in AGR-7 Capsule 3.

- Type N, with Inconel 600 sheath, Spinel ($MgAl_2O_4$) insulation, and sleeved with Nb.

- High-temperature irradiation resistant (HTIR, Mo/Nb wire), with Nb sheath, Al_2O_3 insulation, and sleeved with Mo.

The selection of these TCs relied on the established performance of commercial TCs, furnace testing in support of the AGR-5/6/7 test, and on feedback from prior AGR experiments. Among commercial TCs, standard base metal TCs (Types K and N) decalibrate (drift) at high temperatures due to metallurgical changes (>600°C for Type K and >1000°C for Type N). Based on commercial data, and AGR-1 experience, Type N TCs (both standard and Spinel insulated) were deemed appropriate and selected for the low-temperature capsules (2, 4, and 5 as shown in Table 2). For the high-temperature capsules (1 and 3), the Cambridge Type N TCs were used in locations expected to experience temperatures between 1000°C and 1200°C, and HTIR TCs were used in locations expected to experience temperatures above 1200°C (Table 2). A summary of TC type and placement within the test train is provided in Table 10 of the AGR-5/6/7 irradiation experiment test plan (PLN-5245).

Table 2. AGR-5/6/7 TCs by capsule.

Capsule	Installed TCs	TC Type (# TCs)	TC Temperature Range (°C)
1 (bottom)	17	Spinel (1) HTIR (9) Cambridge (7)	780–1400
2	8	Type N (8)	740–900
3	17	Spinel (4) HTIR (6) Cambridge (7)	680–1500
4	6	Type N (6)	780–940
5 (top)	6	Type N (6)	700–820

2.2.2 Sweep Gas System

Independent gas lines route a mixture of inert helium and neon gases through each of the five capsules to provide temperature control and to sweep released fission-product gases to the fission-product monitoring system (FPMS). Figure 5 shows a simplified flow path for the AGR-5/6/7 sweep gas from the mass-flow controller to the FPMS. Sweep-gas flow, originating from gas-supply bottles, is routed to the mass-flow controller cabinet, where the helium and neon gases (low-neutron-activation inert gases) are blended for each capsule. The blending of sweep gases is accomplished by a computerized mass-flow controller before the gas enters the test train, based on feedback from the control TC. The sweep gas is then routed to the capsule inlet isolation panel, which can be used to isolate inlet gas flow to each capsule independently during reactor outages or in the event of a failure. Upon exiting the capsule and test train, the gas flows through the outlet isolation panel to another panel containing a particulate filter, moisture detector, and three-way valve. The valve routes the gas either to the designated fission-product monitor or to the standby, backup fission-product monitor. After passing through the FPMS, the gas lines combine into a common exhaust header that routes the gas through a silver-zeolite filter. The exhaust gas is finally routed to the ATR stack.

Helium and neon sweep gases have the following specifications:

- Purities of ≥99.99% by volume for each gas to limit the amount of contamination to the test articles and to limit the background activity

- New gas-bottle verification: thermal conductivity and moisture measurements are performed for both the helium- and neon-gas lines

- Moisture content of <5 ppm H_2O within the sweep gas to reduce possible reactions with the graphite contained in the test capsule

- Gas flow of ≤50 sccm at a pressure of about 7–21 kPa-gauge (or 1–3 psig).

To prevent capsule to capsule gas leakage, a nominal helium or neon flow of 1–5 sccm per capsule at about 6.9 kPa-gauge (or 1 psig) above the capsule pressure will be provided via a mass-flow controller into the lead-out cavity, for a total flow of 5–20 sccm, which then flows into the common plenums between capsules. Through tubes are only present in Capsules 2 – 5, Capsule 1, being the bottom capsule, does not require through tubes.
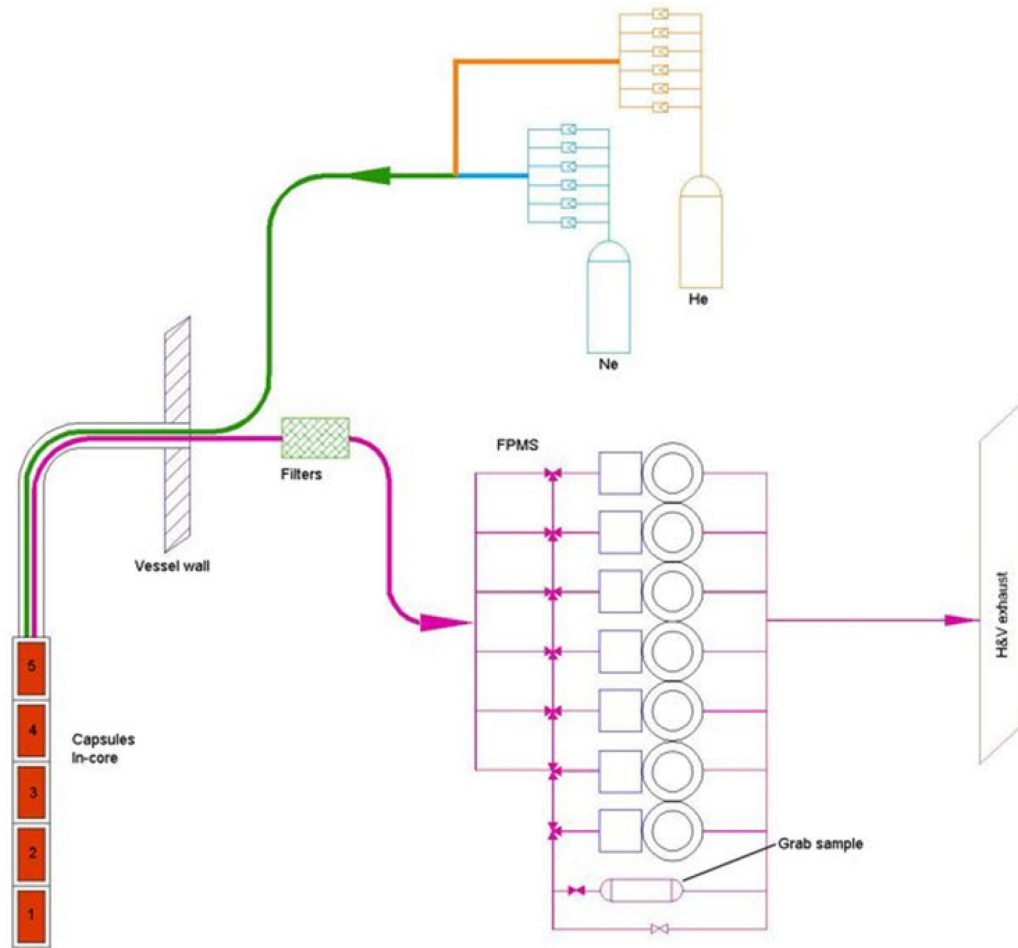
Figure 5. Simplified flow path for AGR-5/6/7 sweep gas.

2.2.3   Fission Product Monitoring System

Each AGR-5/6/7 capsule is continuously monitored for fission gas (FG) release by the FPMS. The FPMS consists of seven sets of gross-radiation monitor and spectrometer detector pairs. One detector set is designated for each of the five capsules, while the two remaining detector sets serve as spares. A detector set is illustrated in Figure 6. Under normal operation, computerized data acquisition, analysis, and storage occur continuously without operator intervention.

Sweep gas carries released fission-product gases from the capsules to the detector system under normal conditions with a transit time expected to be about 150 seconds. The sweep gas passes in front of the gross-radiation monitor, which uses a thallium-doped sodium iodide (NaI[Tl]) detector to detect each fuel-particle failure up to the first 250 failures.

Flow continues to the spectrometer system, which uses a high-purity germanium (HPGe) detector. The spectrometer detector systems measure the concentrations of various krypton and xenon isotopes in the sweep gas from each capsule. During normal operation, 8-hour counting intervals are used to measure the concentrations of Kr-85m, Kr-87, Kr-88, Kr-89, Kr-90, Xe-131m, Xe-133, Xe-135, Xe-135m, Xe-137, Xe-138, and Xe-139. The select nuclides were chosen because they are chemically inert fission-product gases with relatively short half-lives, allowing each isotope to reach equilibrium concentration in the fuel during each reactor cycle. These measured concentrations are converted to per-capsule release rates for each isotope, which are automatically stored and backed up.

During reactor outages, the capsules are swept with pure helium; the remaining effluent is analyzed for FG. Of particular interest are the FG concentrations of Xe-133, Xe-135, and Xe-135m, which are measured and recorded for at least 2 days following each reactor shutdown. These xenon concentrations are used to calculate concentrations of their parent iodine isotopes, which are an indication of fuel performance.
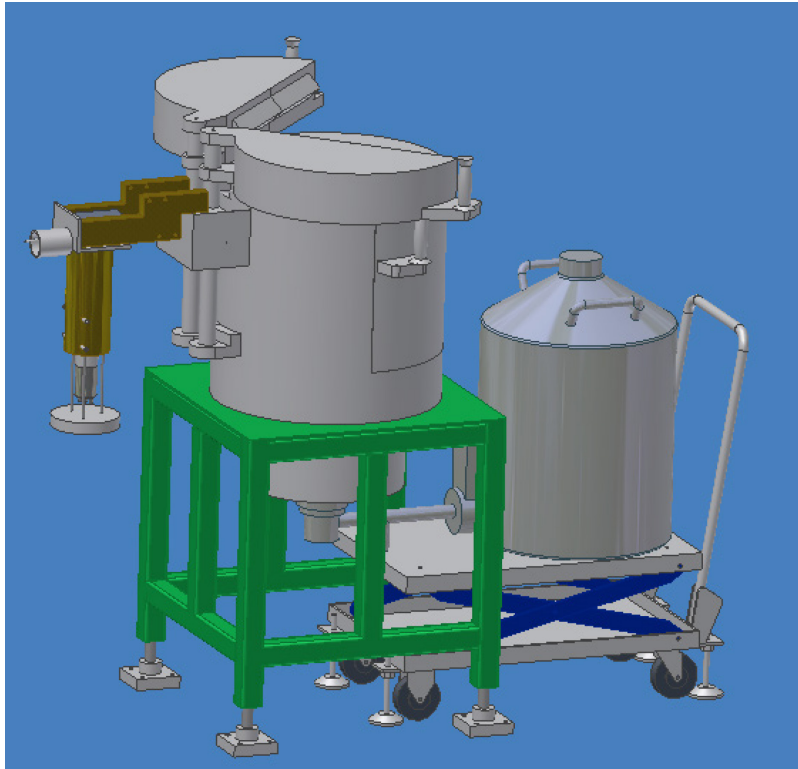
Figure 6. Gross-radiation monitor and spectrometer detector for one AGR-5/6/7 sweep gas line.

3. ANALYTICAL METHODOLOGIES

Most of the physical parameters describing irradiation conditions of the AGR test fuel are calculated using analytical models. This includes fission-power density, fast neutron fluence, and burnup for fuel compacts, calculated from neutronics depletion code; fuel temperature, calculated based on thermal-simulation code; and fission-gas R/B, calculated based on the measured release rate per capsule and calculated birthrate. After completion of each cycle, an as-run neutronics analysis is performed using actual ATR operating parameters. The heating rate and fast fluence from neutronics analysis, combined with neon fraction in the gas flow to each capsule, are used in the thermal model to calculate daily fuel-compact temperatures. During this time, the R/B ratios are also calculated using fission-product-isotope birth rates, calculated by the neutronics code. Detailed model descriptions for the AGR-5/6/7 as-run fission-product release, thermal, and neutronics analyses will be reported in a separate engineering calculation and analysis report (ECARs) for each analysis. The following subsections provide a summary of each of the simulation methodologies that are specific to the AGR-5/6/7 experimental design and irradiation conditions.

3.1 Neutronics Analysis

Neutronics analysis of the AGR-5/6/7 test train was performed using JMOCUP, a coupling code developed at INL that combines the continuous-energy Monte Carlo N-Particle (MCNP) transport code (LANL 2004) and the depletion code ORIGEN (Croff 1983). The JMOCUP depletion methodology was used to model and deplete the AGR-5/6/7 TRISO fuel compacts in the northeast flux trap of ATR, based on a hypothetical 13-cycle irradiation schedule. This AGR-5/6/7 depletion analysis was performed for use in the capsule, test-train, and filter-design iterations and final design activities. A detailed description of the JMOCUP system and verification and validation of the preliminary JMOCUP depletion calculation for AGR-5/6/7 experiment were documented in ECAR-2961 (Sterbentz 2017). The similarity in test-train design between AGR-3/4 and AGR-5/6/7, in conjunction with the similarity in reactivity worth of the two test-train configurations and the low worth of the fuel compacts, allowed the same JMOCUP Monte Carlo depletion methodology and software modules to be used in both the AGR-3/4 neutronics calculation (Sterbentz 2015) and the AGR-5/6/7 neutronics calculation.

The JMOCUP depletion calculation coordinated three depletions: (1) the ATR driver core, (2) the AGR-5/6/7 TRISO compacts, and (3) the AGR-5/6/7 hafnium capsule shroud (i.e., the thermal neutron filter). The ATR driver core consists of 840 depletion cells in the MCNP model, or three radial and seven axial cells per each of the 40 driver elements in the serpentine ATR core. The 194 AGR-5/6/7 fuel compacts were homogenized, and each was split into four axial segments for a total of 776 compact depletion cells. The hafnium shroud had 40 depletion cells, two azimuthal by 20 axial segments. Therefore, there were 1656 depletion cells in the MCNP full-core ATR model. JMOCUP depleted each cell at each time step. The ATR driver-fuel depletion cells each contain nine actinide isotopes and 24 fission-product isotopes, the concentrations of which, along with their fission and radiative-capture cross-sections are tracked and updated at each time step. Similarly, the compacts have 21 tracked actinides and 71 tracked fission products. In the hafnium-shroud cells, the six naturally occurring hafnium isotopes are tracked. The MCNP code calculates cell flux and specified nuclear reaction rates for every isotope in each depletion cell at every time step. Using these data, updated isotopic concentrations and one-group cross sections are fed to the ORIGEN input files along with the cell-average neutron flux for the next ORIGEN depletion calculation.

The neutron transport problem in the JMOCUP method is solved using the KCODE option in the MCNP code. For the KCODE option to be effective, the ATR driver fuel must be simultaneously depleted along with the AGR-5/6/7 experiment depletions. Modeling the depletion of the entire ATR core provides realistic neutron and gamma sources for analyzing the AGR-5/6/7 experiment's radiation environment. The effects of important operational details (such as the positions of the outer shim control cylinders and neck shims) can be considered on a daily average basis using this methodology. The ATR

operating parameters used in the depletion model include the total core power, lobe powers, rotational movement of the outer shim control cylinders, and withdrawal of neck shim rods. The AGR-5/6/7 compacts are solid cylinders composed of TRISO particles and a graphite binder matrix with selected fabrication data presented in PLN-5245 (Collin 2018). The TRISO particle compacts are homogenized in the MCNP full-core models. The specific results of the neutronics analyses include:

- Compact fission heat rates (W/cm^3)

- Compact burnup in percent fissions of initial metal atoms (%FIMA)

- Compact fast neutron fluence (E > 0.18 MeV)

- Neutron/gamma heat rates (W/cm^3) for the AGR-5/6/7 experiment structural components, ATR coolant, and neutron filter

- Compact actinide and fission-product concentrations at end-of-irradiation

- Birth rates of fission-gas isotopes per capsule (atoms/sec)

- End-of-cycle I-135 concentrations (no decay).

Verification that the calculation executed properly was done through both technical checkers and post-processing of calculated data. The as-run JMOCUP depletion calculation for AGR-5/6/7 experiment based on the actual ATR operating conditions will be documented in the form of an ECAR, as was done for the previous experiments. The ECAR can be used as a basis for the qualification of the neutronics data.

3.2 Thermal Analysis

The Abaqus finite-element stress and heat transfer code (Abaqus 2014) was used to perform the daily as-run thermal analysis for the AGR-5/6/7 capsules (Hawkes et al. 2019). These calculations were performed using compact and capsule components' heat-generation rates and fast neutron fluence provided by the neutronics analysis (see Section 3.1) and with additional operational input for daily helium/neon gas-mixture compositions and flow rates. The entire AGR-5/6/7 test train was described by a finite-element mesh formed from approximately 1,200,000 hexahedral finite-element bricks (Figure 7). Each compact was discretized with ~3,500 of such brick elements.

Figure 7. Cut-away view of finite element mesh of entire capsule train.

Fuel-compact thermal conductivity was taken from historical correlations that account for the temperature of heat treatment, irradiation temperature, fast neutron fluence, and the TRISO-particle packing fraction (Gontard and Nabielek 1990). In order to adjust for matrix density differences, the compact matrix thermal conductivity was scaled according to the ratio of the AGR-5/6/7 compact matrix density (1.75 g/cm^3 for Capsules 2–4 and 1.73 g/cm^3 for Capsules 1 and 5) to the compact matrix density used to develop the correlations (1.75 g/cm^3). The result was then combined with particle thermal conductivity obtained from Folsom et al. (2015), following an approach described by Gonzo (2002) to obtain an effective thermal conductivity for the compact at a given TRISO-particle volume-packing fraction.

The AGR-5/6/7 graphite holders are made of IG-430 nuclear-grade graphite. Material properties for unirradiated graphite IG-430 were determined as follows: specific heat values, as function of temperature, were taken from American Society for Testing and Materials (2014); density and expansion coefficients (measured at room temperature, 20°C) were taken from Windes et al. (2017) and Swank et al. (2012); and thermal diffusivities for temperature range 20–1000°C were taken from Windes et al. (2013). Unirradiated thermal conductivity as a function of temperature is calculated as the product of the diffusivity, specific heat, and density. The effect of irradiation on graphite thermal properties was accounted for by incorporating multipliers for thermal expansion and thermal conductivity, expressed as a function of temperature and fast neutron fluence. These multipliers were taken from the Japanese multiplier data (Shibata et al. 2010) and used to adjust density and thermal conductivity of the graphite holders under actual irradiation conditions.

Heat produced mainly in the fuel compacts and graphite holders was transferred through the gas gaps surrounding the compacts and graphite holders via a gap-conductance model using the gap width and the conductivity of the sweep gas. Heat transfer across every gap was considered by both radiation (15–20% of the heat transfer depending on the temperature of the compacts) and conduction (80–85%). Because the thermal capacitance of the sweep gas is very low, advection was not considered in the sweep gas, and it was modeled as stationary. The convective heat transfer from the sweep gas would be <0.01% of the heat transfer across the gap because of the low density, low flow rate, and low thermal capacitance. The thermal conductivity of the sweep gas was determined using a set of correlations from Brown University for mixtures of noble gases (Kestin et al. 1984). All gas gaps were modeled as changing linearly with time in response to the graphite dimensional change with fast neutron fluence. The rate of diameter changes for the graphite IG-430 specimens due to fast neutron fluence was taken from (Windes 2012). The gas gap change in thermal models was accomplished by having the gas-gap conductivity of each capsule change with fast neutron fluence.

Like the previous AGR models, the offset of the graphite holder was also considered in the AGR-5/6/7 thermal models. The graphite-holder offset was possibly caused by wearing down of the nubs—due to vibration in the reactor and a slight bit of clearance between the outside of the nubs and the capsule wall—that held the holder away from the capsule wall. The impact of the holder offset can be seen in Figure 8, where the image on the right shows increased temperature on the southwest side, as the holder is offset in the southwest direction, making a bigger gap on the southwest side. This holder offset helped in reducing residuals (measured minus calculated) for many TC locations throughout the holder(s) in each capsule. The fuel temperatures reported in Section 5.2.2 below were calculated by the thermal models with the same graphite-holder offset for all capsules. The TC residuals could be reduced by as much as 15 °C on average, when the offset is optimized for each individual capsule.

The thermal model provides daily temperature distributions for all components of the AGR-5/6/7 capsules. Figure 9 shows a typical temperature distribution for the entire AGR-5/6/7 test train. As expected, Capsule 3 is the hottest capsule, followed by Capsule 1. Capsule 5 is the coldest of the capsules. Beside temperatures for each finite element of all compacts, the AGR-5/6/7 thermal models also predict temperatures for all TCs. Thus, TC readings during the first cycle (162B) were used for calibration of the AGR-5/6/7 thermal model, adjusting input parameters within their expected ranges to achieve the best match between measured and predicted TCs. Figure 10 shows a history plot of the TC residual temperatures (measure minus calculated) for all full power days for all cycles. A modest match between calculated and measured TCs during the first cycle was achieved. The continuing good match between measured and calculated TCs for Cycles 163A–168A indicates that thermal models simulate the thermal conditions well. Capsule 5 shows excellent agreement between the measured and calculated TC temperatures and Capsule 4 shows good agreement with largely negative TC residuals indicating slightly overpredicting capsule temperature. Capsule 2 TC residuals varied within a wider range [between -60°C and 60°C] and Capsule 1 has even larger variation in predictions compared to actual TCs due to the highest number of TCs located throughout this capsule. However, the TC residuals in Capsule 1 and 2 lie

on both sides of the horizontal line at zero, indicating the current thermal model provides a reasonable fit to data. Capsule 3 had a good agreement during the first four cycles, but TC residuals were much larger during the last three cycles, which might indicate an unexpected change in the Capsule 3 gas gap that impacted temperature at TC locations, but was not captured by the thermal model. The TC residual plots over time ended when TCs failed.

As with the as-run neutronics analysis, verification that the calculation executed properly was done through both technical checkers and post-processing of calculated data.
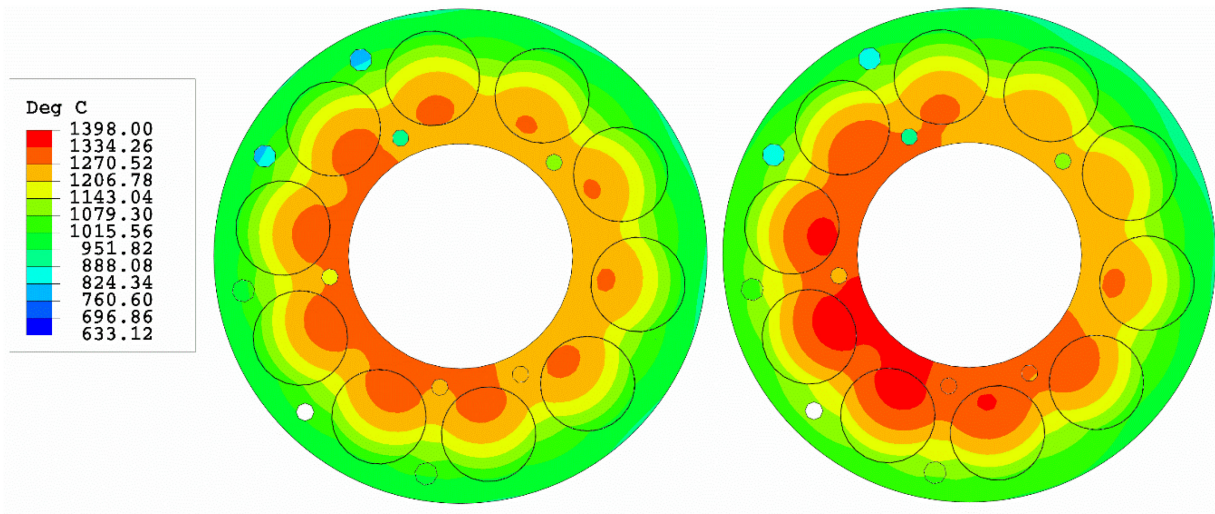
Figure 8. Straight on top-down view temperature contours of the Capsule 1 graphite holder and fuel compacts at axial mid-plane. Left is capsule centered; right is capsule offset 0.0254 mm in southwest direction.
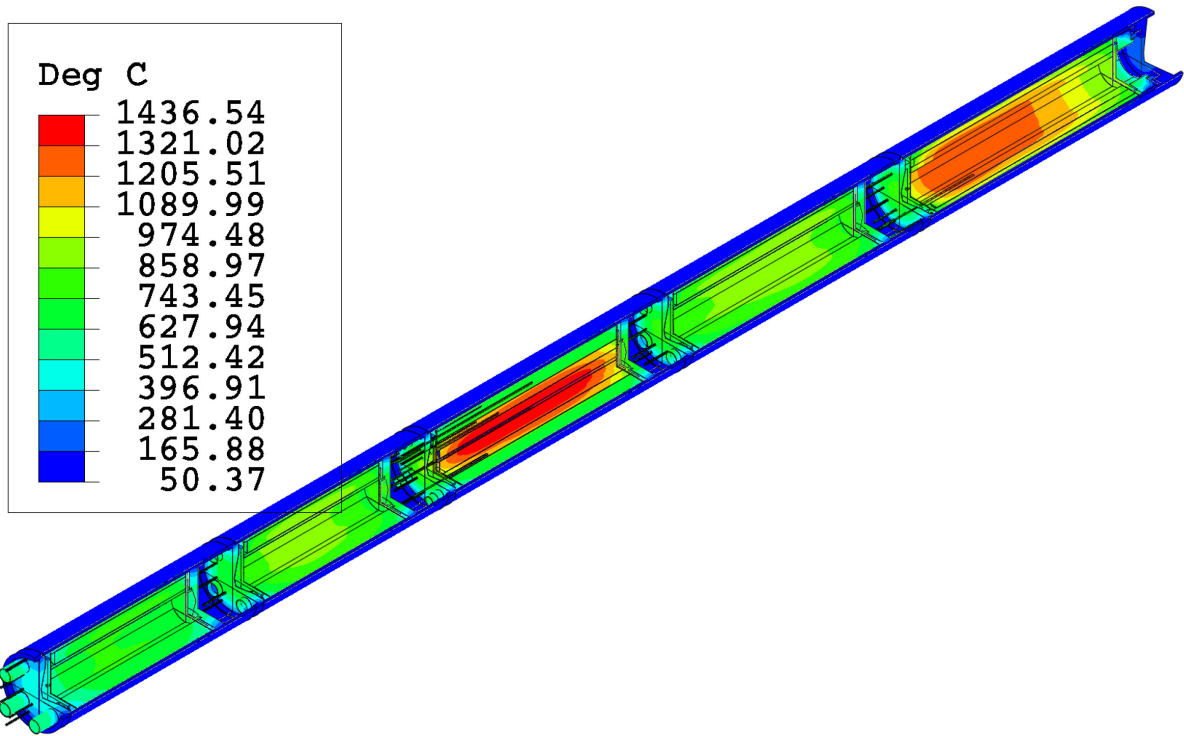
Figure 9. Cut-away view of temperature distribution of entire capsule train.
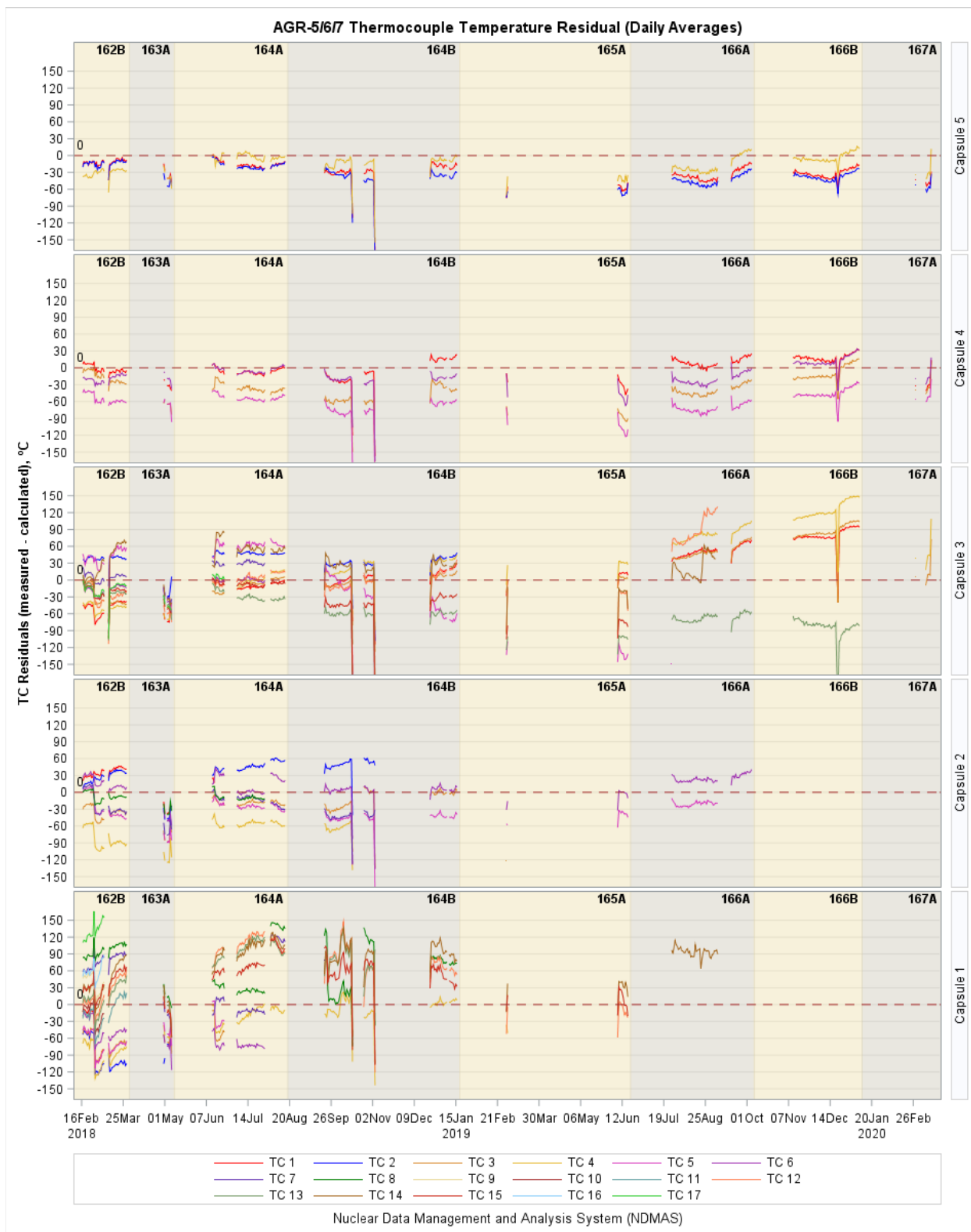
Figure 10. Difference between measured and calculated temperature for TCs in AGR-5/6/7 capsules.

3.3 Release Rate Calculation

The radionuclides of interest decay in transit from the capsule to the counters. The actual transport time for each capsule is calculated from outlet-gas flow rates and the capsule-specific volumes through which samples flow to reach the respective monitoring detector. Given a certain measured activity, A (μCi), the radionuclide release rate, R (atoms/s), of a particular nuclide can be calculated as (Scates 2010):

$$R = 3.7 \times 10^4 \frac{Ae^{\lambda V_T/f}}{(1 - e^{-\lambda V_S/f})}$$

where V_S is the sample volume (mL), λ is the nuclide-decay constant (s^{-1}), f is the capsule volumetric flow rate (mL/s), and V_T is the transport volume from the capsule to the sample volume (mL). The transport volumes were determined during a lead-out flow test performed at the beginning of the AGR-5/6/7 irradiation. This conversion formula was derived under the assumption that equilibrium release conditions were established (Scates 2010).

There are several factors that could make it difficult to assess the actual radionuclide release rate from fuel compacts in AGR-5/6/7 capsules from the measured activities at detectors: (1) wide range of outlet flow rates over the entire irradiation span, (2) capsule pressure variation over time, and (3) three different designs for the five capsules (Figure 3). For the previous experiments (AGR-1, -2, and -3/4), gas flow rates were kept at the same level of 30 sccm for all capsules and capsule designs were similar for each experiment, so the equilibrium release conditions were similar for all capsules and transport times were well defined. On the contrary, outlet gas flow rates for all AGR-5/6/7 capsules are not stable over time: Capsule 1 outlet flow rates varied the most from ~2 sccm to 58 sccm (excluding zero flow during gas line isolation) and outlet flow rates for Capsules 2-5 varied within a smaller range between 40 and 70 sccm. These gas flow regime variations from capsule to capsule and over time complicated the conversion from FG activities measured at detectors to release rate at the capsule exits due to high uncertainty in transport time estimations. Differences in capsule design can also affect the time that FG isotopes spend inside each capsule, resulting in different FG ratios existing each capsule. In addition, the pressure variations for the five capsules and leadout contribute to the uncertainty between the corrected release rate and actual release rate from compacts.

The performance of a nuclear fuel test is typically evaluated using the R/B ratio, which is the ratio of the released activity of an isotope from the fuel to the predicted creation rate of the isotope during irradiation. Daily fission-product birth rates for the following isotopes were provided by as-run neutronics calculations: Kr-85m, Kr-87, Kr-88, Kr-89, Kr-90, Xe-131m, Xe-133, Xe-135, Xe-135m, Xe-137, Xe-138, and Xe-139. Release rates obtained from the FPMS and calculated birthrates were used to calculate the capsule R/B ratios for the radionuclides of interest.

4. DATA MANAGEMENT

Preservation and management of the AGR experimental data are critical contributions to the experiment's ability to meet its objectives. INL's ART program established the Nuclear Data Management and Analysis System (NDMAS) to ensure that INL ART data are qualified for use and stored in a readily accessible electronic form that can be analyzed to extract useful results. The system is described in the Nuclear Data Management and Analysis System Plan (Lybeck 2016).

During the entire course of the irradiation period, three streams of data are continually generated:

- Fuel-irradiation data, which include thermocouple readings, sweep-gas flow rates, pressure, and moisture-monitor readings

- FPMS data, which include gross gamma (GG) counts

- ATR operating-condition data, which include lobe powers, outer-shim control-cylinder positions, neck-shim positions, and control-rod positions.

AGR-5/6/7 data also comprise the following calculated quantities resulting from release-rate calculations, neutronics modeling, and thermal modeling performed after the end of each ATR cycle:

- Fission-product release-rate data, which include release rates and R/B ratios per capsule for twelve krypton and xenon isotopes: Kr-85m, Kr-87, Kr-88, Kr-89, Kr-90, Xe-131m, Xe-133, Xe-135, Xe-135m, Xe-137, Xe-138, and Xe-139

- Neutronics data, which include fission-power density, fast neutron fluence, burnup for fuel compacts, fission/gamma power density for non-fuel components, and fast neutron fluence for graphite holders

- Thermal data, which include temperatures for fuel compacts and TC locations.

NDMAS provides a single controlled repository for all AGR-5/6/7 data and makes the data available to users on an easily accessible website. During the experiment, the website shows progress of irradiation in almost real time after the data are generated. The data processing is scheduled to run hourly to add new data to the monitoring displays, allowing researchers to quickly identify and correct any issues. The Highcharts JavaScript library is used to generate compact interactive plots that are useful for monitoring as-run experimental conditions. Many of the plots in this document are examples of the displays available on the website.

As was done for the previous AGR experiments, detailed model descriptions for the as-run fission-product release analysis, thermal analysis, and neutronics analysis will be reported in separate ECARs for each analysis and each experiment. These ECARs serve as the basis for determining qualification status of the calculated results which have been captured and stored in the NDMAS database. Because the corresponding ECARs for AGR-5/6/7 analyses have not yet been issued, all calculated results (R/B ratios, temperatures, and neutronics data) presented in this report are considered preliminary.

5. MONITORING AND CALCULATED RESULTS

The AGR-5/6/7 experiment started on February 16, 2018 (ATR Cycle 162B), and ended on July 22, 2020 (ATR Cycle 168A), which result in nine cycles spanning over two-and-half years. This brought the total irradiation duration to approximately 360.9 EFPDs (instead of the planned 500 EFPDs). Instrumentation data are available for all cycles, but calculated results are available for only eight cycles (up to Cycle 167A). The measured and calculated data are displayed on the 'AGR-5/6/7 Irradiation' webpage for online test-condition monitoring by experiment staff members.

5.1 Monitoring Data

Measurements from instruments in ATR and the AGR-5/6/7 test train are essential for control of the specified experimental irradiations and provide necessary data inputs to simulation codes. The ATR- and capsule-measured data are transferred to the NDMAS and automatically processed every hour during the entire irradiation period. A summary of instrumental data is documented in this section.

5.1.1 Advanced Test Reactor Power History

Among the nine ATR cycles during AGR-5/6/7 irradiation: six are regular cycles (i.e., 162B, 164A, 164B, 166A, 166B, and 168A); one is a short high-power powered axial locator mechanism [PALM] cycles (i.e., 165A); and two are intermittent (mostly low-power and about one day high power) short PALM cycles (i.e., 163A and 167A). The overview summary of these cycles presented in Table 3 includes cycle type, time period, number of EFPDs, and northeast lobe power.

Table 3. ATR cycles during the AGR-5/6/7 irradiation.

Cycle #	Cycle Name	Cycle Type	Begin Power Date	End Power Date	Cycle Power Length (days) [a]	Cycle Power Length (EFPD)	Northeast Lobe Power (MW)
1	162B	Regular	2/16/2018	3/29/2018	41	38.5 [b]	14 and 15
2	163A	PALM	4/29/2018	5/8/2018	9	3.0 [c]	5 and 20
3	164A	Regular	6/10/2018	8/17/2018	68	54.9	16
4	164B	Regular	9/18/2018	1/17/2019	121	64.1 [d]	17 and 16
5	165A	PALM	2/28/2019	6/18/2019	111	13.4	19
6	166A	Regular	7/24/2019	10/6/2019	73	62.5	17
7	166B	Regular	11/9/2019	1/10/2020	62	61.2	17
8	167A	PALM	2/27/2020	3/14/2020	16	2.3 [c]	5 and 20
9	168A	Regular	4/13/2020	7/22/2020	99	61.0	20
Total						360.9	
(a) Number of days between the begin-power and end-power for a cycle.							
(b) The 162B cycle ran 14 days at 14 MW and 25 days at 15 MW.							
(c) The 163A and 167A PALM cycles ran most days at 5 MW and about a day at 20 MW.							
(d) The 164B cycle ran 27 days at 17 MW and 37 days at 16 MW.							

ATR data that describe the core neutronics and thermal-hydraulic environment are used to inform the physics and thermal analyses, as well as support temperature control. ATR data used as input for the physics analyses include total core power, individual lobe powers, shim cylinder (hafnium absorber) positions, neck shim positions, and regulatory rod positions. NDMAS receives the ATR operating data at 5-minute increments (summarized in Figure 11 for selected parameters).
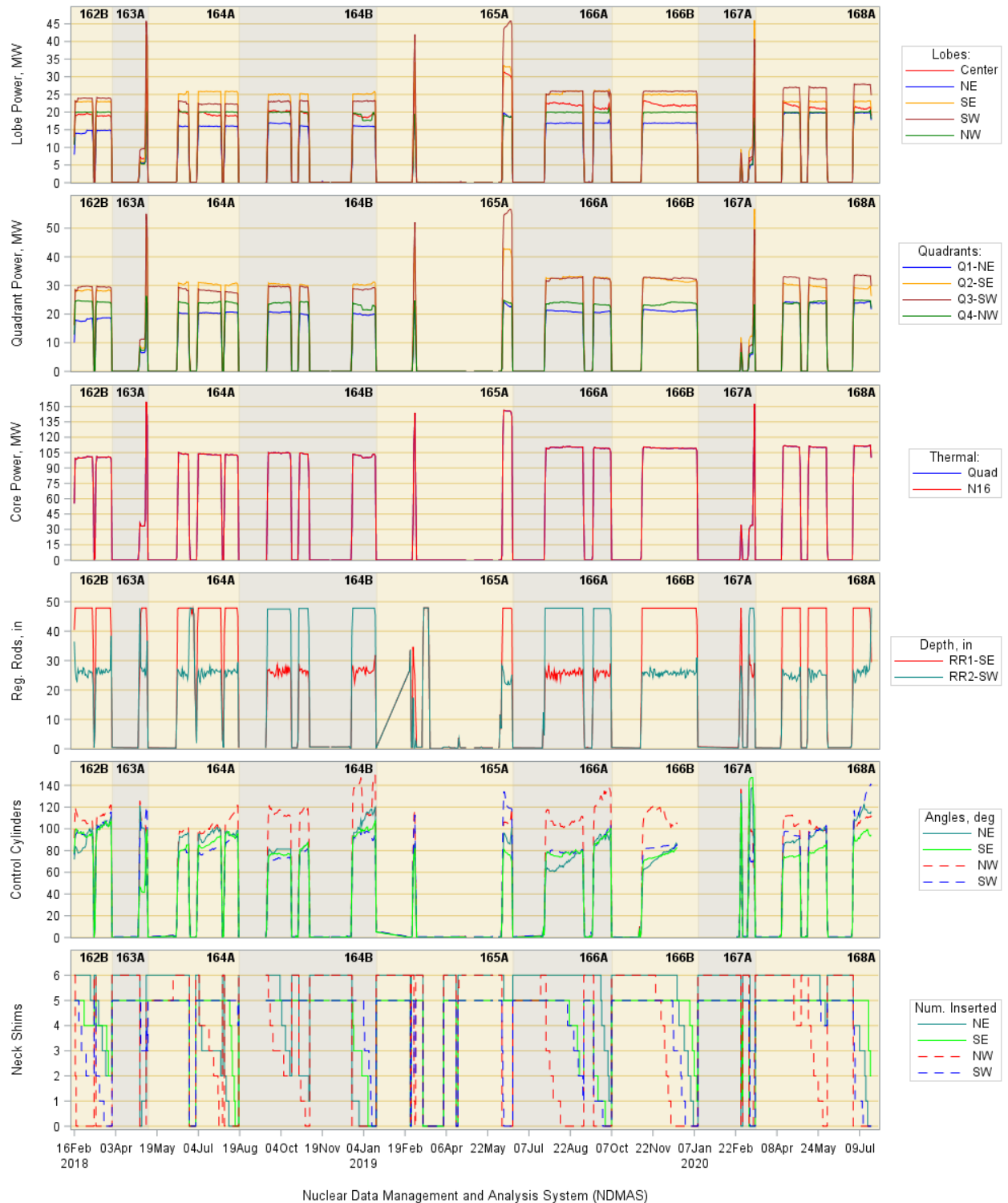
Figure 11. ATR daily operating parameters during AGR-5/6/7 irradiation.

5.1.2 Thermocouple Performance and Data

By the end of Cycle 168A, 48 out of 54 TCs installed in the five AGR-5/6/7 capsules had failed (see Table 4). Among them, 10 TCs in the three upper capsules (3, 4, and 5) were broken before irradiation,

during handling and assembly of the test train. The other 38 TCs failed throughout the irradiation campaign. Most TC failures occurred at scrams, when temperatures dropped rapidly to room temperature after ATR power dropped from full to zero within approximately 5 minutes. Powering up also causes TC failures, but to a lesser extent because powering up is usually much more gradual than powering down. Failures were identified when TC readings stopped or became stuck at the same level when neighboring TC readings were changing. TC failures by capsule are

- Capsule 1: all 17 installed TCs failed, which led to no operational TCs left in this capsule after Cycle 166A (Cycle 6). This is consistent with TC failures in previous AGR experiments because wires of TCs in the bottom capsule had to pass through all other capsules including the high temperature Capsule 3. Multiple TC failures occurred during the first cycle, 162B. Interestingly, the longest surviving TC was exposed to the highest temperature range in this capsule, up to 1400°C.

- Capsule 2: all eight installed TCs failed by the end of Cycle 166B. These Type N TCs were exposed to lower temperatures (up to 900°C) and started to fail from the third cycle, 164A. Capsule 2 TC wires also had to pass through the highest temperature capsule (Capsule 3).

- Capsule 3: five of the 17 TCs were broken during assembly and twelve TCs failed during irradiation, no operational TC remained in this capsule after Cycle 167A. Capsule 3 TC-12 was exposed to temperature as high as 1550°C but still survived for almost six cycles.

- Capsules 4 and 5: only one TC failed in Capsule 4, and this failure occurred during the last cycle of irradiation. This could be because wires of TCs in these capsules do not have to pass through the hottest capsule (Capsule 3). Other TC failures (two in Capsule 4 and three in Capsule 5) occurred before irradiation, during handling and assembly.

Figure 12 shows the readings of all functioning TCs as a function of EFPDs; the plots are discontinued at the time of TC failures. Plots for all TCs are mostly parallel to each other, which indicates similar behavior among the TCs. An exception is TC-5, located in the center of Capsule 3, with gradually decreasing readings during Cycle 164B until its failure on July 26, 2019 (Cycle 166A).

The temperature difference between TCs in the same capsule should generally remain constant over time. Any other trend or discontinuity in the data could suggest that one of the TCs is drifting. Thus, control charts for a pair of the primary- and secondary-control TCs are used for monitoring consistency of the control TCs. Measured TC residuals are also compared with the calculated values from capsule thermal models to demonstrate that the control TCs are behaving as physically expected. Accordingly, no clear TC drift failures among the control TC pairs in the five AGR-5/6/7 capsules have been observed.

Table 4. TC failures in AGR-5/6/7 capsules by the end of ATR Cycle 165A (48 failed out of 54).

Capsule	N$^{\#}$ of Installed: Operational / Failed TCs	Failed TCs	TC Type	Failure Date	ATR Cycle	Associated Event
1	17: 0 / 17	1 9, 10, 16, 17	Cambridge HTIR	3/9/2018	162B	Scram
		11	HTIR	3/29/2018	162B	Scram
		2	Spinel	5/7/2018	163A	High power
		3, 5	Cambridge	6/24/2018	164A	Scram
		6	Cambridge	7/30/2018	164A	Scram

		7	Cambridge	9/20/2018	164B	Ramp up
		13	HTIR	11/5/2018	164B	Scram
		8	Cambridge	1/17/2019	164B	Scram
		4	Cambridge	6/8/2019	165A	Restart
		12	HTIR	6/18/2019	165A	Scram
		15	HTIR	7/25/2019	166A	Ramp up
		14	HTIR	9/07/2019	166A	Scram
2	8: 0 / 8	1	Type N	6/14/2018	164A	Ramp up
		8	Type N	7/30/2018	164A	Scram
		4	Type N	10/24/2018	164B	Ramp up
		2, 7	Type N	11/5/2018	164B	Scram
		3	Type N	3/1/2019	165A	Scram
		5	Type N	9/07/2019	166B	Scram
		6	Type N	10/07/2019	166B	Power-down
3	17: 0 / 17	8 9, 10, 11, 16	Cambridge HTIR	Assembly		Assembly
		17	Cambridge	6/24/2018	164A	Scram
		6, 7	Cambridge	8/2/2018	164A	Restart
		2	Spinel	1/17/2019	164B	Scram
		15	Cambridge	7/25/2019	166A	Ramp up
		5	HTIR	7/26/2019	166A	Ramp up
		12, 14	HTIR	9/07/2019	166A	Scram
		1, 13	Spinel, Cambridge	1/10/2020	166B	Power-down
		3, 4	Spinel	3/14/2020	167A	Power-down
4	6: 3 / 3	2, 4	Type N	Assembly		Assembly
		3	Type N	5/13/2020	168A	Ramp up
5	6: 3 / 3	3, 5, 6	Type N	Assembly		Assembly
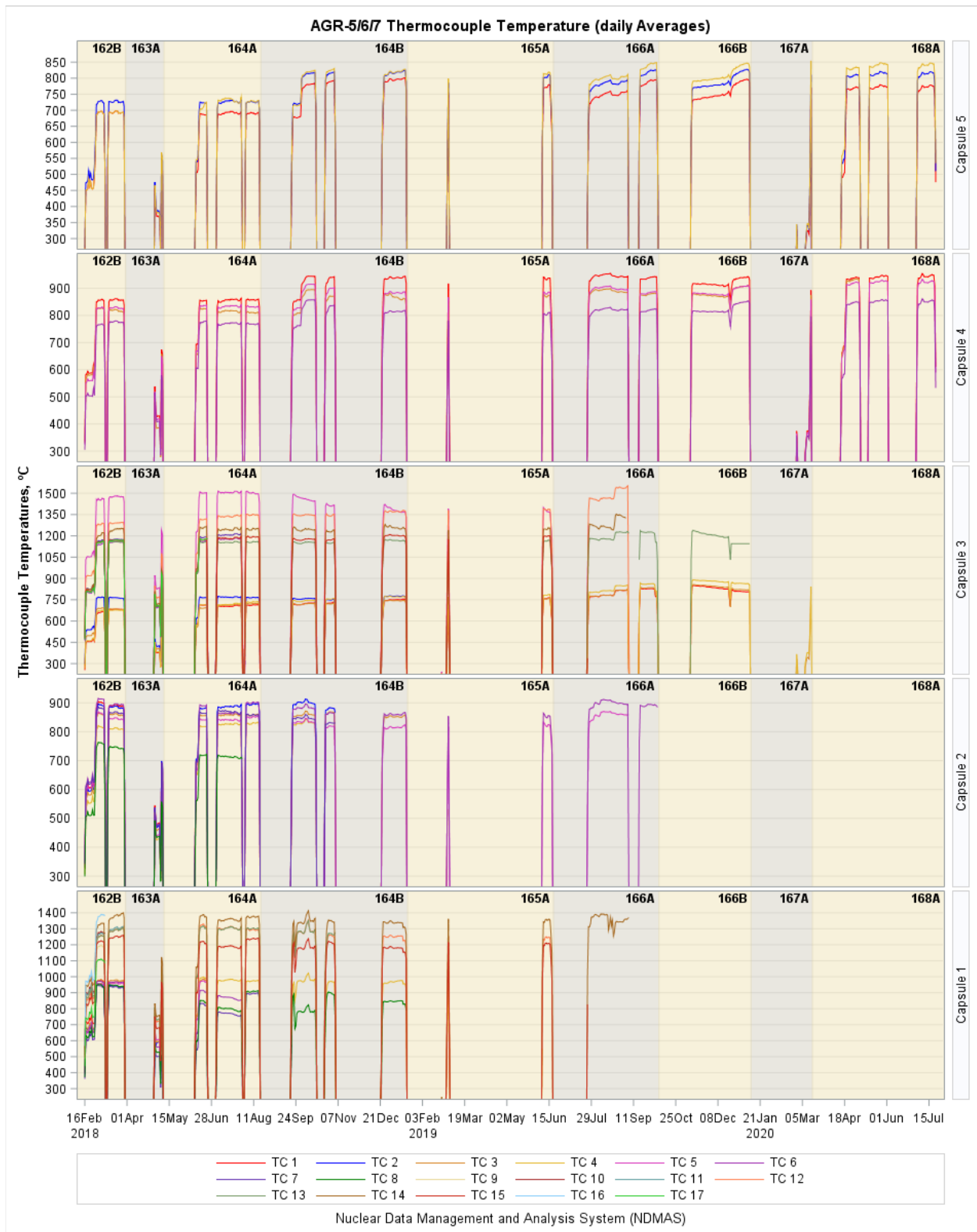
Figure 12. Measured TC temperatures.

5.1.3   Sweep Gas Flows

Several sweep-gas parameters are required for thermal analysis and temperature control. These include pressure, mass-flow rates for each constituent gas, and moisture content. Moisture-content measurements (measured on the outlet side of the capsule and compared to the gas-supply verification measurement) provide indicators of capsule integrity. The mass-flow rates for each constituent gas, measured at the inlet line for each capsule and the lead-out, are referred to as inlet flow rates; the total mass-flow rates, measured at each capsule outlet line, are referred to as outlet flow rates. An additional mass-flow rate is measured at the FPMS. Actual gas-flow rates for the five capsules and lead-out are presented in Figure 13 and Figure 14, respectively. Sweep-gas constituent mass-flow rates (which determine gas-mixture ratios) are used in thermal analyses of the test train.

By design, a nominal helium/neon mixture flow at higher pressure than the capsule pressure was provided via a mass-flow controller into the lead-out cavity, which then flowed into the common plenums between capsules. The intent of this design was to prevent capsule-to-capsule cross gas leakage ensuring FG signatures remain separated by capsule. However, about half-way through irradiation a clog and then a crack formed in the Capsule 1 outlet line (Figure 15) that prevented its FGs from sweeping out to the detector as intended. Instead, some of the Capsule 1 FGs diffused out and contaminated gas in the leadout, and then entered other capsules. To mitigate this issue, the leadout pressure was reduced lower than capsule pressures and the leadout outlet isolation valve was opened allowing the leadout contaminated gas to flow to spare Detector 6. This arrangement allowed some gas flow from the Capsules 2-5 to the leadout, limiting FG leakage into Capsules 2-5 from the leadout. Consequently, capsule inlet flows are higher than outlet flows (red lines are higher than blue lines in Figure 13 for Capsules 2-5 from Cycle 166B); and the leadout outlet and FPM flow rates are not zero as before Cycle 166B as shown by the blue and cyan lines in Figure 14.

The capsule gas line event summary is:

- Shortly after powerup of Cycle 164B (on September 23, 2018), a clog formed somewhere in the Capsule 1 outlet line leading to gas pressure in Capsule 1 increasing beyond its normal level. For part of Cycle 164B, Capsule 1 was operated in a batch mode, where the capsule was isolated and updated gas blends were sent periodically. Eventually, it was determined that at low flow rates, the obstruction growth was halted. For the last half of Cycle 164B, the Capsule 1 flow rate was set at 11 sccm, and no pressure increase was observed.

- During restart of the PALM Cycle 165A (on June 8, 2019), a crack or break in the Capsule 1 gas line occurred somewhere downstream of the clog location, as indicated by a substantial outlet flow increase in Capsule 1 and decrease in the outlet flows of the other four capsules (see the blue line in Figure 13). This is because most of the gas flow from the lead-out flowed into the Capsule 1 outlet line instead of entering other capsules, as designed. This situation was addressed promptly to ensure effective temperature control and accurate fission-gas release measurement for Capsules 2-5.

- With a large amount of dilution gas entering the Capsule 1 exhaust line from the leadout through the crack, it was difficult to interpret the FP measurements from Capsule 1. Therefore, a decision was made to swap the inlet and outlet lines for capsule 1 at the top of the test. This would ensure that only Capsule 1 FGs can reach its detector and at a known flow rate.

- After the lines were swapped, Capsule 1 performed as expected for only a period of time. Then, evidence of a second series of plugs and cracks was observed. Ultimately Capsule 1 became totally plugged, or nearly so.

The detail log of the gas flow operating history in response to gas line issues in Capsule 1 is presented in Appendix A. Gas flow events in the AGR-5/6/7 capsules after gas line problems in Capsule 1 are summarized in Table *5* for easy reference. These gas flow regimes are important in neon fraction

calculation for all capsules, especially for Capsule 1. They also play a key role in interpretation of the FG releases and GG counts data from Capsules discussed in following sections.

Table 5. Summary of gas flow in AGR-5/6/7 capsules after problem in Capsule 1 gas line.

ATR Cycle	Capsule Gas Flow History
164B	A clog developed in the Capsule 1 outlet line, leading the program to periodically shut off the gas flow through this capsule from September 23 to October 16, 2018
	From October 16, 2018, gas flow in Capsule 1 was successfully re-established at 11 sccm.
165A (PALM)	A crack or break in the outlet line at a point downstream of the clog caused a sudden increase in the Capsule 1 outlet flow.
	Gas flows to the other capsules were increased and the lead-out flow was increased to 50 sccm (and then 60 sccm) to ensure lead-out flow was entering Capsules 2–5
166A	During outage, the inlet- and outlet-gas lines for Capsule 1 were swapped to prevent FG leakage to other capsules.
	At this point, Capsule 1 inlet line had a crack, so the neon/helium mixture for the lead-out and Capsule 1 was kept the same, allowing the Capsule 1 neon fraction to be accurately defined.
	August 1-16, 2019: the clog appeared to be clearing, as indicated by an increase in outlet flow. The crack was also closing because more flow was being forced through Capsule 1.
	From August 16, 2019: a new clog developed in the new Capsule 1 outlet gas line causing an increase in pressure; intermittent flow was implemented to avoid exceeding pressure limits.
166B	Flow to Capsule 1 was isolated during the entire power cycle
	November 9 to December 21, 2019: flows to Capsules 2-5 were also suspended.
	Beyond December 21, 2019: flows to Capsules 2-5 were resumed and the leadout outlet line was opened with lower pressure, so some gas from capsules can now flow out to the leadout.
167A (PALM)	Flow to Capsule 1 was isolated and the leadout outlet line was opened with lower pressure than all capsules.
168A	Flow to Capsule 1 was mostly isolated with several unsuccessful attempts to flow small amount of gas for FG release measurement; the leadout outlet line was opened with lower pressure than pressure in Capsules 2-5.
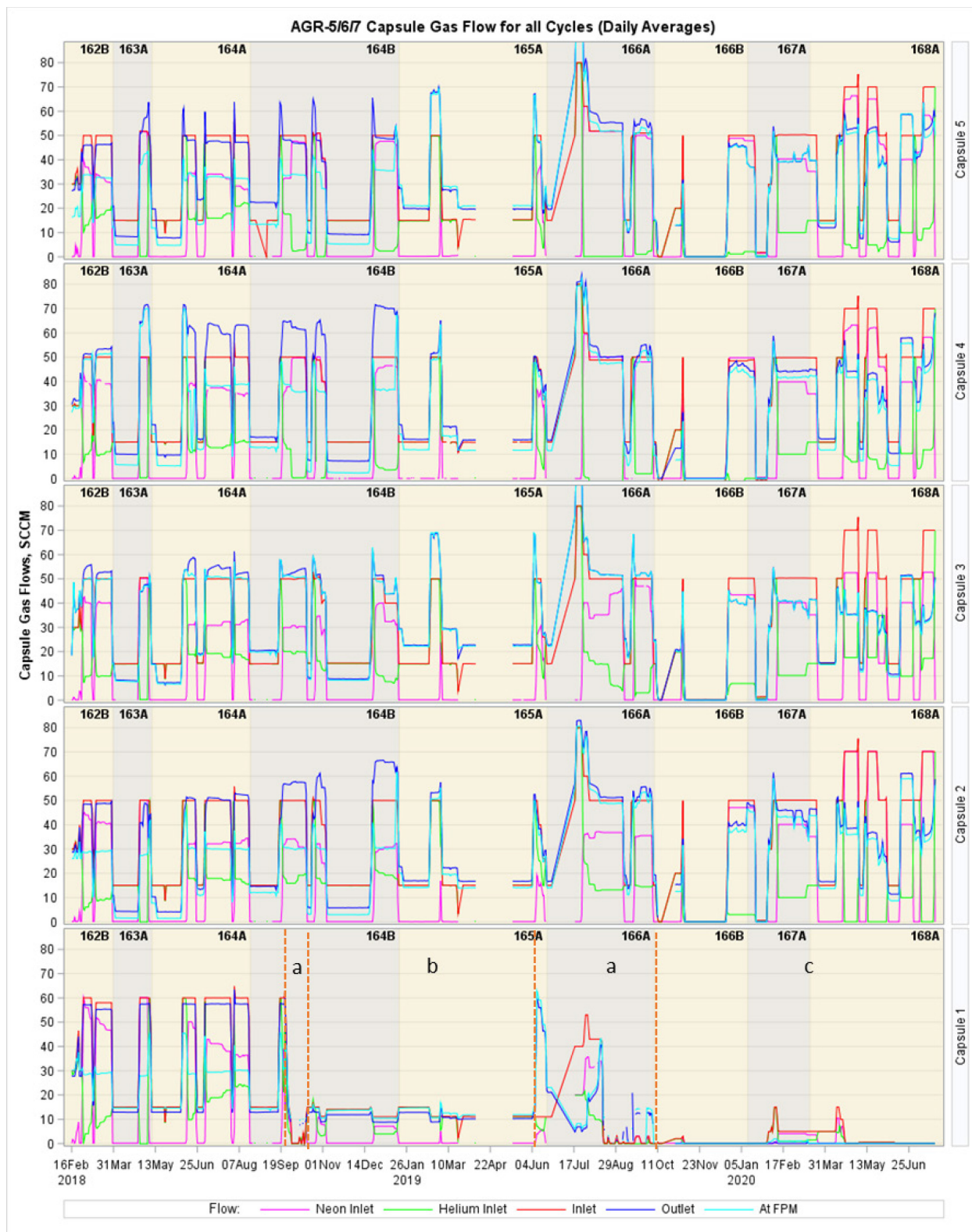
Figure 13. Capsule sweep-gas flow rates with Capsule 1 flow history: a – intermittent flow, b – stabilized low flow rate, and c – mostly isolated gas line with an unsuccessful attempt to reestablish flow during Cycles 167A and 168A.
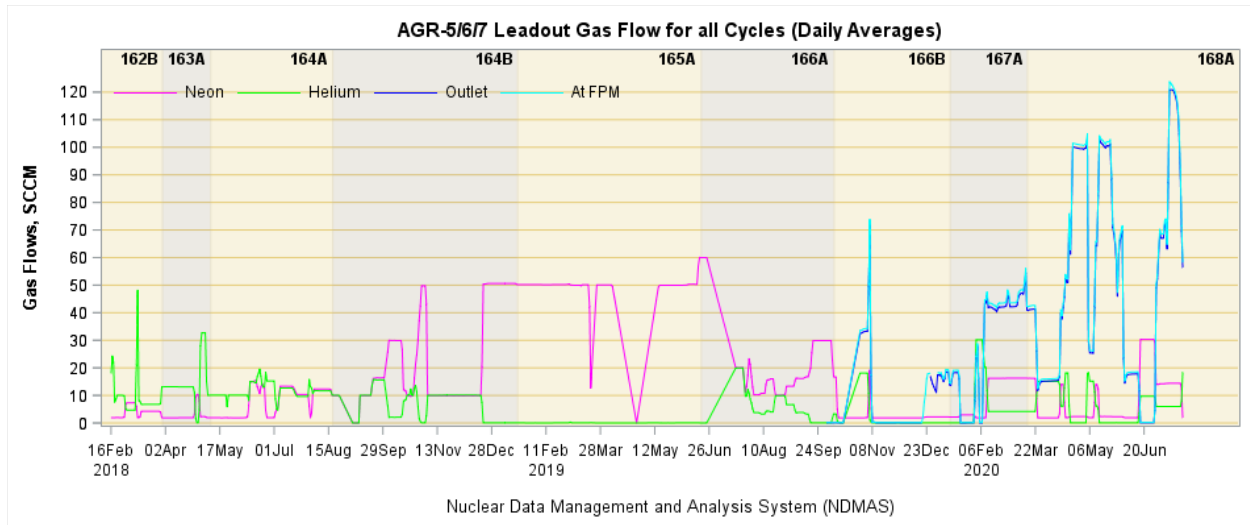
Figure 14. Lead-out sweep-gas flow rates: outlet isolation valve was opened from Cycle 166B.

PLUG AND CRACK

At the beginning of Cycle 165A, a crack opened in the outlet line of Capsule 1. At first flows from capsules 2 - 5 were flowing into the leadout and then into the break, but we made adjustments to achieve the flow paths shown in this figure.
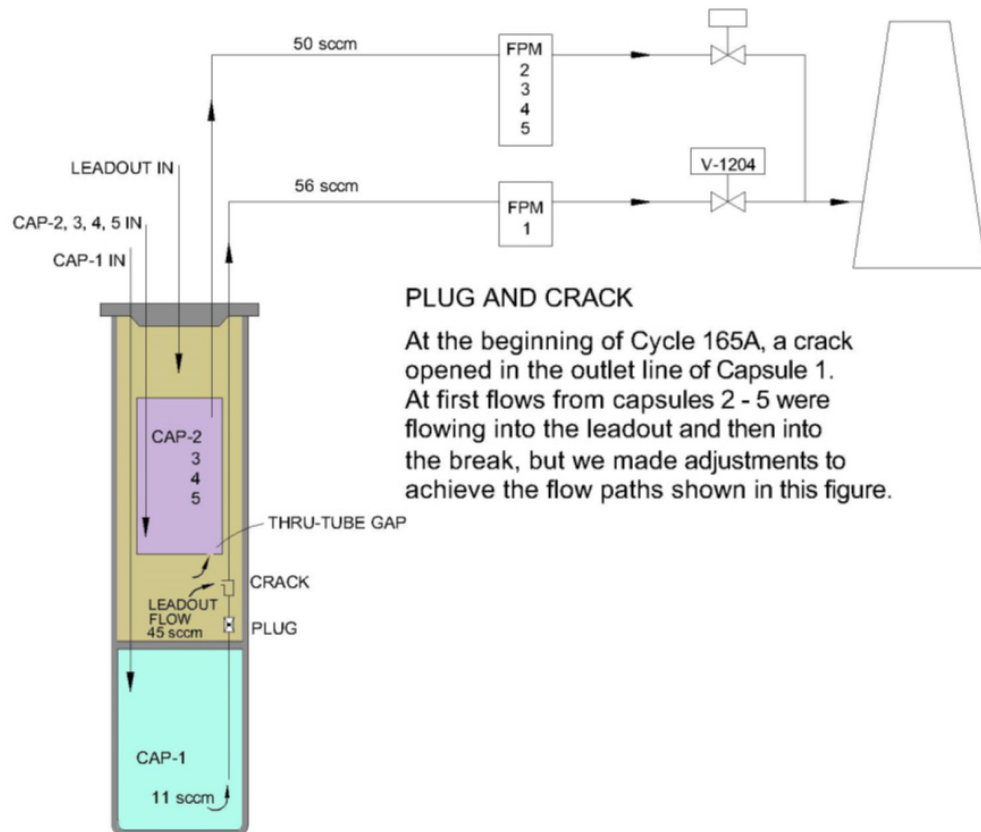
Figure 15. Simplified schematic showing the location of the initial capsule 1 plug and crack.

5.1.4   Fission-gas Release Monitoring Results

The performance of a nuclear fuel test is typically evaluated using the R/B ratio, which is the ratio of the released activity of an isotope from the fuel to the predicted creation rate of the isotope during irradiation. Daily fission-product birth rates for the following twelve isotopes were provided by as-run neutronics calculation: Kr-85m, Kr-87, Kr-88, Kr-89, Kr-90, Xe-131m, Xe-133, Xe-135, Xe-135m,

Xe-137, Xe-138, and Xe-139. Release rates obtained from the FPMS and calculated birthrates were used to calculate the capsule R/B ratios for the radionuclides of interest.

For this report, data on all twelve measured isotopes, Kr-85m, Kr-87, Kr-88, Kr-89, Kr-90, Xe-131m, Xe-133, Xe-135, Xe-135m, Xe-137, Xe-138, and Xe-139, are displayed. Release activities are generally reported as an average for the eight-hour interval during normal irradiation conditions to reduce measurement uncertainty. However, during the initial test of the leadout flow system, release rates were recorded at a much higher frequency (i.e., every 20 minutes), so those measurements usually have higher measurement uncertainty. To preclude the use of data with high measurement uncertainty in the analysis of fission-gas release, values where uncertainties are greater than 50% are omitted. Negative values are also excluded. These filters remove data from the short lead-out flow runs or incomplete measurements while leaving other runs unaffected.

On average, capsule measured R/B values can be on the order of 1E-06 for krypton and 1E-07 for xenon, except for the two very-long-life isotopes, Xe-131m and Xe-133 with half-life of 11.9 and 5.2 days, respectively (Table 6). R/B values for the longest-life isotope, Xe-131m, are peaked at 4.9E-02 (or 4.9%). Uncertainties in the R/B data are a little more than 6% on average for selected krypton and xenon isotopes (i.e., Kr-85m, Kr-87, Kr-88, Xe-135, Xe-137, and Xe-138 in Table 6). These isotopes have moderate half-lives that are sufficiently short to reach equilibrium in the capsule, but also long enough to provide a measurable and stable signal in the FPMS detector; and are measured with lower uncertainty. Releases for isotopes with extra-short-half-lives (i.e., Kr-90, Xe-139) or extra-long-half-lives (i.e., Xe-131m) are associated with much higher uncertainty (greater than 30% on average). The reason for high uncertainty for short-lived isotopes is a weaker signal at the detector, especially when there was insufficient flow to carry them fast enough to reach their perspective FPMS; and for long-lives isotopes is the inability to reach equilibrium conditions within a capsule.

Table 6. AGR-5/6/7 measured R/B and uncertainty statistics for krypton and xenon isotopes.

Isotope	Half-life (min)	Measured R/B			Uncertainty [a] (%)		
		Average	Minimum	Maximum	Average	Minimum	Maximum
Kr-85m	268.7	3.38E-06	2.15E-10	1.24E-04	6.8	5.8	49.5
Kr-88	170.4	2.14E-06	7.35E-11	7.38E-05	6.9	5.8	46.1
Kr-87	76.0	1.14E-06	5.60E-10	3.25E-05	6.4	5.8	24.6
Kr-89	3.2	1.74E-07	5.74E-10	1.44E-05	9.6	5.8	48.4
Kr-90	0.5	1.01E-06	3.02E-09	3.44E-05	30.6	10.6	49.7
Xe-131m	17162.0	3.56E-03	6.14E-06	4.90E-02	40.6	6.4	50.0
Xe-133	7558.9	2.00E-05	4.28E-09	1.26E-03	17.3	5.9	50.0
Xe-135	545.8	8.27E-07	1.78E-11	3.34E-05	6.8	5.8	48.5
Xe-135m	15.3	3.28E-07	6.10E-10	5.53E-05	6.6	5.8	38.6
Xe-138	14.1	1.19E-07	6.51E-11	3.56E-06	6.3	5.8	47.4
Xe-137	3.8	7.94E-08	1.61E-10	4.35E-06	8.7	5.8	48.0
Xe-139	0.7	1.49E-07	3.72E-10	5.43E-06	30.6	8.2	50.0

[a] Only R/B values with uncertainty less than 50% and a standard 8-hour interval are used.

Green rows are for shortest isotopes with uncertainty less than 10% on average.

Red rows are for either too short or too long isotopes high uncertainty (more than 30% on average).

The daily averages of the measured capsule R/B in each of the five AGR-5/6/7 capsules for the twelve measured isotopes are presented as a function of irradiation days in Figure 16 for krypton and Figure 17 for xenon. These plots can be used to examine the relationships to fuel temperature and to assess possible particle failures. The following observations can be made:

1. For all cycles, R/B values for the shortest half-life isotope, Kr-89 (cyan dots in Figure 16), are few, unstable, and high uncertainty (30% on average) and R/B values for the longest half-life isotope, Xe-131m (pink dots in Figure 17), are unrealistically high and have the highest uncertainty (40% on average). In addition, R/B values for the second-shortest isotope, Xe-139 (cyan dots in Figure 17) are also unstable and have high uncertainty (30% on average). Therefore, R/B data for these three isotopes will not be analyzed further.

2. During the first 5 cycles (162B – 165A) gas flows in all capsules were within normal, as-designed ranges, even when the Capsule 1 gas line clog developed downstream of the outlet gas line during 164B. The R/B trends are (excluding the three isotopes mentioned in the first paragraph):

   - R/B values were stable in all capsules and corresponded well to changes in fuel temperature as shown in Figure 18. During the short PALM Cycles 163A the ATR only reached full power for one day at the end of the cycle, which led to much lower fuel temperatures in all capsules, and therefore, R/B data are much lower. This behavior is consistent with the absence of spikes in gross gamma temporal profiles that typically occur during in-pile particle failure events.

   - The main objective of AGR-7 Capsule 3 fuel irradiation was to test fuel performance beyond normal operating condition, so its compacts were maintained at the highest temperature in the test train (Figure 18). As a result, Capsule 3 R/B values are much higher than R/B in Capsules 2, 4 and 5, where fuel temperatures are significantly lower. The lower fuel temperatures at the beginning of each cycle and the low-power PALM cycle 163A clearly led to lower R/B in all the capsules.

   - High R/B values in Capsule 1 during this time were caused by the second-highest fuel temperature in the test train and higher as-fabricated exposed kernel (EK) fraction (Pham and Scates, 2019).

3. For Cycle 166A, an almost total clog in Capsule 1 outlet gas line caused intermittent gas flow rates (Table 5), which led to intermittent R/B data for Capsule 1 (see bottom frame in Figure 16 and Figure 17 from 200 EFPDs to the end of 166A). As a result, some of accumulated FGs in Capsule 1 diffused out via a crack in the gas line and contaminated gas in the leadout. Then, the contaminated gas in the leadout flowed through the other four capsules, resulting in various amounts of Capsule 1 FGs leaked to the other four capsules during this cycle. This FG leakage was first detected by synchronizing behavior of Capsule 2 R/B for longer-lived isotopes (i.e., Kr-85m, Kr-88, Xe-133, Xe-135) in with Capsule 1 R/B right from 200 days of irradiation to the end of this cycle (Frame 4 in Figure 16 and Figure 17). The same trend became apparent for Capsules 4 and 5 near the end of Cycle 165A. However, the fluctuating behavior is much less apparent for Capsule 3, instead R/B for all isotopes were gradually increasing during that time.

4. For Cycle 166B:

   - Near the end of ATR Cycle 166A, a significant number of in-pile failures occurred in Capsule 1, causing a substantial increase in FG activity and saturation of the FPMS HPGe detector and increased activity in the 1A primary that was picked up by the GG NaI(Tl) detectors (Scates 2021). This event prompted an analysis (ECAR-4802) to assess the impact of FG release from the AGR-5/6/7 capsules at the ATR stack monitor. The analysis demonstrated that 100% particle failure from Capsule 1 (over 300,000 particles) would result in an off-site dose increase of 0.057 mrem/y, less than the dose limit (0.1 mrem/yr) specified in 40 CFR 61.93(4)(i) as the criterion for additional radionuclide emission rate monitoring.

   - ECAR-4802 also established criteria for single day averages, based on the activity of each isotope, that would be required for the total FG activity to reach a total dose of 0.0098

27

mrem/y if accumulated over 200 days, a level that is less than 10% of the 40 CFR 61.93(4)(i) criterion of 0.1 mrem/yr.

- As a precaution, gas flows were suspended for the whole test train during the first half of Cycle 166B, and the Capsule 1 gas line was isolated during the entire cycle. At the same time, the leadout outlet isolation valve was opened, allowing Capsule 1 FG to discharge through the leadout to one of the spare detectors (6) to limit FG leakage to other capsules.
- As a result, R/B data were collected only for Capsules 2-5 during the second half of 166B and no release data for Capsule 1was collected. However, the FG leakages into Capsules 2, 4, and 5 are still observable by elevated R/B for longer-lived isotopes during that time.

- At the same time, R/B for extra-short isotopes (i.e., Kr-89 in Figure 16 and Xe-137 in Figure 17) increased at much smaller fraction relative to R/B during earlier cycles for Capsules 2, 4, and 5. This is because the impact of FGs leakage is smaller for shorter isotopes due to decay over the transport time from Capsule 1 to other capsules, especially the top capsules 4 and 5. R/B data for these two isotopes can be used to assess if any in-pile particle failures in these capsules occurred during this time.

- For Capsule 3, R/B for all isotopes, except the longest-lived (i.e., Xe-131 m and Xe-133) are slightly higher than levels at the end of the previous cycle, 166A. This indicated only insignificant FGs leakage from Capsule 1 but cannot exclude in-pile particles failures. Note that some particle failures were considered possible in this capsule due to high fuel temperature well beyond normal operating conditions of a high temperature gas reactor.

5. For the PALM cycle 167A, R/B in all capsules are lower because of significantly lower fuel temperatures, as shown in Figure 18.
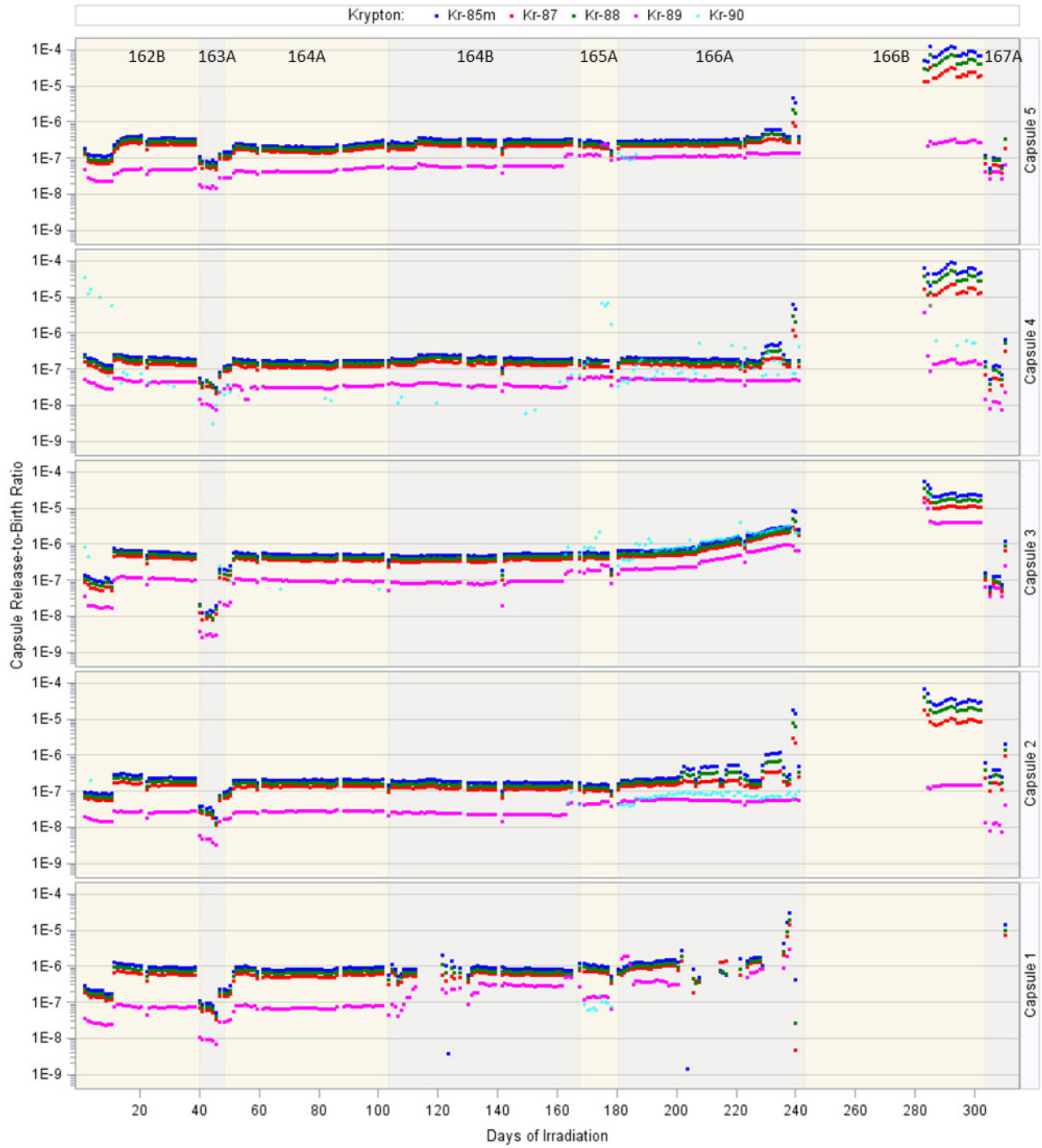
Figure 16. Measured R/B in AGR-5/6/7 capsules for krypton isotopes.
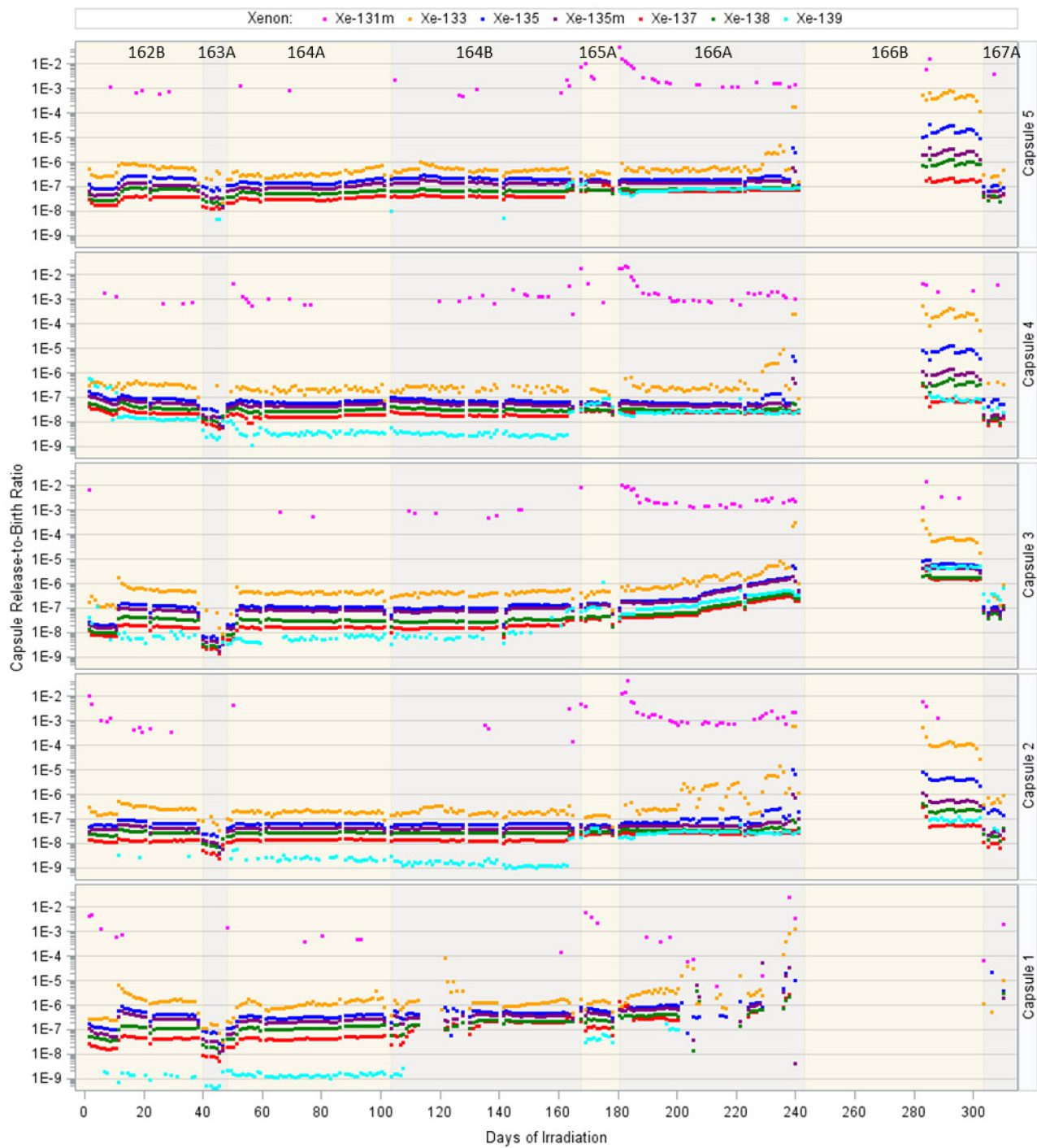
Figure 17. Measured R/B in AGR-5/6/7 capsules for xenon isotopes.
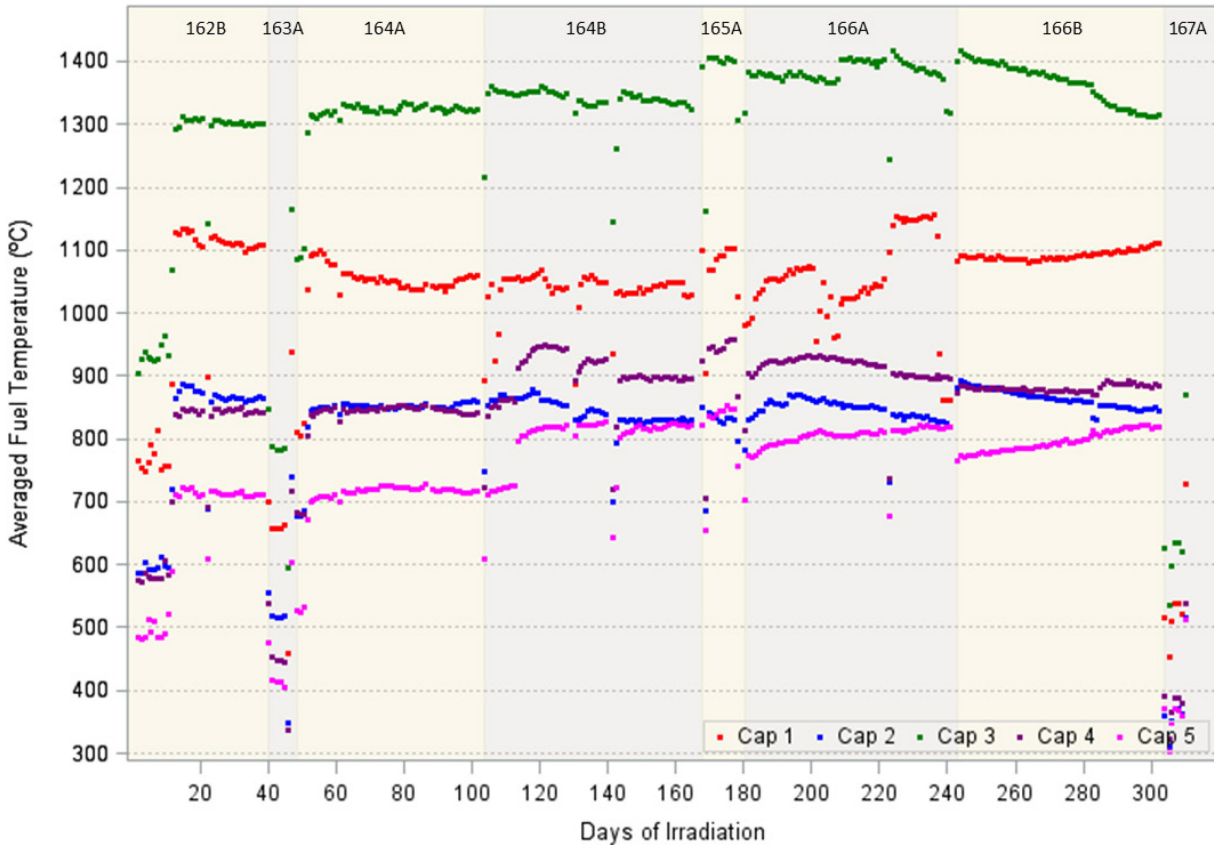
Figure 18. Capsule average fuel temperature.

5.1.5   Particle Failure Monitoring Results

5.1.5.1   Particle failure evidence

For each capsule, the sweep gas carries released fission-product gases from the capsule to the corresponding detector system, which uses a thallium-doped sodium iodide (NaI[Tl]) detector to measure GG count rates. The temporal GG count profile can help detect each fuel-particle failure up to the first 250 failures. A particle failure would cause a rapid rise and drop (or spike) in the temporal profile of the measured GG-count rate and raise the baseline gamma count afterward. The spike is the result of a sudden release of stored fission-product inventory inside a just-failed particle, which can be visually detected. However, accurate particle failure detections can be difficult when multiple failures occur at once and in the presence of possible FG leakage into the capsules. Therefore, the GG counts data are used only to provide supporting evidence for failures, but not to determine the exact number of failures.

The GG counts were recorded every 3.5 seconds, which resulted in a large amount of GG data. Subsequently, daily peak and average GG counts in five capsules and two spare detectors are plotted (Figure 19) to spot possible in-pile failures manifesting in substantially higher daily peaks and an subsequent increase in daily averages cannot otherwise be explained. Areas of interest are then examined in further detail using 5-min peaks and average GG data to spot typical peak values caused by particle failure, as shown in Figure 20 through Figure 22. The following evidence can be seen:

1. Up to the end of Cycle 165A, both GG averages and peaks are low and stable, which is a good indication that in-pile particle failures are unlikely in all capsules. Stable R/B values for all isotopes in

all capsules (see Figure 16 and Figure 17) up to this cycle further confirm this fact. It is still possible that one or more failures occurred without causing the expected evidence.

2. For PALM Cycle 167A: the ATR reactor was at full power for less than a day and fuel temperature were low in all capsule, which resulted in low GG counts, except for the last data point at the end of the cycle. No failure evidence was detected.

3. For the three remaining regular cycles (166A, 166B, and 168A), the GG count averages increased in all capsules relative to previous cycles and numerous significant peaks were visible in several capsules. Therefore, a more detailed look at the 5-minute GG plots is presented in Figure 20 through Figure 22; failure evidence will be discussed in following paragraphs.

4. For 166A (Figure 20), during the outage the inlet- and outlet-gas lines for Capsule 1 were swapped to prevent FGs released by Capsule 1 from spilling to the lead-out and entering other capsules. Flow to Capsule 1 was intermittent due to a new clog that developed in the swapped outlet line, leading to its flow suspension.

   - The first observed particle failure in Capsule 1 occurred on August 4, 2019. After that, basing on GG plot in Figure 20, a large number of spikes are evident for Capsule 1 between September 30, when Capsule 1 outlet flow resumed, and October 4, 2019. These spikes and subsequent increases in averages indicate numerous failures occurred in Capsule 1. GG counts were not always available due to intermittent flow to Capsule 1, so exact number of failures in this capsule cannot be determined by GG counts.

   - For the remaining four capsules, the small spikes are synchronized across capsules as they are correlated with spikes in Capsule 1, which might contribute to the response of the other capsule GG detectors when activity in the gas lines enters the 2C cubicle. Also, GG count increases during that time can be explained by FG leakage from the leadout gas contaminated with Capsule 1 FGs. This is because the leadout outlet was still closed as originally designed and gas in the leadout would have to pass through Capsules 2-5.

5. For 166B (Figure 21): Capsule 1 gas line was isolated, and flows to the other four capsules were suspended during the first half of this cycle; the leadout outlet was opened with lower pressure than pressure in Capsules 2-5 when flows in these capsules resumed (Table 5). As a result, the following GG counts trends can be seen:

   - During the first half of 166B, GG data from all capsules were just background noise when gas flows were suspended as shown in Figure 19. Unfortunately, any particle failures during this time cannot be detected by GG counts.

   - During the second half of 166B, the increase in GG counts from the four Capsules 2-5 without spikes of peak GG counts could lead to the conclusion that some FGs from Capsule 1 still leaked to Capsules 2-5 (Figure 21). An increase in R/B values for all isotopes in these capsules (see Figure 16 and Figure 17) also further confirms this theory.

6. For 168A (Figure 22 and Figure 23): The Capsule 1 gas line was isolated, and the leadout outlet line was opened with lower pressure. Subsequently for Figure 22:

   - Capsule 1 GG counts decreased to a very low level as expected because of the flow suspension (the decrease in activity is due to the decay of radioisotopes present in the gas line).

   - Capsule 2 had a few spikes in peak GG count together with increases in average values, which led to the belief that a few particle failures were possible. It is possible that some of the Capsule 2 GG count increase can also be contributed to FG leakage from Capsule 1 due to their proximity (if the leak(s) in Capsule 1 are near the capsule head, as expected, then they are in close proximity to the base of Capsule 2 where leadout gas can enter through the gaps where the through tubes penetrate the capsule base).

   - Capsule 3 had more than a dozen GG spikes typical of particle failure. These spikes and subsequent increase in GG background indicate that particle failures occurred in this capsule.

32

- Capsules 4 and 5 had no apparent spikes, so their variations in GG counts could be attributed to a small leakage of FGs from Capsule 1.
- For Figure 23 (July 2-22, 2020): no clear spikes were apparent during this time. High GG counts in Capsules 2-5 during this period were likely caused by FG leakage from Capsule 1.

In conclusion, the data indicate a large number of failures in Capsule 1 since the middle of Cycle 166A; numerous failures in Capsule 3 and perhaps a small number of failures in Capsule 2 during Cycle 168A. No clear failure evidence was apparent for the top two Capsules 4 and 5.
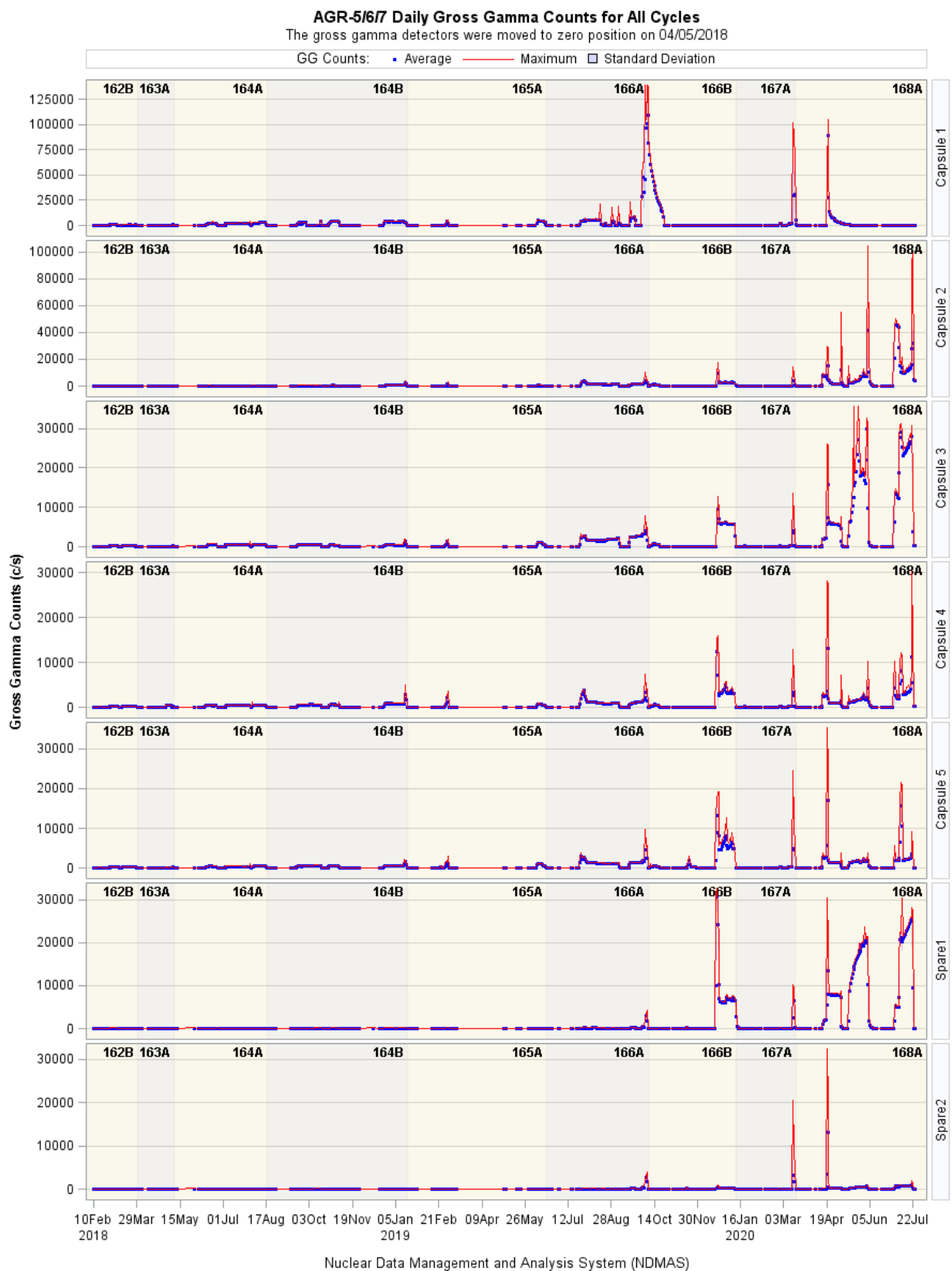
Figure 19. AGR-5/6/7 daily average and maximum GG counts for five capsules and two spare detectors.
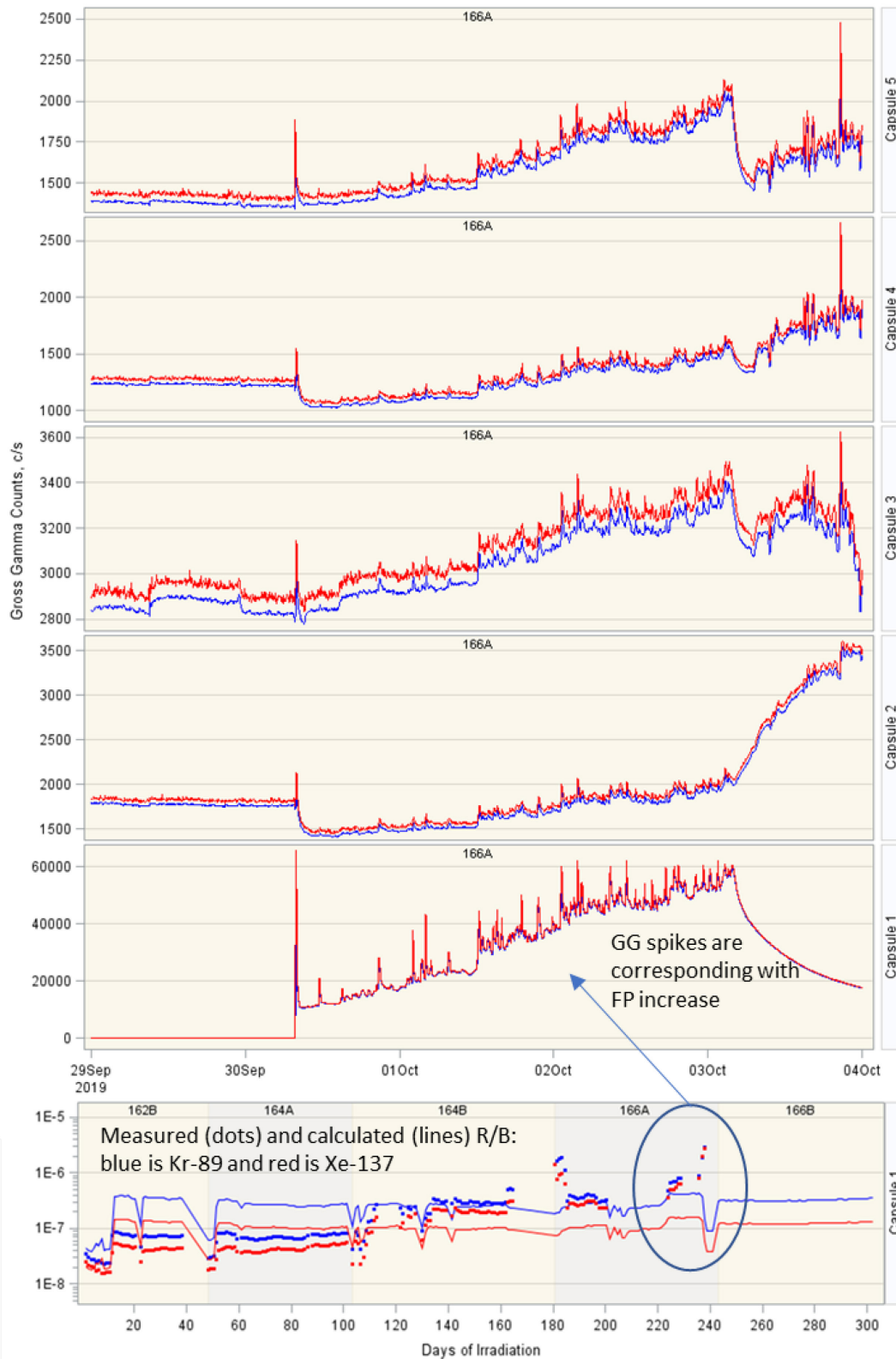
Figure 20. Typical spikes associated with particle failures are observable in Capsule 1 based on 5-minute peak and average GG counts near the end of Cycle 166A.
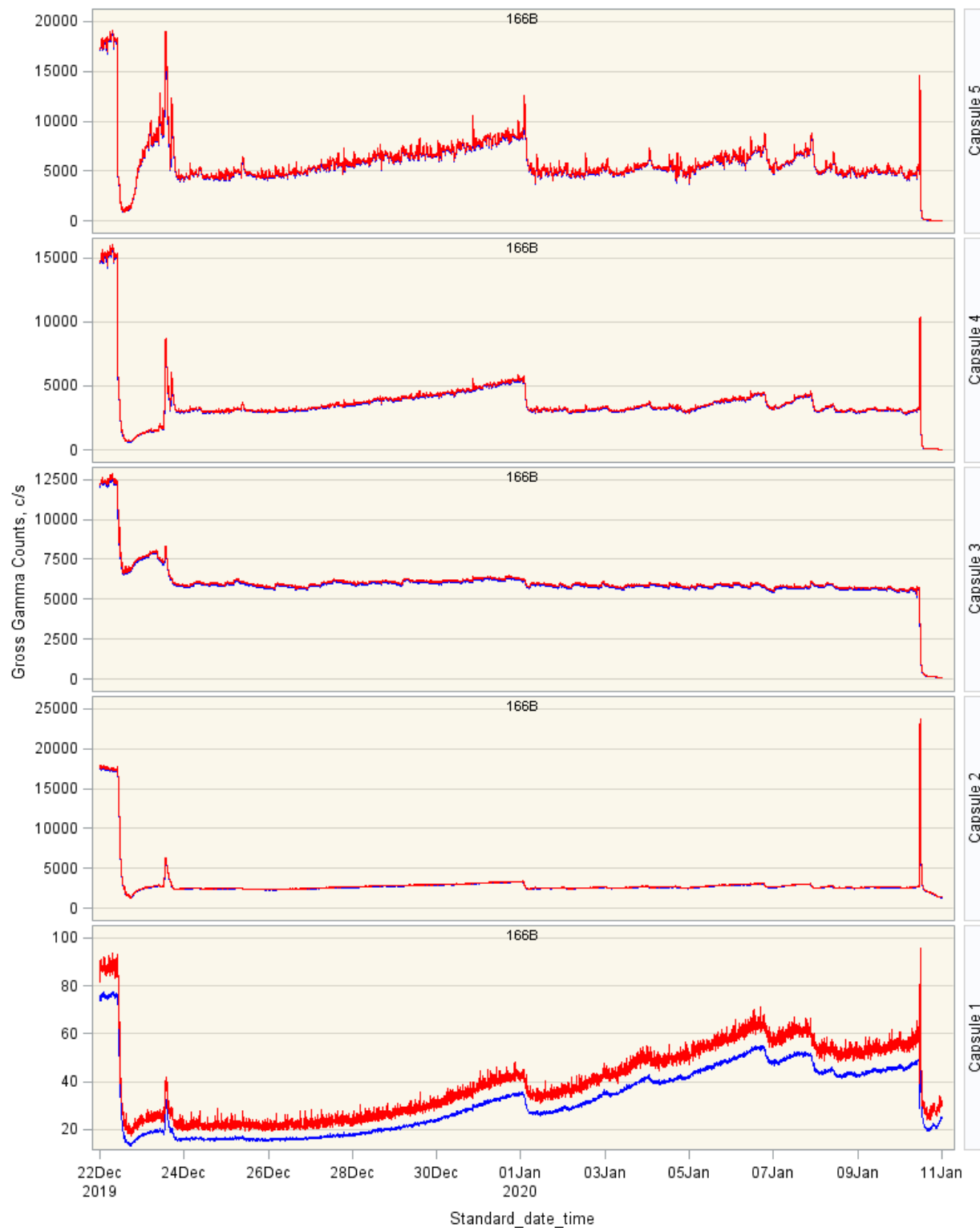
Figure 21. No clear spikes associating with particle failures are observable in Capsules 1- 5 during 166B.
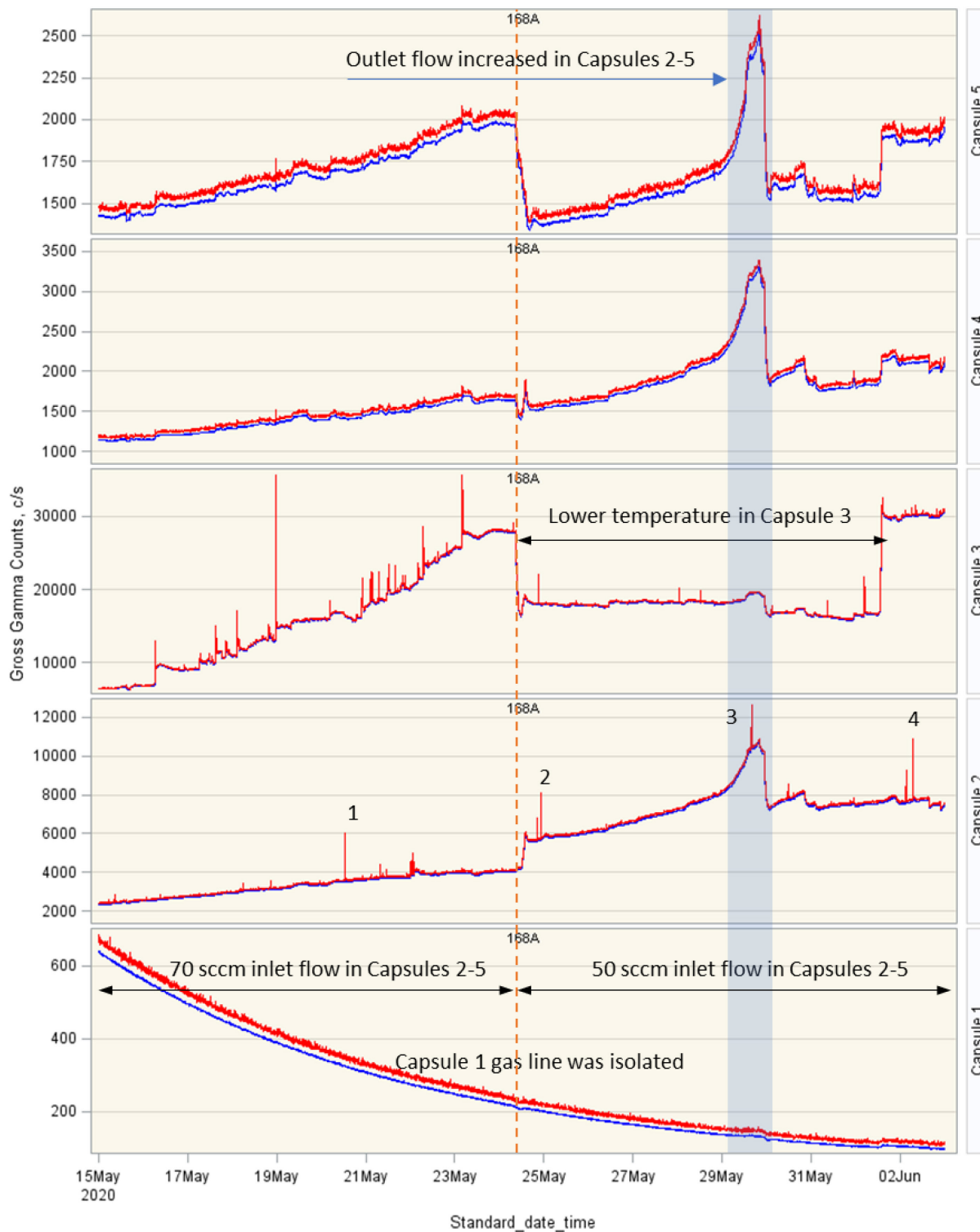
Figure 22. Typical spikes associating with particle failures are observable in Capsules 2 and 3 based on 5-minute peak and average GG counts between May 15 and June 4, 2020 during 168A.
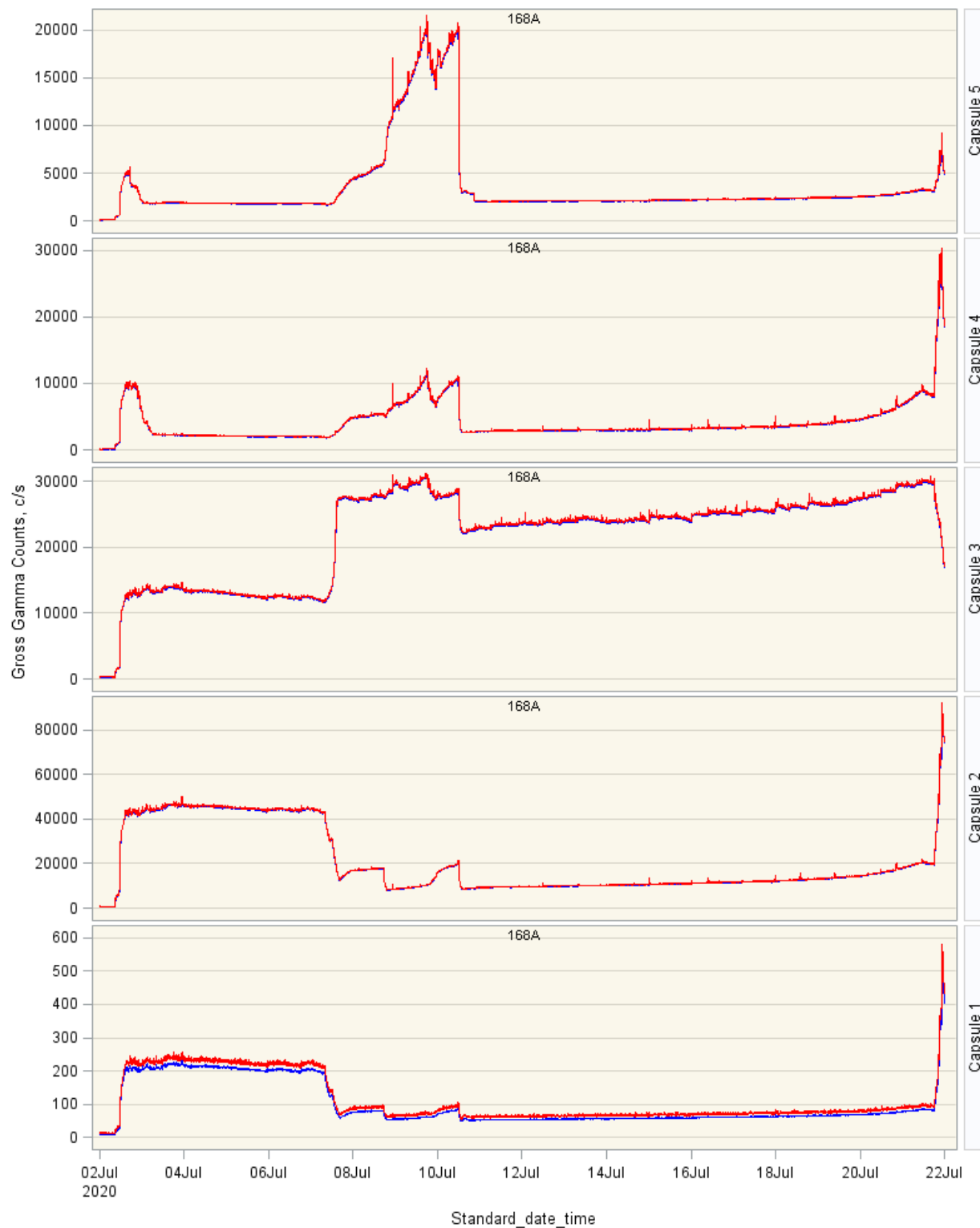
Figure 23. Typical spikes associating with particle failures are observable in Capsules 2 and 3 based on 5-minute peak and average GG counts between July 2 - 22, 2020 during 168A.

5.1.5.2   Particle failure estimation

According to the fabrication quality data for fuel compacts used in the AGR-5/6/7 capsules, there could be as many as 17 EK defects and 1.52 kernels worth of dispersed uranium (DU) in Capsule 1, which resulted in 26.3 and 23.1 as-fabricated equivalent EKs for krypton and xenon isotopes, respectively, as shown in Table 7 (Pham and Scates, 2019). This is because the release from one DU kernel is equivalent to ~6 EKs for krypton isotopes and ~4 EK for xenon isotopes. Capsules 3 and 4 have the least number of equivalent EKs of ~2 for krypton and ~1 for xenon isotopes, which were solely due to DU because no EK defect was likely to exist in these two capsules. As designed, in-pile particle failures are expected in Capsule 3 due to high irradiated fuel temperatures that were beyond normal operating temperatures for a hypothetical high temperature gas reactor. Capsule 1 fuel temperature is also much higher than the remaining three capsules. The GG count monitoring presented in the previous subsection indicated that in-pile particle failures likely occurred in Capsules 1, 2, and 3 but not in the two top capsules 4 and 5. An attempt was made by the FPMS staff to accurately estimate the number of in-pile failures based on manually aligning spikes in GG counts and peaks in hourly isotope activities for long-lived isotope such as Xe-133. This exercise also concluded that particle failures occurred in Capsules 1, 2, and 3.

Table 7. Numbers of equivalent EKs calculated from DU and EK fractions.

Capsule	Total Particles	Dispersed Kernels	Estimated Exposed Kernels	Assumed Exposed Kernels	Equivalent Exposed Kernels for Krypton	Equivalent Exposed Kernels for Xenon
Capsule 1	307625	1.52	16.58	17	26.3	23.1
Capsule 2	72480	0.36	0.53	1	3.2	2.5
Capsule 3	54360	0.27	0.40	0	1.7	1.1
Capsule 4	52728	0.26	0.38	0	1.6	1.1
Capsule 5	81432	0.40	4.39	4	6.5	5.6

In this section, R/B for short-lived isotopes, Kr-89 and Xe-137, will be used to estimate the number of in-pile particle failures in each capsule. This is because R/B data for the isotopes with half-lives less than ~3 minutes are not stable and have high measurement uncertainty; and R/B data for long-lived isotopes were likely contaminated with Capsule 1 FGs as shown in Section 5.1.4. This FG leakage in Capsules 2-5 can be seen by substantial increases in R/B during Cycle 166A (Figure 16 and Figure 17), especially when there is no evidence of particle failures in Capsules 4 and 5 based on spikes in the GG counts. However, R/B increases during Cycle 166A were not the same for all isotopes as R/B for relatively long-lived isotopes (i.e., Kr-85m, Xe-133) increased much more than the increase for short-lived isotopes (i.e., Kr-89, Xe-137 with approximately 3 minutes half-life). This is because it took some time for Capsule 1 FGs to diffuse to other capsules, especially for the top Capsules 4 and 5, and most activities of short-lived isotopes were decayed.

The total number of particle failures ($N_{failures}$) in each capsule can be estimated as the ratio between capsule measured R/B and predicted R/B per EK, based on the AGR-3/4 R/B per EK model as a function of fuel temperature reported in (INL, 2019), as follows:

$$N_{failures} = \frac{R/B_{measured} * N_{particles}}{R/B_{1\_predicted}}$$

where: $R/B_{measured}$ is the measured R/B per capsule

$N_{particles}$ is the number of particles per capsule

$R/B_{1\_predicted}$ is the predicted R/B per an EK.

The number of in-pile particle failures ($N_{irr\_failures}$) is the difference between estimated total number of failures ($N_{failures}$) and estimated number of equivalent EKs ($N_{EK\_failures}$), which were reported in (Pham and Scates, 2019) as:

$$N_{irr\_failures} = N_{failures} - N_{EK\_failures}$$

The capsule daily measured and predicted R/B data for Kr-89 and Xe-137 are presented in Figure 24 for five AGR-5/6/7 capsules to show how well AGR models (AGR-3/4 model for R/B per EK and AGR-1 for R/B per DU kernel) perform in predicting R/B values for AGR-5/6/7 capsules. For clear visual presentation of plots, only data when fuel temperatures are close to specification and R/B values with uncertainty < 50% were included in the plots. Therefore, three PALM cycles (163A, 165A, and 167A) were excluded because of significantly lower temperatures most of the time. According to the measured versus predicted plots, good model prediction performance can be seen prior to the identified occurrence of in-pile failures (i.e., through the end of ATR Cycle 164B). For both isotopes, Kr-89 and X-137, the AGR model predicted best for Capsule 2, under-predicted for Capsules 4 and 5, and over-predicted for Capsules 1 and 3. It is worth mentioning that uncertainty in the number of equivalent EKs in each capsule can also contribute to differences between measured and predicted R/B data in all capsules.

The estimated in-pile failures and as-fabricated equivalent EKs are presented in Figure 25. For estimating the number of failures, it has been assumed that all failures occurred near the highest temperature location within a capsule. Model over-prediction will result in negative in-pile failures when no in-pile failure occurred, instead of the expected zero minimum. The results are:

- The most negative number of estimated in-pile failures is for Capsule 1 (bottom panel in Figure 25), where as much as 26 equivalent EKs were estimated, but the actual equivalent EKs could be much lower. Evidence of multiple particle failures occurred in Capsule 1 toward the end of Cycle 166A (Figure 20) is consistent with a sharp increase in the estimated number of in-pile failures (up to a few hundred failures are possible). After 166A, no R/B measurements in Capsule 1 were available because of zero outlet flow for this capsule.

- A slight increase in the estimated number of in-pile failures in Capsules 2 and 3 during ATR Cycle 166A was likely caused by small leakage of FGs from Capsule 1 because no evidence of failure was observed for these cycles according to plots in Figure 20. FG leakage from Capsule 1 to Capsules 4 and 5 were very insignificant, especially for the short-lived isotopes, Kr-89 and Xe-138. This resulted in the same level of estimated number of failures as earlier cycles.

- When the gas line problem in Capsule 1 was worsening during Cycle 166B, but its valve was not isolated, the FG leakage to all other four capsules are apparent by the increase in R/B without GG spikes as evidence of particle failures presented in Figure 21.

- For Cycle 168A, the Capsule 1 gas line was totally isolated in addition to opening the leadout outlet isolation valve, allowing gas flow out from capsules to the leadout to minimize FGs leaking to the capsules. Consequently, the estimated number of failures is more accurate than results for Cycle 166B. However, R/B data for this cycle were not available in time for this report, so estimated number of failures will be discussed in the as-run report.

In conclusion, no in-pile failures likely occurred in Capsules 4 and 5. A few hundred failures may have occurred in Capsule 1 by the end of Cycle 166A, when the last R/B are data available. Additionally, the failure predictions are likely over-estimated due to FG leakage from Capsule 1.
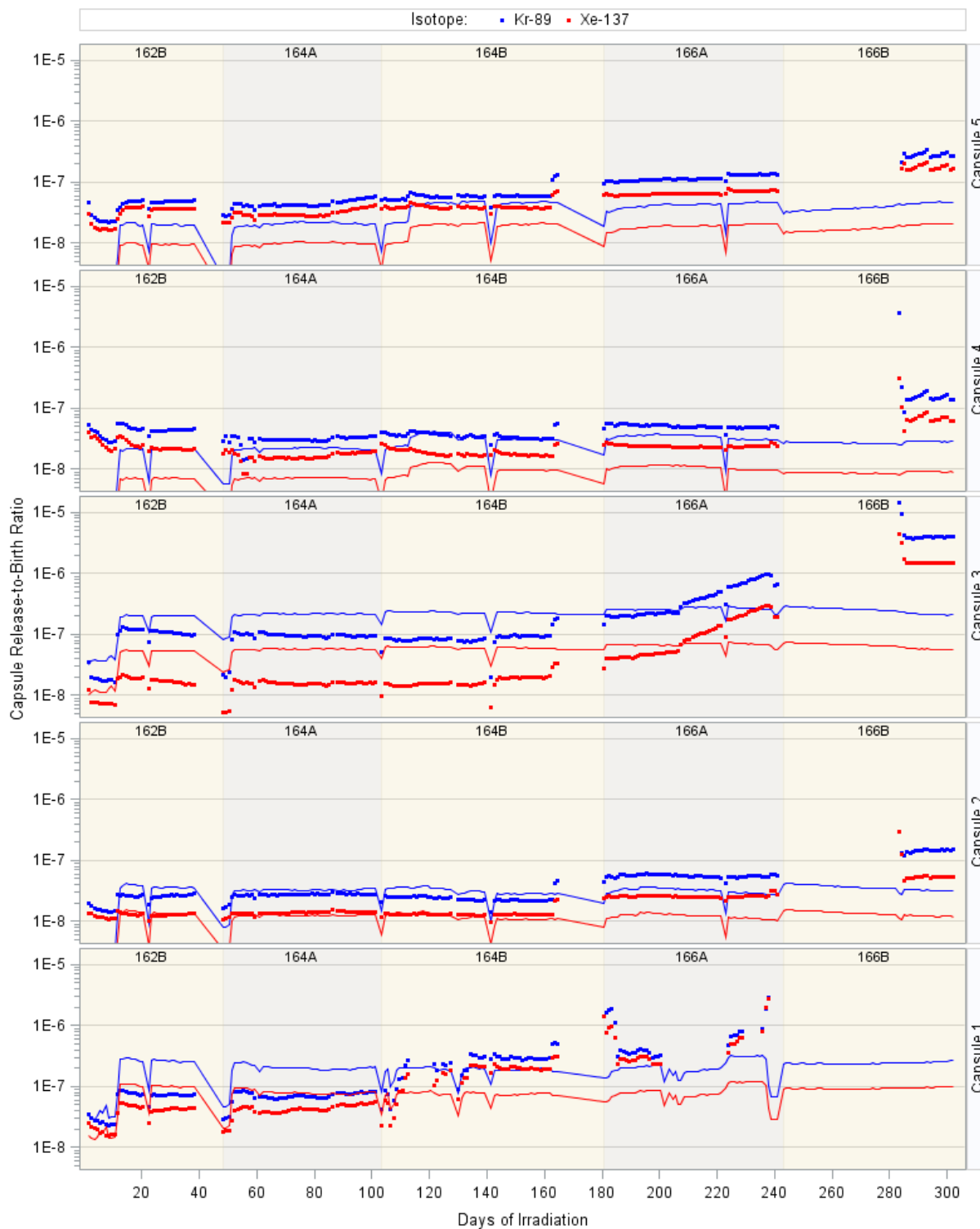
Figure 24. Measured (dots) and predicted capsule R/B for Kr-89 and Xe-137 isotopes.

41
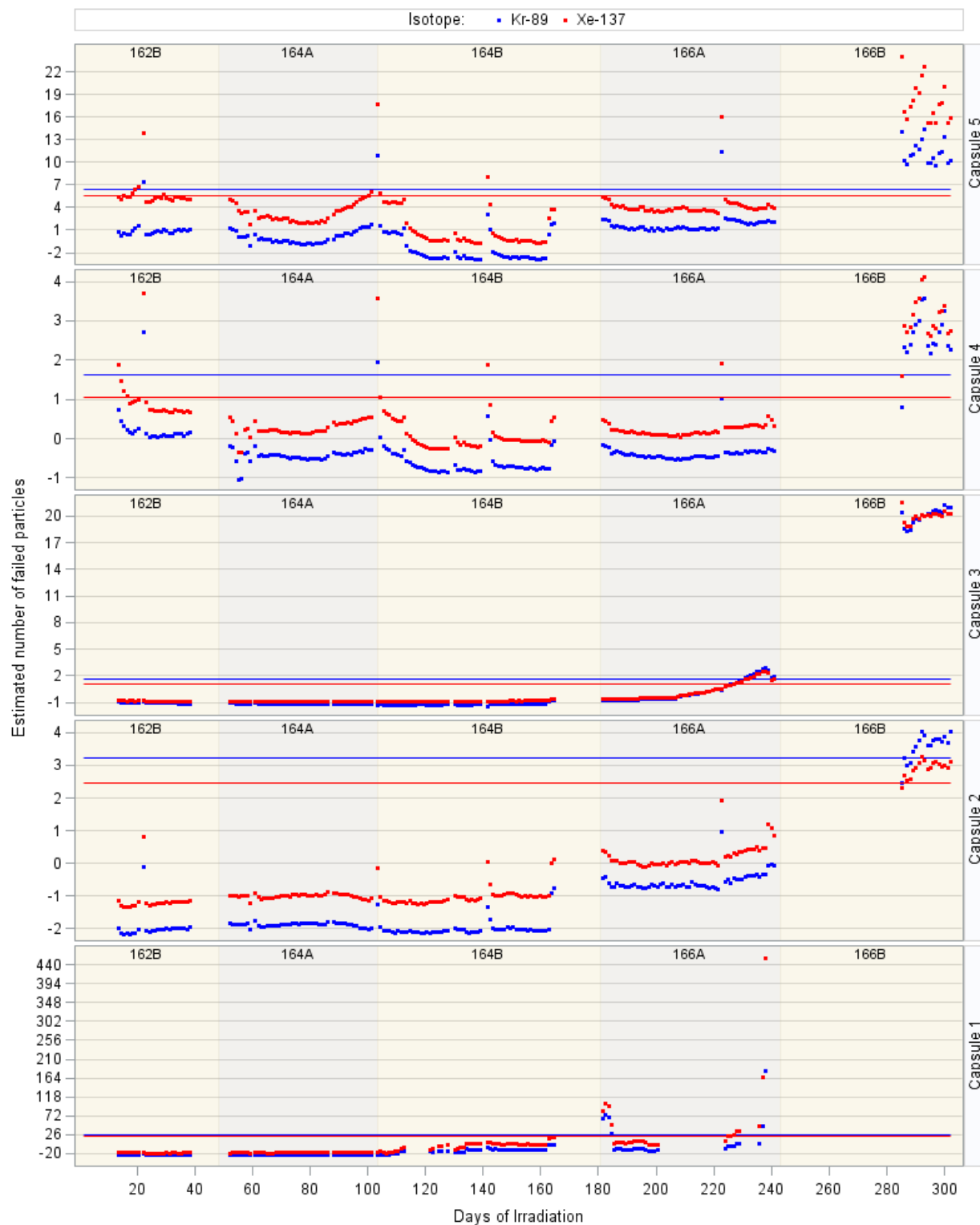
Figure 25. Estimated number of particle failures for AGR-5/6/7 capsules based on Kr-89 (blue color) and Xe-137 (red color): lines are as-fabricated equivalent EKs and dots are in-pile failures.

5.2 Physics Analysis Results

Calculated physics results for AGR-5/6/7 capsules are also used to control experiment conditions, so they are generated and made available as soon as practically possible. Below is a summary of test-relevant calculated data including neutronics and temperature results for the nine cycles: 162B, 163A (low-power PALM), 164A, 164B, 165A (PALM), 166A, 166B, 167A (low-power PALM), and 168A, which were reported in ECAR-5321 (Sterbentz 2020).

5.2.1   As-run Neutronics Analysis Results

The neutronics analysis provides daily values of fission power density (W/cm^3) and fast neutron fluence (n/m^2) for the 194 AGR-5/6/7 compacts and non-fuel components, and burnup (%FIMA) for all compacts. Fast neutron fluence is defined as those neutrons with energies greater than 0.18 MeV. For each time step, neutronics data include:

- For fuel compacts: 776 values of fission power density and fast neutron fluence (4 axial segments per compact); and 194 values of burnup (one per compact).

- For non-fuel components: 907 values of neutron and gamma heat rates for graphite holders, capsule shell, neutron filters (shrouds), capsule lids, spacers, thru tubes, TCs, and gas lines; 45 values of fast neutron fluence for graphite holders in five capsules.

The daily powers per particle in milliwatts per particle are converted from the provided fission power density, compact volume, and number of particles per compact. The daily capsule-peak power per particle plots in Figure 26 show that the AGR-5/6/7 compacts meet the requirement of SPC-1352 (Marshall 2017)—i.e., "The instantaneous peak power per particle shall be ≤400 mW/particle.*"*
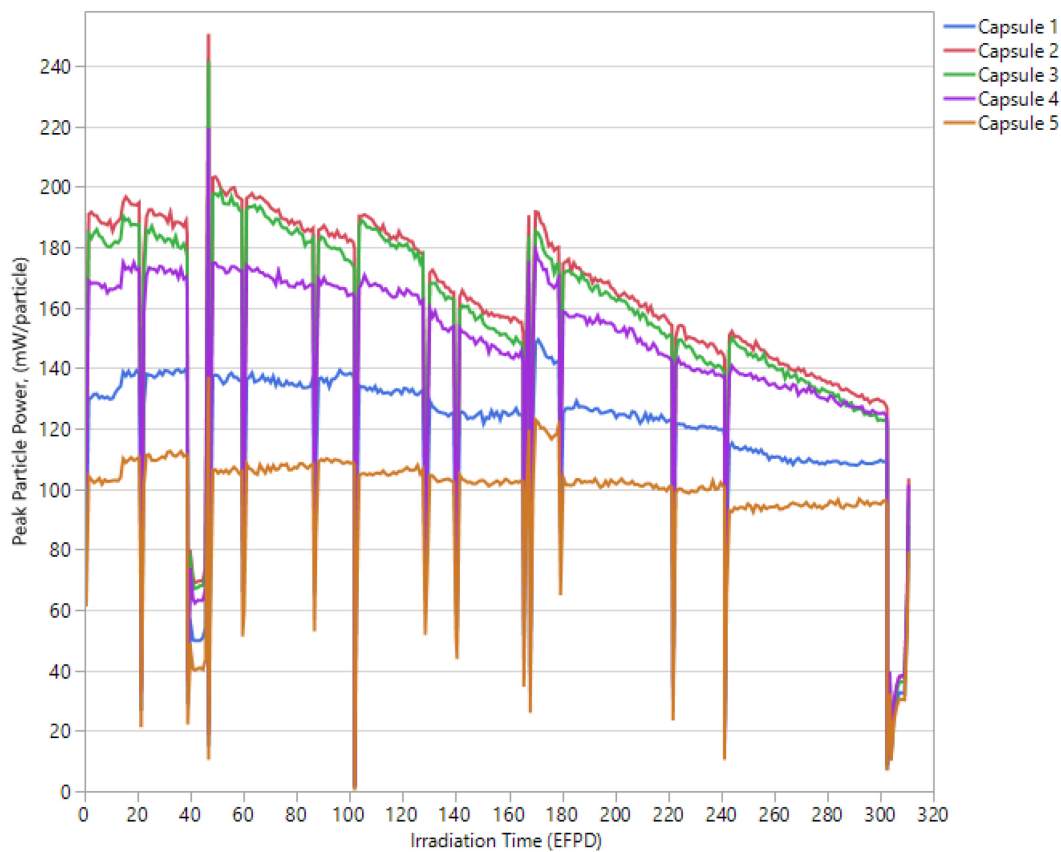
Figure 26. Calculated daily capsule-peak particle power.

For each compact, minimum, average, and maximum values are calculated based on the provided values from the four axial segments per compact. For each capsule, these values are calculated from per-compact values. The daily calculated compact power densities are plotted versus irradiation time by capsule in Figure 27, fuel compact burnups in each capsule are in Figure 28, and fast neutron fluences are given in Figure 29. The power density in the three middle capsules (2, 3, and 4) decreased more rapidly as each cycle progressed than in the two peripheral capsules (1 and 5), as shown in Figure 27. Capsules 2 and 3 were near the ATR core midplane and exposed to the highest thermal-neutron levels (Table 8). Thus, their compacts sustained the greatest burnups (Figure 28) and fluence (Figure 29). Capsule 4 was exposed to slightly lower thermal-neutron levels, which led to less burnup and fluence. The bottom Capsule 1 and top Capsule 5 received the least fast fluence and accumulated least burnup. The average burnup and fast neutron fluence, accumulated at the end of Cycle 167A, for each of 194 compacts are presented in Appendix A.

The burnup and fast neutron values for AGR-5/6/7 test fuel reached more than two-thirds of their requirements by the end of Cycle 167A, after approximately 300 EFPDs of irradiation, which is a little less than two-thirds of the 500-EFPD schedule specified in PLN-5245 (Collin 2018).

Table 8. Minimum, average, and peak compact burnup and fast fluence at the end of 167A.

Capsule	Compact Burnup (% FIMA)			Compact Fast Neutron Fluence (10^{25} n/m^2, E >0.18 MeV)		
	Specification at the end of irradiation: Minimum > 6% for all compacts *Maximum > 18% for at least one compact*			Specification at the end of irradiation: *Minimum >1.5 for all compacts Maximum ≤7.5 for all compacts and ≥5.0 for at least one compact.*		
	Minimum Compact	Capsule Average	Peak Compact	Minimum Compact	Capsule Average	Peak Compact
5	5.65	6.95	7.97	1.37	2.10	2.78
4	10.56	11.50	12.12	3.24	3.69	4.07
3	11.62	12.45	12.93	4.17	4.37	4.47
2	11.61	12.68	13.23	3.68	4.09	4.39
1	4.65	7.75	9.95	1.32	2.60	3.59
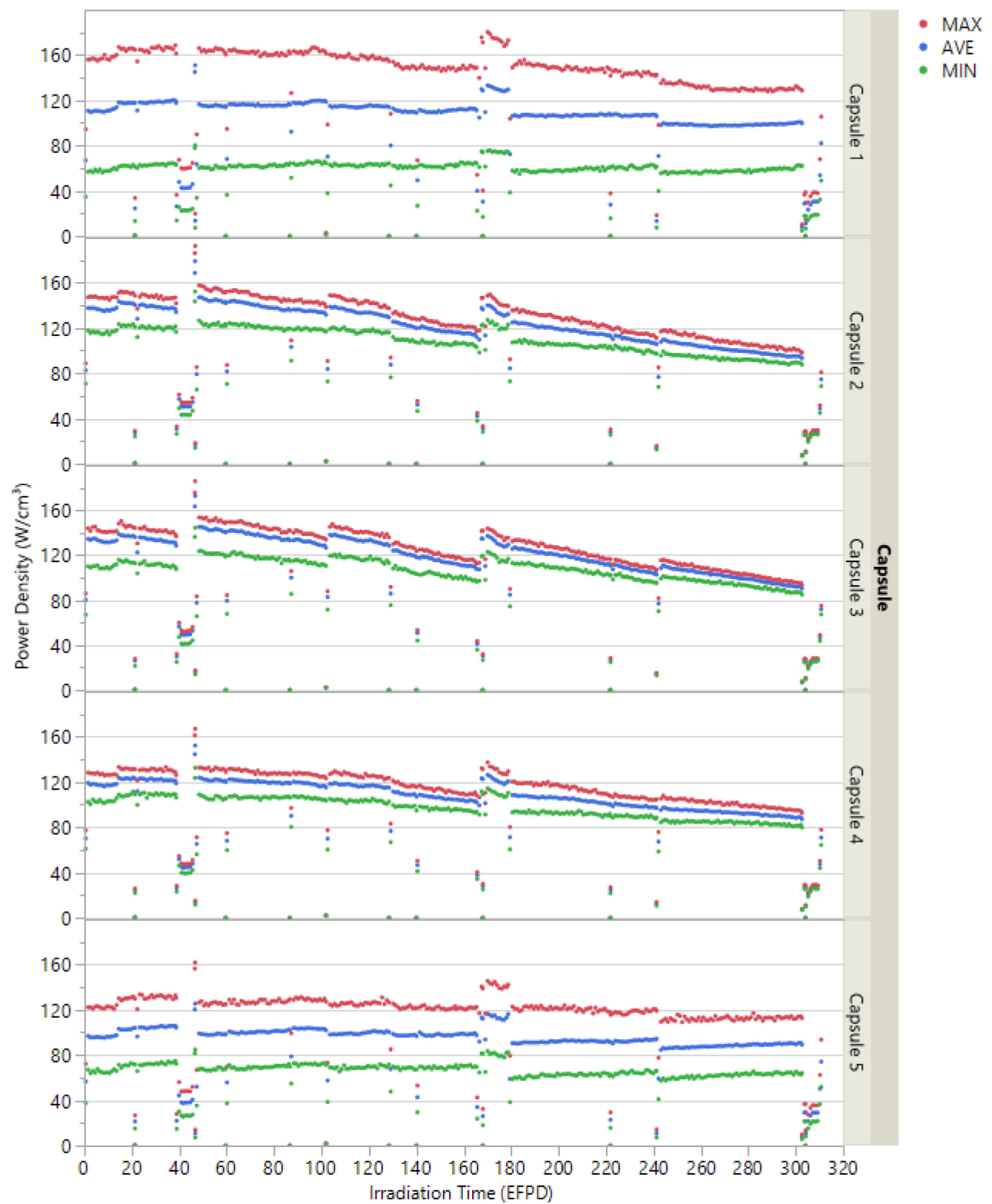
Figure 27. Calculated daily minimum, maximum, and volume-averaged compact power density.
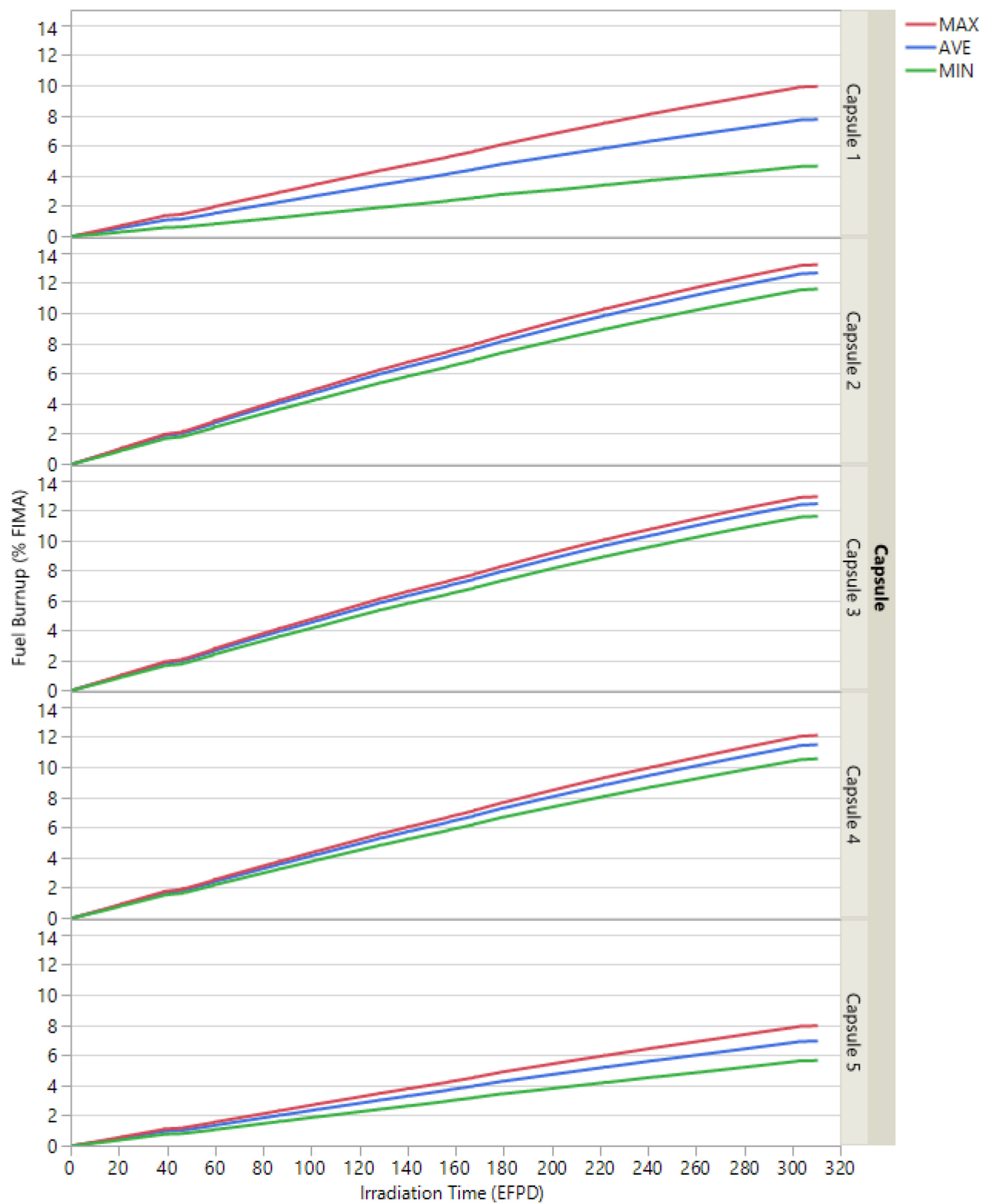
Figure 28. Burnup versus irradiation time in EFPD.
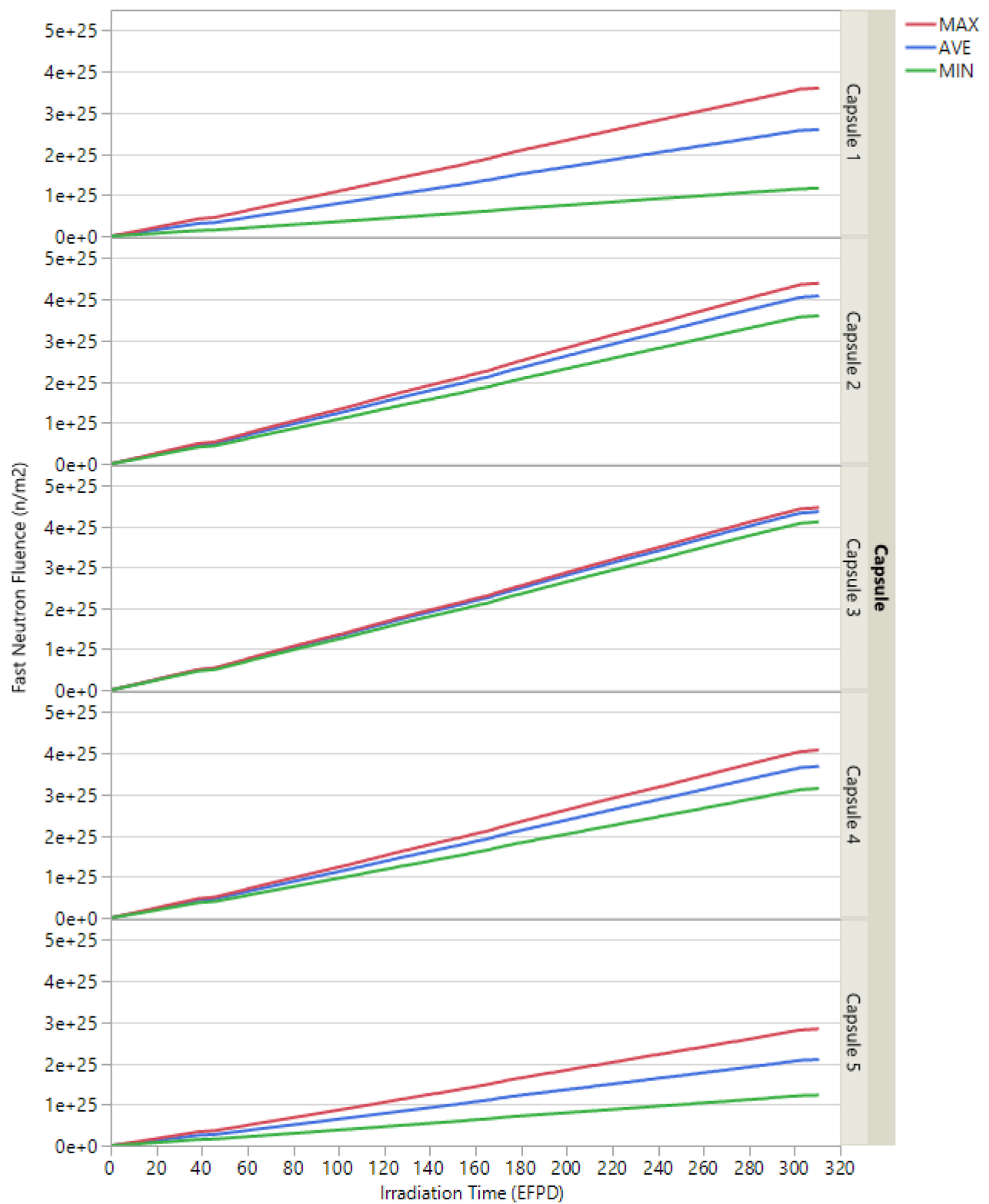
Figure 29. Fast neutron fluence (E >0.18 MeV) versus irradiation time in EFPD.

5.2.2   As-Run Thermal Analysis Results

The AGR-5/6/7 thermal model provides detailed temperatures calculated for each finite-element volume of 194 fuel compacts for each time step (or each day). These temperatures are used to calculate instantaneous and time-averaged minimum, volume-averaged, and peak fuel temperatures per compact and per capsule, which are presented in Figure 30 and Figure 31, respectively. The instantaneous fuel temperatures remained relatively constant only in Capsules 1 and 2, except for the first 10 days of 162B and the two low-power PALM cycles 163A and 167A. The daily peak temperature from all capsules is 1536°C (fuel compacts in Capsule 3), which is well below the specification of 1800°C. Thus, this constraint was met in all capsules (as can be seen in Figure 30).

According to history plots of neutronics parameters in Figure 27 through Figure 29, during the two low-power PALM cycles (163A and 165A), compact fission power, burnup, and fluence in all capsules are significantly lower than other remaining cycles. This is because the ATR NE lobe power, where AGR-5/6/7 test train was located, was only ~5MW instead of the normal 17-20 MW range, except for the last day of the cycle. During these two low-power cycles, the AGR-5/6/7 fuel compacts accumulated very insignificant burnup in the range from 0.15 (Capsules 1 and 5) to 0.30 % FIMA (Capsules 2, 3, and 4) per capsule on average. In addition, the low fission powers during these power cycles led to significantly lower fuel temperatures in all capsules.

Therefore, the time-average temperature calculations were performed for two scenarios: the first one included all days of irradiation and the second one excluded two low-power PALM cycles (163A and 167A). The daily plots of time-average fuel temperatures are presented in Figure 31 for both scenarios. The time-average values of the volume-average and peak compact temperature at the end of Cycle 167A for both scenarios are also presented in Table 9 for each capsule and each experiment. The exclusion of two low-power PALM cycles increases time-average temperatures between 20 to 30 °C by the end of irradiation. The minimum, volume-averaged and peak values of time-averaged temperatures at the end of Cycle 167A for each of 194 compacts are presented in Appendix A for both scenarios for easy reference.

Table 9. Compact temperature per capsule and experiment at the end of 167A.

Capsule and Experiment	Time-Averaged Minimum Temperature (°C)	Time-Averaged Volume-Averaged Temperature (°C)	Time-Averaged Peak Temperature (°C)
All Capsule 5 compacts	458 / 469	736 / 753	840 / 860
All Capsule 4 compacts	546 / 561	838 / 859	948 / 973
All Capsule 2 compacts	532 / 545	811 / 831	924 / 946
All Capsule 1 compacts	611 / 623	1018 / 1040	1243 / 1270
All AGR-5/6 compacts	**458 / 469**	**914 / 934**	**1243 / 1270**
All AGR-7 Capsule 3 compacts	**964 / 989**	**1288 / 1318**	**1407 / 1439**

The detailed daily fuel temperatures are used to calculate fractions of fuel that were exposed to each temperature range to compare against fuel-temperature specifications. By the end of Cycle 163A, the estimated fuel compact proportions within several pre-defined temperature ranges were lower than specifications for both AGR-5/6 and AGR-7 experiments. Therefore, to increase fuel temperatures in Capsules 4 and 5 after 110 EFPDs, the control TC setpoints in these capsules were increased by 90°C from Cycle 164B to the end of irradiation and the control TC setpoint in Capsule 3 was also increased by 50°C starting two-thirds of the way through Cycle 166A. The fractions of fuel exposed to each time-average temperature range and contributing capsules by the end of Cycle 167A are presented in Table 10 together with corresponding specifications. The following conclusions can be drawn:

- For AGR-5/6 fuel compacts, the actual fuel proportions are close to specifications for the two middle temperature ranges. Fuel proportions are lower than the specification of 10% for the highest temperature range due to lower Capsule 1 temperatures especially towards the end of irradiation. Fuel proportions are higher than the specification of 30% for the lowest temperature range due to lower temperatures in Capsules 2 and 4. All fuel compacts in Capsule 5 contributed to this lowest temperature range because the time-average peak fuel temperature in Capsule 5 was less than 900°C by the end of irradiation, as shown in Figure 31. Also, less than 1% of AGR-5/6 fuel experienced time-average temperature lower than 600°C.

- For AGR-7 Capsule 3 compacts, the time-average peak fuel temperature by the end of irradiation was near the lower bound of the specification if temperatures during the two low-power cycles were excluded.

Table 10. Time-averaged temperatures at the end of 167A (Note: fuel distribution calculation excludes extreme low-temperature periods at the beginning of the first cycle 162B and the PALM cycles 163A and 167A).

| Temperature range	Contributing capsule(s)	Actual data	Specification
AGR-5/6 Experiment – Capsules 1, 2, 4, and 5			
≥ 600 °C and < 900 °C	1, 2, 4, 5	41.0%	30%
≥ 900 °C and < 1050 °C	1, 2, 4	25.0%	30%
≥ 1050 °C and < 1250 °C	1	30.6%	30%
≥ 1250 °C and < 1400 °C	1	1.2%	10%
Time average, peak temperature		1243 °C	1350 ± 50 °C
Time average, minimum temperature		458 °C	≤700 °C
AGR-7 Experiment – Capsule 3			
Time average, peak temperature		1439 °C	1500 ± 50 °C
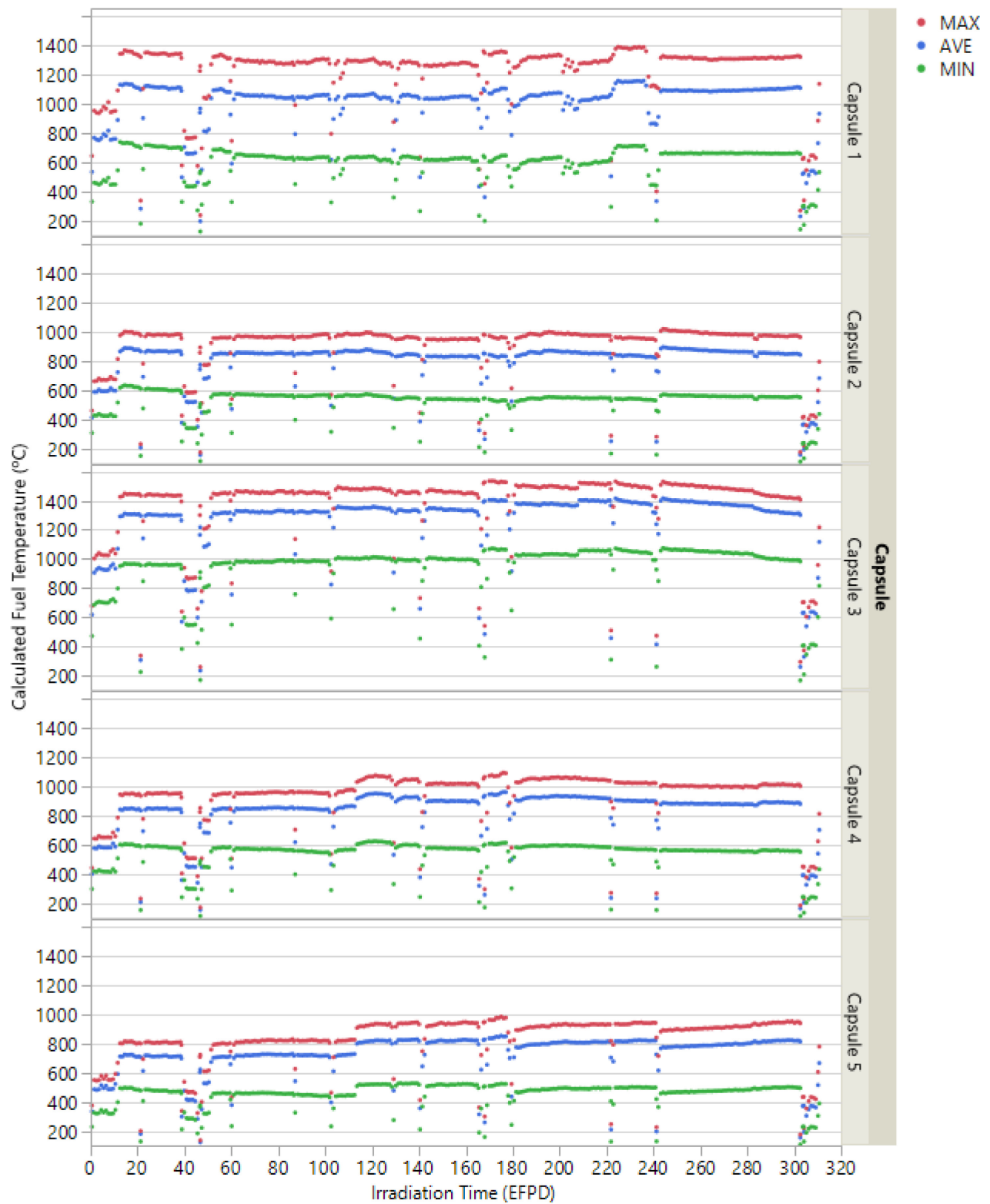
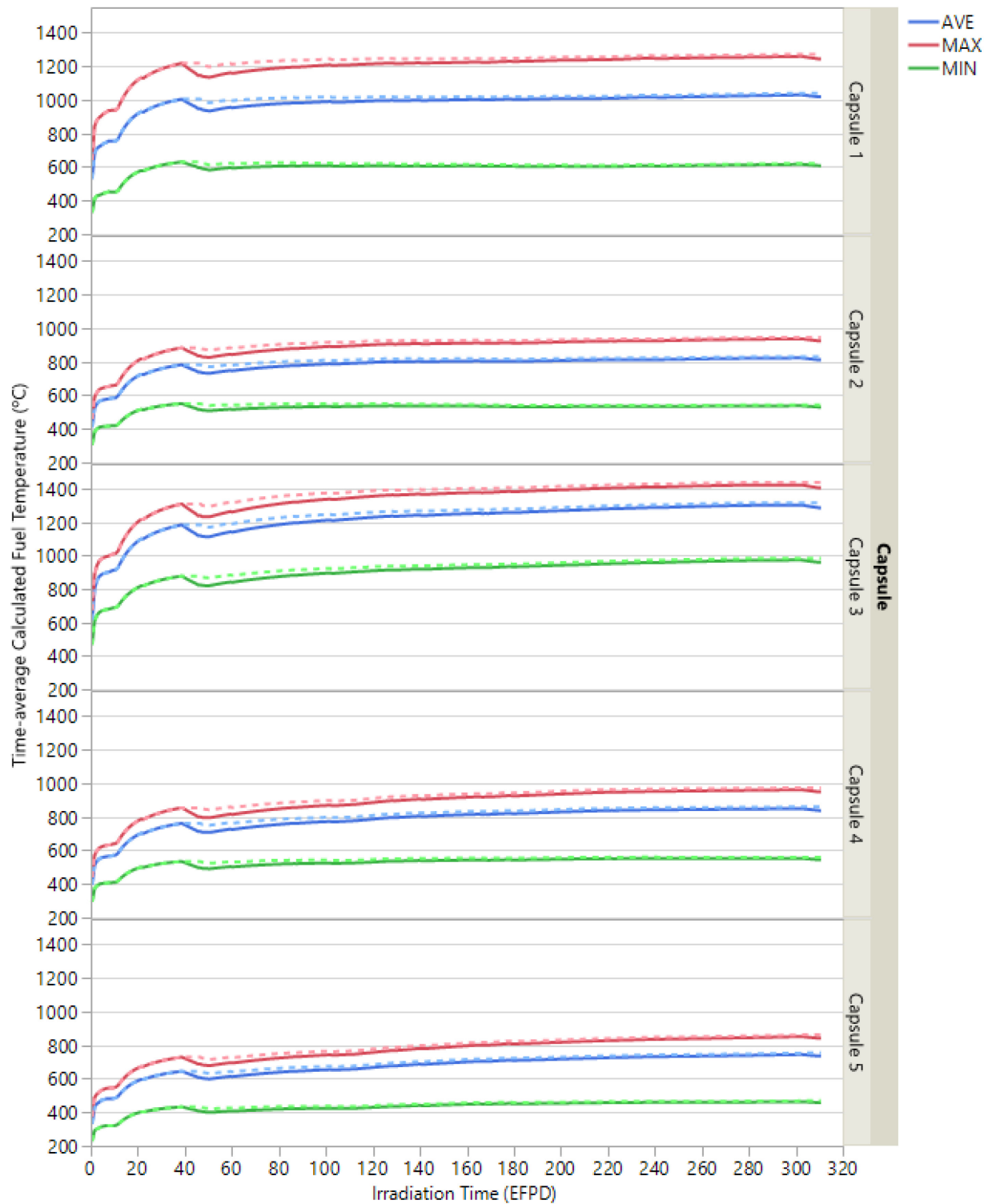Figure 30. Calculated daily minimum, maximum, and volume-averaged fuel temperatures.

Figure 31. Calculated time-averaged minimum, time-averaged maximum, and time-averaged volume-averaged fuel temperatures: solid lines are included all days and dashed lines are excluded two low-power PALM cycles 163A and 167A.

5.3 Fuel Temperature Control

A range of irradiation fuel temperatures were specified for each AGR-5/6/7 capsule to achieve the desired fuel-compact temperature distribution in the test train [per SPC-1352 (Marshall 2017)]. The goal for AGR-5/6 was to adequately bound the irradiation conditions expected in an HTGR, which led to time-averaged target irradiation temperatures from less than 900°C to over 1250°C that will conservatively span the range expected in a prismatic reactor. The primary goal of AGR-7 was to demonstrate the available performance margin with respect to temperature for UCO fuel; thus, its fuel was tested at a higher time-averaged peak temperature target of 1500°C. To shape the temporal and spatial fuel power distribution (subsequently, fuel temperature distribution) in the capsules, two techniques are used to adjust the neutron-flux incident to the AGR 5/6/7 test train. These techniques include placing a neutron filter around the capsules and raising the power throughout the irradiation, as discussed in Section 2.1.

Before irradiation, preliminary neutronics and thermal analyses were performed for AGR-5/6/7 capsules based on the original 13-cycle schedule, as documented in ECAR-2961 (Sterbentz, 2017) and ECAR-2966, respectively. Besides confirming the AGR-5/6/7 requirements of fast fluence and burnup are met, the neutronics analysis provides heat rates and fast fluence for input to the thermal models. In turn, the thermal analysis provides confirmation that the chosen gas-gap widths and gas mixtures will allow the test fuel to meet the temperature requirements. The predicted fuel and TC temperatures were also used to determine corresponding setpoint temperatures for the designated control TC for each capsule. Besides the primary control TC, two TCs additional were selected as a backup and second backup TC for use in the event of primary TC failure. Corresponding setpoint temperatures are also defined to these backup TCs.

During irradiation, instantaneous temperature control is based on temperature feedback from the designated control TC for each capsule and is performed by varying the sweep-gas composition (between 100% helium for high conductivity and 100% neon for low conductivity). A single blend of inert gases from a capsule-specific gas controller is routed by an independent gas line to each capsule to provide temperature control.

The control TC setpoints were periodically adjusted in response to changing events in a capsule, including TC drift, irradiation-induced changes in gas-gap widths and material thermal conductivities, and replacement of the designated control TC due to failure. These TC setpoint adjustments were based on fuel temperatures, as calculated by the as-run thermal analysis. After completion of each cycle, the as-run thermal analysis is performed based on the fast fluence and heat rate (predicted by the as-run neutronics analysis using actual ATR operating conditions) and actual neon/helium gas mixtures in AGR-5/6/7 capsules. Calculated fuel temperatures were compared against requirements, as shown by plots in Figure 32 for AGR-5/6 and Figure 33 for AGR-7. The contribution of the fuel portion from each capsule to each temperature range was color-coded and displayed in these interactive plots. Based on these plots, control TC setpoints were adjusted accordingly to improve the match with fuel-temperature requirements.

The AGR-5/6/7 TCs performed consistently with previous AGR irradiation experiments: of the 54 installed TCs, 48 had failed by the end of Cycle 168A. The six surviving TCs are in the top two Capsules 4 and 5, so they were used to maintain fuel temperature as intended. The three bottom capsules had no operational TCs left (i.e., Capsules 1 from Cycle 166B, Capsule 2 from Cycle 167A, and Capsule 3 from 168A). When all TCs failed in a capsule, the appropriate neon fraction was determined based on the thermal models so fuel temperatures could be maintained as close to specified levels as possible. The exception was Capsule 1 during the last cycle 168A, when its gas line was totally isolated. Thus, Capsule 1 neon fraction was not well-defined and had to be bounded by neon fraction in the leadout, including portions of outflow gas from Capsules 2-5.

For the AGR-5/6 capsules (1, 2, 4, and 5), the low portion of fuel in the middle range of temperatures (i.e., 900–1050°C) at the end of Cycle 164A (see Figure 32) prompted the first TC setpoint adjustment on

September 30, 2018 (Cycle 164B), when the control TC setpoints for Capsules 4 and 5 were raised by 90°C to increase fuel temperatures. As a result, the portion of AGR-5/6 fuel in the 900–1050°C range increased from 20 to 25.7%, which is closer to the 30% requirement. In addition, the TC setpoint in Capsule 2 has been increased by 40°C from Cycle 166A. On the other hand, the decreasing fraction of fuel for the highest range (i.e., 1250–1350°C) is caused by a decrease in Capsule 1 fuel temperatures over time. To meet the requirement for this temperature range, the TC setpoint for Capsule 1 was increased by 70°C for the last one-third of Cycle 166A. However, the last TC in Capsule 1 failed during Cycle 166A and flow issues were worsening over the last three cycles, causing fuel temperature to drop back below the target temperature.

Figure 32. Time-averaged fuel temperature fraction by range for AGR-5/6 capsules (excluded two low-power PALM cycles 163A and 167A).

54

By the end of the fourth cycle, 164B, the time-averaged fuel temperature for AGR-7 Capsule 3 was about 120°C less than specification. Therefore, the TC setpoint for Capsule 3 was increased by 50°C beginning with Cycle 166A. As a result, the calculated time-averaged peak fuel temperature by the end of Cycle 167A was only ~60°C lower than the specification if Cycles 163A and 167A were excluded from time-averaging: 1439°C calculated versus 1500°C required, as shown in Table 10. Figure 33 also shows ~4.05% of Capsule 3 fuel experienced time-averaged temperature >1450°C range by the end of Cycle 166B.
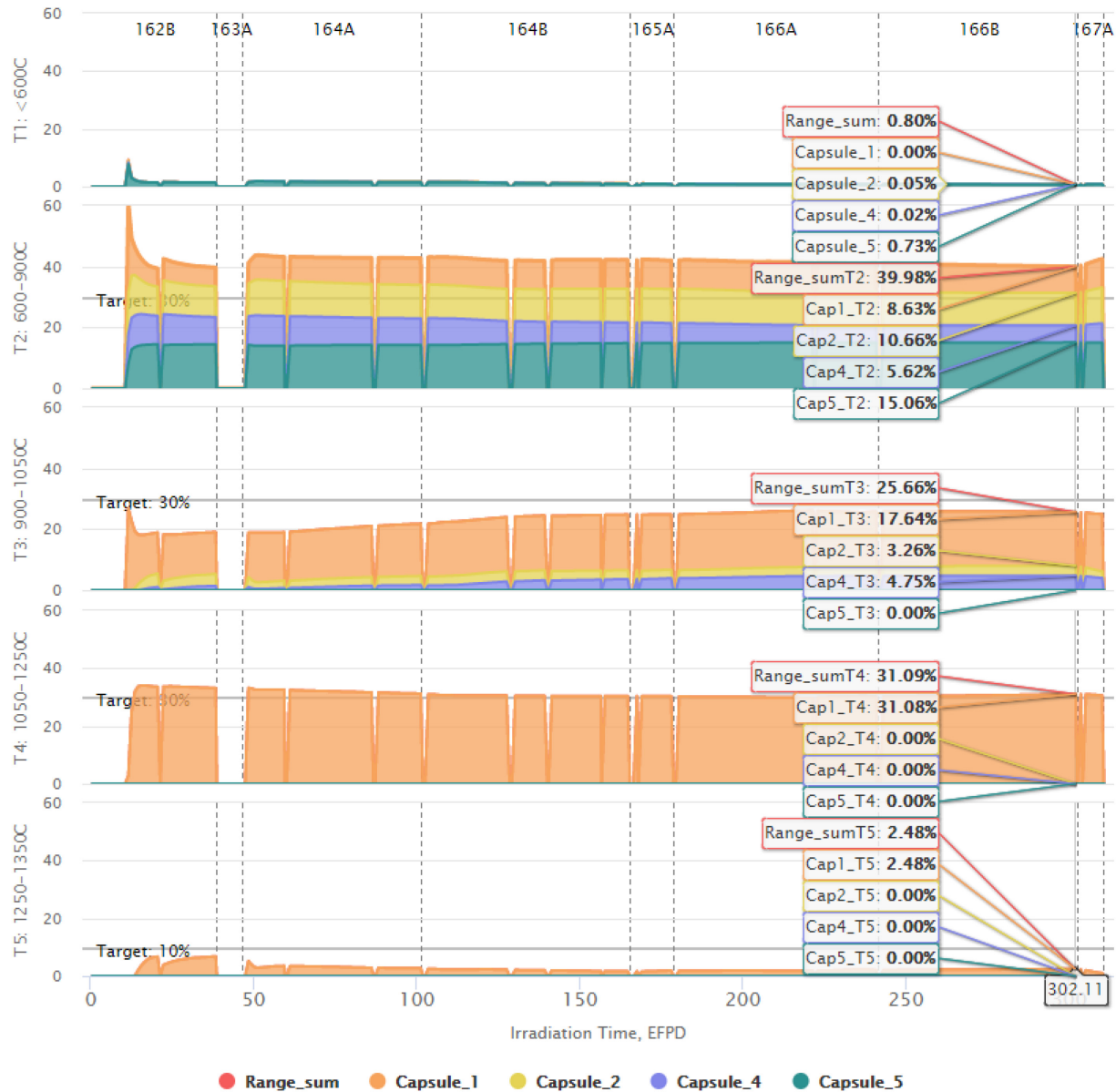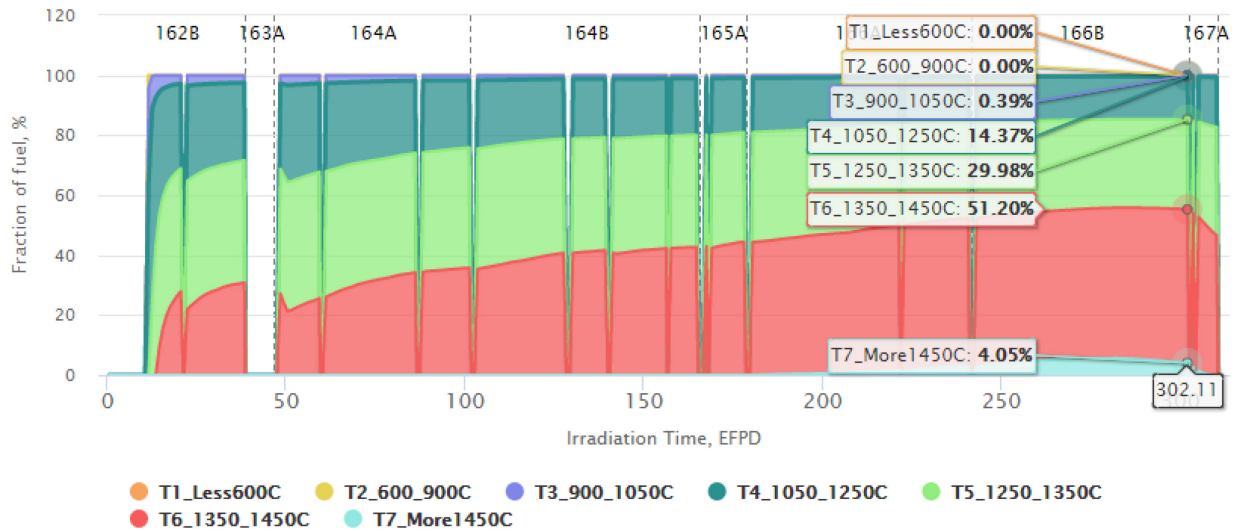

Figure 33. Time-averaged fuel-temperature fraction by range for AGR-7 capsule 3 (excluded two low-power PALM cycles 163A and 167A).

6.   CONCLUSION

The AGR 5/6/7 fuel test has been irradiated for nine complete cycles (four short of the planned 13-cycle schedule), resulting in approximately 360 EFPDs. At the end of Cycle 167A, burnup, fast fluence, and temperature histories may be summarized as follows:

- Capsule-average burnups ranged from 6.95% FIMA in Capsule 5 to 12.68% FIMA in Capsule 2

- Capsule-average fast fluences ranged from 2.10×10^{25} n/m^2 in Capsule 5 to 4.37×10^{25} n/m^2 in Capsule 3

- For AGR-5/6 capsules (1, 2, 4, and 5), the time-averaged volume-averaged fuel temperatures, on a capsule basis, at the end of the four completed irradiation cycles ranged from 753°C in Capsule 5 to 1040°C in Capsule 1, when temperatures during the two low-power PALM cycles were excluded. The actual fuel proportions are close to the specification of 30% for the two middle temperature ranges (between 900 °C and 1250 °C); lower than the specification of 10% for the highest temperature range ($\geq$ 1250 °C); and higher than the specification of 30% for the lowest temperature range (< 900 °C).

- For AGR-7 Capsule 3, the time-averaged peak fuel temperature is 1439°C (close to the specification of 1500 ± 50 °C) when data from the two low-power PALM cycles were excluded from time averaging.

The TCs performed consistently with previous AGR irradiation experiments: of the 54 installed TCs, 48 had failed by the end of Cycle 168A. The six surviving TCs are in the top two Capsules 4 and 5, so they were used to maintain their fuel temperatures as intended. The three bottom capsules had no operational TCs left (i.e., Capsules 1 from Cycle 166A, Capsule 2 from Cycle 167A, and Capsule 3 from 168A). When all TCs failed in a capsule, the appropriate neon fraction was determined based on thermal models so fuel temperatures could be maintained within specified range. The exception was Capsule 1 during the last cycle 168A, when its gas line was totally isolated. Thus, Capsule 1 neon fraction was bounded by neon fraction in the leadout, including portions of outflow gas from Capsules 2-5.

During the first five cycles (162B – 165A), fission-gas isotope R/B ratios were stable in the 10^{-8}–10^{-6} range and no in-pile particle failures were observed based on the GG counts. During this time, the higher exposed kernel fraction and high fuel particle temperatures in Capsule 1 led to the maximum R/B value of around 2×10^{-6} for Kr-85m.

The gas line issues in Capsule 1 occurred from the fourth cycle (164B) and were rigorously mitigated to minimize crosstalk between capsule gas lines. Capsule 1 fission-product release measurements were not possible during the last three cycles (166B, 167A, and 168A) due to its gas flow isolation. Capsule 1 gas line issues still caused FG leakage to the other four capsules to various degrees over time starting from Cycle 166A. By the end of Cycle 166A, a significant number of in-pile failures occurred in Capsule 1, causing a substantial increase in FG activities. In addition, numerous particle failures were also observed in Capsule 3 and perhaps a small number of failures might have occurred in Capsule 2 during Cycle 168A. No in-pile failures are likely in the top two capsules (4 and 5) based on the absence of typical spikes in GG counts and low failure estimates by the end of Cycle 168A using the AGR-3/4 R/B per EK model. Increased and unstable R/Bs in Capsules 4 and 5 can be contributed to FG leakage from Capsule 1.

The results of this test will provide irradiation-performance data for the reference fuel manufactured at pilot scale for a typical HTGR temperature range (AGR-5/6) as well as at temperatures beyond the normal range (AGR-7). Together with previous AGR data, AGR-5/6/7 data will form a link between fabrication processes, fuel-product properties, and irradiation performance.

7.   REFERENCES

Abaqus, 2014. Abaqus Version 6.14-2 documentation. Dassault Systèmes.

ASTM, 2014. *Standard practice for testing graphite and boronated graphite materials for high-temperature gas-cooled nuclear reactor components*. Designation C781-08, ASTM International, West Conshohocken, Pennsylvania.

Collin B.P., 2018, "AGR-5/6/7 Irradiation Experiment Test Plan," PLN-5245, Rev. 1, January 25, 2018.

Croff, A.G., 1983, "ORIGEN2: A Versatile Computer Code for Calculating the Nuclide Compositions and Characteristics of Nuclear Materials", *Nuclear Technology*, Vol. 62, pp. 335–352.

Demkowicz P. and B.T. Pham, "Fission Gas Activity Criteria for Operation of the AGR-5/6/7 Experiment in the Advanced Test Reactor," ECAR-4802, Rev. 0, December 2019.

Folsom, C., C. Xing, C. Jensen, H. Ban, and D.W. Marshall, 2015. "Experimental measurement and numerical modeling of the effective thermal conductivity of TRISO fuel compacts," *Journal of Nuclear Materials*, 458, 198–205.

Gontard, R. and H. Nabielek, 1990. *Performance Evaluation of Modern HTR TRISO Fuels*. Report HTA-IB-05/90, Forschungszentrum Jülich GmbH (FZJ).

Gonzo, E.E., 2002. "Estimating Correlations for the Effective Thermal Conductivity of Granular Materials," *Chemical Engineering Journal*, 90, 299–302.

Hawkes, G.L., J. W. Sterbentz, and M. Plummer, 2019, "Thermal Model Details and Description of the AGR-5/6/7 Experiment," *ICAPP 2019 – International Congress on Advances in Nuclear Power Plants, France, Juan-les-pins, May 12-15, 2019*.

Kestin, J., K. Knierim, E.A. Mason, B. Najafi, S.T. Ro, and M. Waldman, 1984. "Equilibrium and Transport Properties of the Noble Gases and Their Mixtures at Low Density," *Journal of Physical and Chemical Reference Data,* 13, 229–303.

LANL, X-5 Monte Carlo Team, 2004, *MCNP—A General Monte Carlo N-Particle Transport Code, Version 5*, Volume I, LA-UR-03-1987, Los Alamos National Laboratory, April 24, 2003 (Revised 6/30/2004) and Volume II, LA-CP-0245, Los Alamos National Laboratory, April 24, 2003 (Revised 6/30/2004).

Lybeck, N.J., 2016, "Nuclear Data Management and Analysis System Plan", PLN-2709 Rev. 5, January 18, 2016.

Marshall D.W., 2017, "AGR-5/6/7 Fuel Specification," SPC-1352, Rev. 8, March 9, 2017.

Murray P.E., 2018, "Thermal Analysis of the AGR-5-6-7 Experiment," ECAR-2966, Rev.5, October 23, 2018.

Pham B.T. and Scates D.M., 2019, "AGR-5/6/7 Release-to-Birth Ratio Data Analysis for Cycles 162B, 163A, 164A, and 164B," INL/EXT-19-54457, Rev. 0, June 2019.

Pham, B.T., Einerson, J.J., Scates, D.M., Maki, J.T., and Petti, D.A., 2019, AGR-1, AGR-2 and AGR-3/4 Release-to-Birth Ratio Data Analysis, INL/EXT-14-32970, Rev. 2, May 2019.

PLN-3636, 2020, "Technical Program Plan for INL Advanced Reactor Technologies Advanced Gas Reactor Fuel Development and Qualification Program," Rev. 9, June 25, 2020.

Scates, D.M., 2010, "Fission Product Monitoring and Release Data for the Advanced Gas Reactor 1 Experiment," *Proceedings HTR 2010, Prague, Czech Republic, October 18–20, 2010*, Paper 52.

Scates, D.M., 2021, "Release-to-Birth Ratios for AGR-5/6/7 Operating Cycles 162B through 168A", ECAR-5352, Revision 0, May 2021.

Shibata T., Motokuni Eto, Eiji Kunimoto, Shusaku Shiozawa, Kazuhiro Sawa, Tatsuo Oku and Tadashi Maruyama, *Draft of Standard for Graphite Core Components in High Temperature Gas-cooled Reactors,* Japan Atomic Energy Agency Research 2009-042, Jan 2010.

Sterbentz, J.W., "JMOCUP As-Run Daily Depletion Calculation for the AGR-3/4 Experiment in the ATR Northeast Flux Trap," ECAR-2753, Rev. 1, Idaho National Laboratory, July 25, 2015.

Sterbentz, J.W., 2017, "JMOCUP Physics Depletion Calculation for the Design of the AGR-5/6/7 TRISO Particle Experiment in ATR Northeast Flux Trap," ECAR-2961, Rev.1, June 13, 2017.

Sterbentz, J.W., 2020, "JMOCUP Physics Depletion Calculation for the As-Run AGR-5/6/7 TRISO Particle Experiment in ATR Northeast Flux Trap," ECAR-5321, Rev. 0, Idaho National Laboratory, December 8, 2020.

Swank D., Lord J., Rohrbaugh D., and Windes W., 2012, "AGC-2 Graphite Pre-irradiation Data Package," INL/EXT-10-19588, Rev 1, October 9, 2012.

Windes, W.E., Rohrbaugh, D.T., and Swank, D.W., 2017, "AGC-2 Irradiated Material Properties Analysis," INL/EXT-17-41165, May 22, 2017.

Windes, W.E., W. D. Swank, D. Rohrbaugh, and J. Lord, 2013, "AGC-2 Graphite Preirradiation Data Analysis Report," INL/EXT-13-28612, Rev 1, August 7, 2013.

Windes, W.E., 2012, "Data Report on Post-Irradiation Dimensional Change of AGC-1 Samples," INL/EXT-12-26255, June 27, 2012.

APPENDIX A

Capsule 1 Gas Flow Operating History

The following is a log of the gas flow operating history in response to gas line issues in Capsule 1:

- Capsule 1 inlet flow was set to 60 sccm almost from the start of the irradiation until the first week after powerup for Cycle 164B (the fourth cycle). Capsule 1 was the only capsule designed to have no communication with the lead-out. The outlet-flow rate (blue line) was slightly lower than the inlet (red line). Ideally, these two flows should have been identical. The slight difference is likely due to calibration errors between the two instruments.

- The clog, which developed in the Capsule 1 outlet line during Cycle 164B, led the program to periodically shut off the gas flow through this capsule from September 23 to October 16, 2018, while maintaining the same gas mixture to keep the capsule temperature as close to the specification as possible. During this time, no fission-gas release measurements were possible for Capsule 1 because of the intermittent nature of the flow.

- Beginning October 16, 2018, gas flow in Capsule 1 was re-established at 11 sccm, which resulted in a stable capsule-inlet pressure. This enabled resumption of the measurement of fission-gas release from Capsule 1.

- At the beginning of the following cycle (PALM cycle 165A), a sudden increase in the Capsule 1 outlet flow was observed. This was attributed to a crack or break in the outlet line at a point downstream of the clog. Gas flows to the other capsules were increased to compensate for this new path out of the test. Also, the lead-out flow was increased to 50 sccm (and then 60 sccm) to ensure lead-out flow was entering Capsules 2–5. During the outage of the following cycle (166A) the inlet- and outlet-gas lines for Capsule 1 were swapped to prevent FGs released by Capsule 1 from spilling to the lead-out and entering other capsules. In this new configuration, Capsule 1 inlet gas has the potential of mixing with the lead-out gas due to 'now-inlet' gas line crack or break. Therefore, the neon/helium mixture for the lead-out and Capsule 1 was kept the same, and this allows the Capsule 1 neon fraction to be accurately defined.

- As Cycle 166A progressed, evidence was obtained indicating the hole in the (now) Capsule 1 inlet line was a crack, rather than a complete severing. This is because gas-blend changes on Capsule 1 were reflected very quickly on the control TC readings. If the opening in the line were a complete break, we would expect gas blend changes to be seen slowly in the capsule because of the mixing that would take place in the lead-out. Additionally, as the cycle progressed, the clog appeared to be clearing. The indications are (1) on July 31, 2019 at 3:00, the outlet flow on Capsule 1 more than doubled, indicating a piece of material making up the clog had broken loose; (2) subsequent to that event, the flow continued to gradually increase for approximately 11 days; and (3) at that point (August 11 @1:00), the flow and pressure in Capsule 1 began a slow exponential rise. Although, no mechanism for this has been identified, the evidence was that the crack was closing: more flow was being forced through Capsule 1. Flows and pressures in the other capsules showed corresponding drops.

- From August 16, 2019 (166A), a new clog started to develop in the new Capsule 1 outlet gas line causing a sudden increase in pressure, which prompted operators to shut down flow to Capsule 1. After that date Capsule 1 flow became intermittent to avoid exceeding pressure operating limit while still have some fission gas release measurements.

- For Cycle 166B, because the gas line situation in Capsule 1 was getting worse and a substantial increase in FGs at Capsule 1 detector was seen due to possible in-pile particle failures toward the end of Cycle 166A, the flow to Capsule 1 was isolated during Cycle 166B. At the same time, to prevent FGs in Capsule 1 from entering other capsules, the leadout outlet was opened and pressures in Capsules 2-5 were increased higher than Capsule 1 and the leadout. Capsules 2-5 were isolated for half of this cycle.

- During the short PALM cycle, 167A, to resume measurement of FG release from Capsule 1 the gas relieve valve was opened and a small flow of ~5 sccm was delivered to Capsule 1. However, the outlet gas line was completely clogged resulting in zero Capsule 1 outlet flow.

- For Cycle 168A, during a few days right after powering up, the Capsule 1 inlet flow started with 15 sccm but a (suspected) completely clogged outlet gas line led to zero outlet flow. This caused substantial increase in FG activities in all other four capsules, which indicated leakage of Capsule 1 FGs to Capsules 2-5. Therefore, Capsule 1 inlet flow was gradually dropped to zero for the remainder of this cycle, resulting in a decrease in FG activities in other four capsules.

APPENDIX B

Compact Time-averaged Temperature, Burnup, and Fast Neutron Fluence at the End of 167A

The low fission powers during the two low-power PALM cycles (163A and 167A) led to significantly lower fuel temperatures in all capsules. Therefore, the time-average temperature calculations were performed for two scenarios: the first one included all days of irradiation and the second one excluded two low-power PALM cycles. The time-average fuel temperatures in Table 11 for both scenarios.

Table 11. Compact time-averaged temperature, burnup, and fast neutron fluence at the end of 167A.

Capsule	Compact	Time-averaged Minimum Temperature (°C)	Time-Averaged Volume-averaged Temperature (°C)	Time-Averaged Peak Temperature (°C)	Burnup (% FIMA)	Fast neutron Fluence (10^{25} n/m^2, E >0.18MeV)
Capsule 5	5-1-1	489 / 500	691 / 708	797 / 817	7.77	2.66
Capsule 5	5-1-2	489 / 500	690 / 708	796 / 816	7.77	2.64
Capsule 5	5-1-3	495 / 507	702 / 719	811 / 831	7.94	2.76
Capsule 5	5-1-4	496 / 508	701 / 719	810 / 830	7.97	2.78
Capsule 5	5-2-1	683 / 700	769 / 787	822 / 842	7.53	2.45
Capsule 5	5-2-2	683 / 699	768 / 786	821 / 841	7.52	2.44
Capsule 5	5-2-3	693 / 710	781 / 800	835 / 855	7.64	2.55
Capsule 5	5-2-4	693 / 710	780 / 799	834 / 855	7.65	2.56
Capsule 5	5-3-1	704 / 721	779 / 798	825 / 845	7.17	2.21
Capsule 5	5-3-2	704 / 720	778 / 797	825 / 844	7.16	2.2
Capsule 5	5-3-3	714 / 731	791 / 810	838 / 858	7.30	2.3
Capsule 5	5-3-4	714 / 731	790 / 809	838 / 859	7.31	2.31
Capsule 5	5-4-1	720 / 737	784 / 803	826 / 846	6.75	1.96
Capsule 5	5-4-2	720 / 737	785 / 803	826 / 846	6.73	1.95
Capsule 5	5-4-3	731 / 748	797 / 816	839 / 859	6.93	2.03
Capsule 5	5-4-4	731 / 748	797 / 816	840 / 860	6.93	2.04
Capsule 5	5-5-1	659 / 675	740 / 758	805 / 824	6.26	1.68
Capsule 5	5-5-2	658 / 674	740 / 758	805 / 825	6.27	1.68
Capsule 5	5-5-3	668 / 684	751 / 770	818 / 838	6.46	1.75
Capsule 5	5-5-4	669 / 685	752 / 771	819 / 839	6.49	1.75
Capsule 5	5-6-1	459 / 470	618 / 633	719 / 737	5.65	1.37
Capsule 5	5-6-2	458 / 469	616 / 631	718 / 736	5.65	1.37

Capsule	Compact	Time-averaged Minimum Temperature (°C)	Time-Averaged Volume-averaged Temperature (°C)	Time-Averaged Peak Temperature (°C)	Burnup (% FIMA)	Fast neutron Fluence (10^{25} n/m^2, E >0.18MeV)
Capsule 5	5-6-3	465 / 476	626 / 641	730 / 748	5.91	1.42
Capsule 5	5-6-4	465 / 476	627 / 642	731 / 749	5.93	1.43
Capsule 5 compacts		**458 / 469**	**736 / 753**	**840 / 860**	**6.95**	**2.10**
Capsule 4	4-1-1	547 / 561	755 / 775	865 / 887	11.82	3.87
Capsule 4	4-1-2	546 / 561	754 / 774	864 / 886	11.77	3.85
Capsule 4	4-1-3	554 / 568	768 / 788	880 / 903	12.09	4.05
Capsule 4	4-1-4	554 / 569	767 / 787	879 / 902	12.12	4.07
Capsule 4	4-2-1	751 / 770	848 / 870	911 / 934	11.79	3.79
Capsule 4	4-2-2	750 / 770	848 / 869	910 / 934	11.78	3.77
Capsule 4	4-2-3	763 / 782	863 / 885	927 / 951	12.08	3.97
Capsule 4	4-2-4	762 / 782	862 / 884	926 / 950	12.12	3.99
Capsule 4	4-3-1	787 / 806	874 / 897	929 / 952	11.65	3.69
Capsule 4	4-3-2	786 / 806	874 / 896	928 / 952	11.63	3.68
Capsule 4	4-3-3	799 / 818	889 / 911	943 / 967	11.90	3.87
Capsule 4	4-3-4	798 / 818	888 / 911	944 / 968	11.95	3.88
Capsule 4	4-4-1	808 / 828	888 / 910	933 / 957	11.37	3.57
Capsule 4	4-4-2	807 / 827	887 / 909	933 / 956	11.35	3.56
Capsule 4	4-4-3	819 / 839	900 / 923	947 / 971	11.63	3.74
Capsule 4	4-4-4	819 / 840	901 / 924	948 / 973	11.66	3.76
Capsule 4	4-5-1	772 / 792	864 / 886	925 / 949	11.01	3.43
Capsule 4	4-5-2	770 / 790	862 / 884	924 / 948	11.00	3.42
Capsule 4	4-5-3	781 / 801	875 / 897	938 / 962	11.25	3.59
Capsule 4	4-5-4	782 / 801	876 / 898	940 / 964	11.29	3.61
Capsule 4	4-6-1	567 / 582	763 / 783	869 / 892	10.58	3.25
Capsule 4	4-6-2	566 / 581	761 / 781	867 / 890	10.56	3.24
Capsule 4	4-6-3	573 / 588	772 / 792	880 / 903	10.80	3.4
Capsule 4	4-6-4	574 / 588	773 / 793	882 / 904	10.83	3.42
Capsule 4 compacts		**546 / 561**	**838 / 859**	**948 / 973**	**11.50**	**3.69**
Capsule 2	2-1-1	532 / 545	730 / 748	836 / 856	11.61	3.68
Capsule 2	2-1-2	532 / 545	730 / 748	836 / 857	11.62	3.68
Capsule 2	2-1-3	539 / 552	742 / 760	851 / 872	11.89	3.87
Capsule 2	2-1-4	539 / 551	740 / 758	848 / 869	11.88	3.87
Capsule 2	2-2-1	723 / 740	822 / 841	889 / 910	12.10	3.81
Capsule 2	2-2-2	724 / 740	822 / 842	889 / 910	12.09	3.8
Capsule 2	2-2-3	735 / 752	836 / 856	905 / 926	12.38	4

Capsule	Compact	Time-averaged Minimum Temperature (°C)	Time-Averaged Volume-averaged Temperature (°C)	Time-Averaged Peak Temperature (°C)	Burnup (% FIMA)	Fast neutron Fluence (10^{25} n/m^2, E >0.18MeV)
Capsule 2	2-2-4	733 / 750	834 / 853	902 / 924	12.38	4
Capsule 2	2-3-1	763 / 781	851 / 871	906 / 927	12.42	3.91
Capsule 2	2-3-2	763 / 781	851 / 871	906 / 928	12.41	3.9
Capsule 2	2-3-3	775 / 793	866 / 887	923 / 945	12.69	4.11
Capsule 2	2-3-4	774 / 791	864 / 884	920 / 942	12.71	4.11
Capsule 2	2-4-1	759 / 776	853 / 872	906 / 928	12.63	3.99
Capsule 2	2-4-2	759 / 776	853 / 873	907 / 928	12.64	3.98
Capsule 2	2-4-3	772 / 789	869 / 889	924 / 946	12.92	4.19
Capsule 2	2-4-4	770 / 787	866 / 886	921 / 943	12.93	4.19
Capsule 2	2-5-1	730 / 746	829 / 849	893 / 914	12.79	4.06
Capsule 2	2-5-2	730 / 746	830 / 850	894 / 915	12.79	4.05
Capsule 2	2-5-3	742 / 758	846 / 865	911 / 933	13.08	4.27
Capsule 2	2-5-4	741 / 757	843 / 863	909 / 930	13.08	4.27
Capsule 2	2-6-1	722 / 738	816 / 835	874 / 895	12.88	4.12
Capsule 2	2-6-2	722 / 738	817 / 836	875 / 896	12.88	4.11
Capsule 2	2-6-3	733 / 750	831 / 850	891 / 912	13.19	4.33
Capsule 2	2-6-4	732 / 749	829 / 849	890 / 911	13.19	4.33
Capsule 2	2-7-1	702 / 718	802 / 821	865 / 885	12.91	4.16
Capsule 2	2-7-2	701 / 717	802 / 821	865 / 886	12.92	4.15
Capsule 2	2-7-3	712 / 728	815 / 834	880 / 901	13.22	4.37
Capsule 2	2-7-4	711 / 728	814 / 833	879 / 900	13.23	4.37
Capsule 2	2-8-1	539 / 551	736 / 754	836 / 857	12.90	4.17
Capsule 2	2-8-2	537 / 550	735 / 753	836 / 856	12.90	4.17
Capsule 2	2-8-3	545 / 558	747 / 765	850 / 871	13.19	4.39
Capsule 2	2-8-4	545 / 558	746 / 764	849 / 870	13.20	4.39
Capsule 2 compacts		**532 / 545**	**811 / 831**	**924 / 946**	**12.68**	**4.09**
Capsule 1	1-1-1	611 / 624	778 / 795	894 / 913	4.76	1.32
Capsule 1	1-1-2	611 / 623	778 / 795	893 / 912	4.65	1.32
Capsule 1	1-1-3	615 / 628	782 / 798	897 / 917	4.84	1.35
Capsule 1	1-1-4	617 / 630	789 / 806	906 / 926	5.08	1.38
Capsule 1	1-1-5	625 / 638	797 / 814	916 / 936	5.41	1.42
Capsule 1	1-1-6	627 / 640	803 / 820	923 / 944	5.55	1.44
Capsule 1	1-1-7	628 / 641	804 / 821	924 / 944	5.58	1.44
Capsule 1	1-1-8	626 / 640	798 / 816	918 / 939	5.35	1.42
Capsule 1	1-1-9	619 / 631	791 / 808	910 / 930	5.10	1.39

Capsule	Compact	Time-averaged Minimum Temperature (°C)	Time-Averaged Volume-averaged Temperature (°C)	Time-Averaged Peak Temperature (°C)	Burnup (% FIMA)	Fast neutron Fluence (10^{25} n/m^2, E >0.18MeV)
Capsule 1	1-1-10	616 / 629	783 / 800	901 / 921	4.86	1.35
Capsule 1	1-2-1	760 / 775	900 / 919	1005 / 1027	6.16	1.7
Capsule 1	1-2-2	759 / 775	899 / 918	1003 / 1025	6.17	1.7
Capsule 1	1-2-3	763 / 778	903 / 922	1008 / 1030	6.23	1.73
Capsule 1	1-2-4	769 / 785	911 / 930	1017 / 1039	6.36	1.77
Capsule 1	1-2-5	777 / 792	921 / 940	1028 / 1050	6.52	1.81
Capsule 1	1-2-6	782 / 798	929 / 948	1037 / 1059	6.64	1.84
Capsule 1	1-2-7	783 / 799	930 / 950	1038 / 1060	6.64	1.83
Capsule 1	1-2-8	779 / 795	925 / 944	1032 / 1055	6.53	1.81
Capsule 1	1-2-9	772 / 787	917 / 936	1024 / 1046	6.39	1.77
Capsule 1	1-2-10	764 / 780	907 / 926	1013 / 1035	6.24	1.73
Capsule 1	1-3-1	837 / 853	985 / 1005	1088 / 1112	6.85	2.03
Capsule 1	1-3-2	836 / 852	983 / 1004	1086 / 1110	6.86	2.03
Capsule 1	1-3-3	839 / 855	987 / 1008	1091 / 1114	6.89	2.06
Capsule 1	1-3-4	845 / 862	996 / 1016	1100 / 1123	7.01	2.12
Capsule 1	1-3-5	854 / 871	1006 / 1027	1111 / 1135	7.14	2.16
Capsule 1	1-3-6	860 / 877	1014 / 1036	1120 / 1145	7.24	2.18
Capsule 1	1-3-7	861 / 878	1016 / 1037	1123 / 1147	7.23	2.19
Capsule 1	1-3-8	857 / 874	1011 / 1032	1118 / 1142	7.14	2.16
Capsule 1	1-3-9	849 / 866	1003 / 1024	1108 / 1132	7.03	2.12
Capsule 1	1-3-10	841 / 858	992 / 1013	1097 / 1120	6.92	2.06
Capsule 1	1-4-1	891 / 909	1045 / 1067	1143 / 1168	7.37	2.33
Capsule 1	1-4-2	890 / 908	1044 / 1066	1141 / 1166	7.38	2.33
Capsule 1	1-4-3	893 / 911	1047 / 1069	1145 / 1170	7.43	2.37
Capsule 1	1-4-4	900 / 917	1055 / 1077	1153 / 1178	7.49	2.43
Capsule 1	1-4-5	908 / 926	1065 / 1088	1164 / 1189	7.64	2.48
Capsule 1	1-4-6	914 / 932	1074 / 1097	1173 / 1199	7.73	2.5
Capsule 1	1-4-7	916 / 934	1077 / 1100	1176 / 1202	7.72	2.5
Capsule 1	1-4-8	912 / 930	1072 / 1095	1172 / 1197	7.63	2.48
Capsule 1	1-4-9	904 / 922	1064 / 1086	1163 / 1188	7.52	2.43
Capsule 1	1-4-10	896 / 914	1053 / 1075	1152 / 1177	7.43	2.37
Capsule 1	1-5-1	907 / 925	1071 / 1093	1163 / 1188	7.82	2.6
Capsule 1	1-5-2	906 / 924	1069 / 1092	1161 / 1186	7.84	2.6
Capsule 1	1-5-3	908 / 926	1072 / 1095	1164 / 1190	7.86	2.64
Capsule 1	1-5-4	914 / 931	1079 / 1102	1172 / 1197	7.91	2.71

Capsule	Compact	Time-averaged Minimum Temperature (°C)	Time-Averaged Volume-averaged Temperature (°C)	Time-Averaged Peak Temperature (°C)	Burnup (% FIMA)	Fast neutron Fluence (10^{25} n/m^2, E >0.18MeV)
Capsule 1	1-5-5	921 / 938	1089 / 1111	1182 / 1208	8.01	2.76
Capsule 1	1-5-6	926 / 944	1097 / 1120	1190 / 1216	8.09	2.78
Capsule 1	1-5-7	927 / 945	1100 / 1123	1192 / 1218	8.10	2.78
Capsule 1	1-5-8	924 / 942	1096 / 1119	1189 / 1214	8.01	2.76
Capsule 1	1-5-9	918 / 936	1088 / 1111	1181 / 1207	7.93	2.7
Capsule 1	1-5-10	912 / 929	1078 / 1101	1171 / 1197	7.88	2.65
Capsule 1	1-6-1	907 / 924	1082 / 1105	1190 / 1216	8.23	2.85
Capsule 1	1-6-2	906 / 923	1081 / 1104	1188 / 1214	8.23	2.85
Capsule 1	1-6-3	908 / 926	1084 / 1107	1192 / 1218	8.24	2.89
Capsule 1	1-6-4	913 / 931	1091 / 1114	1199 / 1226	8.29	2.96
Capsule 1	1-6-5	920 / 938	1101 / 1124	1210 / 1236	8.38	3.02
Capsule 1	1-6-6	926 / 944	1107 / 1131	1216 / 1243	8.47	3.04
Capsule 1	1-6-7	927 / 945	1109 / 1132	1217 / 1244	8.45	3.04
Capsule 1	1-6-8	924 / 942	1106 / 1129	1214 / 1241	8.38	3.02
Capsule 1	1-6-9	918 / 936	1099 / 1122	1207 / 1234	8.31	2.96
Capsule 1	1-6-10	911 / 929	1089 / 1112	1198 / 1224	8.26	2.9
Capsule 1	1-7-1	921 / 939	1108 / 1131	1216 / 1243	8.58	3.07
Capsule 1	1-7-2	920 / 938	1107 / 1131	1217 / 1244	8.57	3.06
Capsule 1	1-7-3	923 / 941	1110 / 1134	1221 / 1248	8.60	3.11
Capsule 1	1-7-4	928 / 946	1117 / 1141	1228 / 1255	8.65	3.19
Capsule 1	1-7-5	935 / 953	1126 / 1150	1236 / 1264	8.72	3.25
Capsule 1	1-7-6	940 / 958	1132 / 1156	1241 / 1269	8.85	3.27
Capsule 1	1-7-7	941 / 960	1133 / 1157	1242 / 1269	8.84	3.27
Capsule 1	1-7-8	937 / 956	1130 / 1154	1238 / 1266	8.74	3.24
Capsule 1	1-7-9	932 / 950	1123 / 1147	1231 / 1259	8.66	3.19
Capsule 1	1-7-10	925 / 944	1114 / 1138	1222 / 1249	8.61	3.12
Capsule 1	1-8-1	912 / 932	1110 / 1134	1217 / 1245	8.91	3.26
Capsule 1	1-8-2	913 / 932	1111 / 1136	1219 / 1246	8.89	3.25
Capsule 1	1-8-3	915 / 935	1115 / 1140	1223 / 1251	8.93	3.31
Capsule 1	1-8-4	920 / 939	1121 / 1146	1230 / 1257	9.02	3.38
Capsule 1	1-8-5	925 / 945	1128 / 1153	1238 / 1265	9.14	3.44
Capsule 1	1-8-6	930 / 949	1132 / 1157	1242 / 1270	9.25	3.46
Capsule 1	1-8-7	930 / 950	1133 / 1158	1243 / 1270	9.26	3.46
Capsule 1	1-8-8	926 / 946	1130 / 1155	1239 / 1267	9.14	3.44
Capsule 1	1-8-9	921 / 940	1123 / 1148	1232 / 1260	9.02	3.38

Capsule	Compact	Time-averaged Minimum Temperature (°C)	Time-Averaged Volume-averaged Temperature (°C)	Time-Averaged Peak Temperature (°C)	Burnup (% FIMA)	Fast neutron Fluence (10^{25} n/m^2, E >0.18MeV)
Capsule 1	1-8-10	915 / 935	1114 / 1139	1223 / 1251	8.95	3.31
Capsule 1	1-9-1	633 / 647	965 / 987	1171 / 1199	9.42	3.38
Capsule 1	1-9-2	634 / 648	966 / 989	1173 / 1200	9.45	3.38
Capsule 1	1-9-3	635 / 649	970 / 993	1177 / 1205	9.52	3.43
Capsule 1	1-9-4	639 / 653	975 / 998	1184 / 1211	9.62	3.51
Capsule 1	1-9-5	641 / 655	981 / 1003	1190 / 1218	9.79	3.57
Capsule 1	1-9-6	645 / 659	984 / 1007	1194 / 1222	9.95	3.59
Capsule 1	1-9-7	644 / 658	984 / 1007	1194 / 1222	9.93	3.59
Capsule 1	1-9-8	642 / 656	981 / 1004	1191 / 1219	9.83	3.57
Capsule 1	1-9-9	639 / 653	975 / 998	1184 / 1212	9.67	3.51
Capsule 1	1-9-10	636 / 650	968 / 991	1176 / 1203	9.54	3.43
Capsule 1 compacts		**611 / 623**	**1018 / 1040**	**1243 / 1270**	**7.75**	**2.60**
All AGR-5/6 compacts		**458 / 469**	**914 / 934**	**1243 / 1270**	**9.09**	**2.96**
Capsule 3	3-1-1	964 / 989	1162 / 1191	1299 / 1330	11.62	4.31
Capsule 3	3-1-2	964 / 989	1163 / 1193	1300 / 1332	11.77	4.41
Capsule 3	3-1-3	965 / 990	1164 / 1193	1300 / 1332	11.79	4.41
Capsule 3	3-2-1	1174 / 1202	1292 / 1322	1375 / 1407	12.43	4.35
Capsule 3	3-2-2	1177 / 1205	1293 / 1324	1376 / 1408	12.60	4.46
Capsule 3	3-2-3	1177 / 1205	1294 / 1324	1375 / 1407	12.61	4.46
Capsule 3	3-3-1	1235 / 1263	1330 / 1360	1394 / 1425	12.66	4.35
Capsule 3	3-3-2	1237 / 1265	1331 / 1361	1394 / 1426	12.83	4.46
Capsule 3	3-3-3	1238 / 1266	1331 / 1361	1394 / 1426	12.87	4.47
Capsule 3	3-4-1	1246 / 1273	1336 / 1366	1396 / 1427	12.73	4.35
Capsule 3	3-4-2	1249 / 1276	1338 / 1367	1397 / 1428	12.89	4.46
Capsule 3	3-4-3	1250 / 1277	1338 / 1368	1396 / 1428	12.93	4.46
Capsule 3	3-5-1	1241 / 1268	1333 / 1362	1395 / 1426	12.70	4.33
Capsule 3	3-5-2	1245 / 1272	1335 / 1365	1397 / 1428	12.86	4.44
Capsule 3	3-5-3	1245 / 1272	1335 / 1365	1396 / 1428	12.88	4.44
Capsule 3	3-6-1	1235 / 1263	1337 / 1367	1405 / 1437	12.57	4.29
Capsule 3	3-6-2	1238 / 1266	1339 / 1369	1407 / 1439	12.73	4.4
Capsule 3	3-6-3	1240 / 1268	1339 / 1370	1407 / 1439	12.77	4.41
Capsule 3	3-7-1	1187 / 1214	1317 / 1347	1402 / 1435	12.30	4.25
Capsule 3	3-7-2	1189 / 1216	1318 / 1348	1403 / 1436	12.47	4.36
Capsule 3	3-7-3	1190 / 1218	1319 / 1350	1404 / 1436	12.50	4.36
Capsule 3	3-8-1	964 / 989	1188 / 1217	1337 / 1369	11.68	4.17

Capsule	Compact	Time-averaged Minimum Temperature (°C)	Time-Averaged Volume-averaged Temperature (°C)	Time-Averaged Peak Temperature (°C)	Burnup (% FIMA)	Fast neutron Fluence (10^{25} n/m^2, E >0.18MeV)
Capsule 3	3-8-2	966 / 990	1189 / 1218	1338 / 1370	11.85	4.26
Capsule 3	3-8-3	966 / 990	1189 / 1218	1338 / 1370	11.86	4.27
All AGR-7 compacts		**964 / 989**	**1288 / 1318**	**1407 / 1439**	**12.45**	**4.37**